

*Republic of Iraq  
Ministry of Higher Education and Scientific Research  
University of Kerbala  
College of Engineering  
Department of Electrical and Electronic Engineering*



# **Design and Implementation for Wireless Power Transfer Prototypes for Research Validation**

*A Thesis*

*Submitted to the Department of Electrical and Electronic  
Engineering, University of Kerbala in a Partial Fulfillment of  
the Requirements for the Degree of Master of Science (M.Sc.) in  
Electrical Engineering*

by

**Haider Hameed Hussein**

Supervised by

**Prof. Dr. Ali Jafer Mahdi**

**Sha'aban /1443**

**March/2023**

بِسْمِ اللَّهِ الرَّحْمَنِ الرَّحِيمِ

يَرْفَعِ اللَّهُ الَّذِينَ آمَنُوا مِنْكُمْ وَالَّذِينَ أُوتُوا

الْعِلْمَ دَرَجَاتٍ

صدق الله العلي العظيم

( المجادلة: من الآية 11 )

*Dedicated to...*

**My family**

# **Acknowledgement**

All thanks to Allah for giving me the strength to complete this study. I express my appreciation and gratitude to my supervisor Prof. Dr. Ali Jafer Mahdi for his continuous encouragement and support during whole stages of my study, his advice and suggestions have contributed essentially in finishing this work.

I am indebted to my colleagues and friends who have presented advice and pointed positive notes.

Finally, I deepest thanks to my family for their continuous support, and encouragement throughout my study.

## Supervisor Certification

I certify that this thesis entitled “Design and Implementation for Wireless Power Transfer Prototypes for Research Validation”, which is prepared by "Haider Hameed Hussein", is under my supervision at University of Kerbala in partial fulfillment of the requirements for the degree of Master of Science (M.Sc.) in Electrical Engineering.

Signature *Alij. mahdi*

Supervisor's name

Prof. Dr. Ali Jafer Mahdi

Date: 31/5/2023

## Linguistic Certification

I certify that this thesis entitled “Design and Implementation for Wireless Power Transfer Prototypes for Research Validation” presented by “Haider Hameed Hussein” was reviewed linguistically. It was amended to meet the English style.

Signature:



Linguistic Supervisor Name:

Assit. Prof. Dr. Muayad Saleem Kod

Date: 16 / 5 / 2023

## Examination Committee Certification

We certify, as examining committee, that we have read the thesis entitled "**Design and Implementation for Wireless Power Transfer Prototypes for Research Validation**", and examined the student "**Haider Hameed Hussein**" in its contents and what is related with, found it meets the standard of a thesis for the degree of Master of Science (M.Sc.) in Electrical Engineering.

Signature: 


Name : *Prof. Dr. Ali Jafer Mahdi*  
(Supervisor)

Date: / / 2023

Signature: 

Name : *Prof. Dr. Ali Abdul Razzaq Altahir*  
(Chairman)


Date: 31/ 5/ 2023

Signature:   
Name : *Prof. Dr. Amel Ahmed Ridha*  
(Member)

Date: 31/ 5 / 2023

Signature:   
Name: *Dr. Manal Hussein Nawir*  
(Member)

Date: 31/ 5/ 2023

Signature:   
Name: *Prof. Dr. Haider I. Shahadi*  
(Head of the Department of Electrical Engineering)  
Date: 7/ 6 / 2023

Signature:   
Name: *Prof. Dr. Laith Sh. Rasheed Alqarawee.*  
Dean of the Engineering College  
Date: / / 2023

## Abstract

Wireless charging stations will become one of the emerging trends in the field of EV charging that has recently received considerable critical attention from researchers and practitioners to respond to the potential power and energy needs of EV. Inductive wireless power transmission (IWPT) is widely adopted in wireless charging techniques in EV applications for its capability to efficiently transmit high power levels over long distances that can reach up to 5 cm. The use of inductive IWPT goes beyond the charging application and can be used in the drivetrain of the electric vehicle. In-wheel motor is an innovative drivetrain design that has recently earned attention from the research community. In this configuration, electric motors are mounted in the wheels of the vehicle and powered wirelessly eliminating the need for power cables, reducing mechanical power loss, providing control freedom and saving more space in the vehicle body design. In this thesis, a one-input one-output inductive wireless power transmission prototype is designed for EV charging and the efficiency under different charging distances is practically determined. The absolute voltage and current waveforms of the voltages and currents (in the transmitted and received sides) are presented to validate the robustness of the proposed prototype for battery charging under various air gap distances. Then, a wireless power transmission system is designed and implemented with a 250 Watt in-wheel electric motor prototype system. The system is based on inductive wireless power transmission technology in which two coils are designed and mutually coupled at 65 kHz. The transmitter coil is driven by a Class-D inverter that is supplied by a 120 V, 10 A battery. The receiver coil supplies the motor drive circuit at different loading conditions. The stability analysis for the proposed WPT model is performed based on points of intersection on graphs of the coupling of coefficients versus the controllers' parameters (i.e. duty



cycles of the converters in the sending and receiving sides). The results show that the WPT model is stabilized in the limited range of duty cycles that achieve the best coupling of coefficients.

# List of Contents

<b>Abstract</b> .....	<b>V</b>
<b>List of Contents</b> .....	<b>VII</b>
<b>List of Symbols</b> .....	<b>IX</b>
<b>List of Abbreviations</b> .....	<b>XI</b>
<b>List of Figures</b> .....	<b>XII</b>
<b>List of Tables</b> .....	<b>XIV</b>
<b>Chapter One: Introduction</b> .....	<b>1</b>
1.1 Introduction .....	1
1.2 OVERVIEW OF WIRELESS POWER TRANSMISSION .....	2
1.3 CATEGORIES OF WPT SYSTEMS .....	3
1.3.1 Inductive WPT Techniques .....	4
1.3.2 Resonant WPT Technique .....	5
1.3.3 Capacitive WPT Techniques .....	6
1.4 OPERATION AND ANALYSIS OF INDUCTIVELY-COUPLED WPT SYSTEM.....	8
1.5 APPLICATIONS OF WPT SYSTEMS .....	10
1.5.1 Biomedical Applications .....	11
1.5.2 Military Applications .....	12
1.5.3 Electric Vehicles .....	13
1.6 Motivations .....	16
1.7 Research Problem.....	17
1.8 Objectives and Contributions .....	20
1.9 Literature Review .....	20
1.10 Thesis Outline .....	27
<b>Chapter Two: Small-Scale WPT System with R-Load</b> .....	<b>28</b>
2.1 Introduction .....	28

2.2 Small Scale Inductive Configuration.....	28
2.3 Calculations of Self-Inductance, Mutual Inductance, Coefficient of Coupling, AND Resonance-Capacitance Parameters.....	31
2.4 Illustration of The Difference Between Spiral and Rectangular Wireless Coil Shapes.....	33
2.5 Modelling and Analysis of Class-D Inverter .....	35
<b>Chapter Three: Design the Large-Scale WPT Prototype Connecting with an AC Motor .....</b>	<b>39</b>
3.1 Large-Scale in-Wheel WPT System.....	39
3.2 Design of the Proposed WPT System.....	39
3.2.1 The Power Electronic Module .....	41
3.2.2 Inductive link design .....	43
3.2.3 Estimation of the Coupling Coefficient .....	47
3.3 Design and Procedure Proposed System .....	49
3.4 Modelling and analysis of a Brushless DC (BLDC) Motor.....	51
3.5 Experimental Implementation of the Large-Scale System .....	53
<b>Chapter Four: Experimental Results .....</b>	<b>56</b>
4.1 Experimental Results of the Small-Scale System .....	56
4.2 Experimental Results of the Large-Scale System .....	61
4.2.1 Stability for Large Scale Prototype.....	75
<b>Chapter Five: Conclusion and Future work.....</b>	<b>78</b>
5.1 Conclusion .....	78
5.2 Future Work .....	79
<b>References .....</b>	<b>80</b>
<b>Appendix A: Photos of the Experimental Setup .....</b>	<b>A</b>

## List of Symbols

Symbol	Definition
$V_s$	Voltage Source
$R_L$	Load resistance
$R_T$	Internal resistance of the transmitter coil
$L_T$	The inductance of the transmitter coil
$I_T$	The current of the transmitter coil
$R_R$	Internal resistance of the receiver coil
$L_R$	The inductance of the receiver coil
$I_R$	The current of the receiver coil
$M$	Mutual inductance
$\omega$	Angular frequency
$P_{in}$	Input power
$P_o$	Output power
$Q_T$	Transmitter quality factors
$Q_R$	Receiver quality factors
$K$	Coupling coefficient
$\eta$	Efficiency
$D_{in}$	The inner diameter in inches
$S$	The distance between turns in inches
$w$	The wire diameter in inches
$N$	The number of turns
$V_d$	The rotating d reference voltage.
$V_q$	The rotating q reference voltage.
$i_d$	The rotating d reference current.
$i_q$	The rotating q reference current.
$L_d$	The rotating d reference inductance.
$L_q$	The rotating q reference inductance.
$\omega_r$	The electrical angular speed.
$\omega_m$	The mechanical angular speed.

$T_e$	The electromagnetic torque.
$P_m$	Mechanical power.
$np$	Number of poles.
$W_1$	Resonance frequency of the primary.
$W_2$	Resonance frequency of the secondary.
$Z_r$	Reflected impedance.
$L_1$	Primary inductance.
$L_2$	Secondary inductance.
$C_1$	Primary capacitive.
$C_2$	Secondary capacitive.
$D_o$	Outer diameter of Transmitter coil
$D_{in}$	Outer diameter of Receiver coil
$a$	The average radius of the plane spiral coil

## List of Abbreviations

<b>Abbreviation</b>	<b>Definition</b>
EVs	Electric Vehicles
WPT	Wireless Power Transmission
IWPT	Inductive Wireless Power Transmission
ICE	Internal Combustion Engine
W-IWM	Wireless In-Wheel Motor
LiC	Lithium-ion Capacitor
ISM	Industrial, Scientific and Medical
SAE	Society of Automotive Engineers
V2G	Vehicle-to-Grid
Tx	Transmitter coil
Rx	Receiver coil
$f_{wpt}$	wireless resonant frequency
PWM	Pulse Width Modulation
MIT	Massachusetts Institute of Technology
BMS	Battery Management System

# List of Figures

Fig. 1.1. Classification of WPT Techniques. ....	4
Fig. 1.2. Inductive WPT coils.....	5
Fig. 1.3. Resonant WPT system. ....	6
Fig. 1.4. Fundamental capacitive WPT system. ....	6
Fig. 1.5. Equivalent circuit of an inductive WPT system. ....	8
Fig. 1.6. An epiretinal prosthesis with WPT. ....	11
Fig. 1.7. RF-based WPT system in a military application [20]......	12
Fig. 1.8. Wireless charging of a military robotic vehicle [19]. ....	13
Fig. 1.9. Scheme of a static charging IWPT system for an electric vehicle [21]. ....	13
Fig. 1.10. The concept of dynamic WPT for EV charging [22]......	14
Fig. 1.11. Power profile from road charging transmitters showing the pulsating nature of dynamic WPT [12]......	15
Fig.2.1. Schematic circuit of the small-scale WPT system, the Tx side.....	30
Fig.2.2. Experimental circuit of the inductive WPT system at Tx side.....	31
Fig.2.3. Schematic circuit of the IWPT system, the Rx side.....	31
Fig.2.4. Experimental circuit of the small-scale WPT system, the Rx side.....	31
Fig.2.5. The implemented static charging WPT prototype.....	32
Fig.2.6. Class D inverter circuit diagram.....	37
Fig.2.7. Voltage and current waveforms of Class D inverter at its different operation...	38
Fig. 3.1. The structure of the proposed system showing its three modules. ....	39
Fig. 3.2. The proposed wireless drive system for an electric vehicle System component. ....	40
Fig. 3.3. Real printed wireless coil by CNC machine.....	46
Fig. 3.4. T-type equivalent circuit of the coupling module.....	49
Fig. 3.5. The Flow Chart the Proposed design procedure and stability validation.....	51
Fig. 3.6. The practical BLDCM with its drive circuit ....	53
Fig. 3.7. The complete transmitter and receiver circuit of the proposed system.....	54
Fig. 3.8. The experimental prototype of the Large Scale system.....	56
Fig. 4.1. The waveforms of the voltage and current in Tx side 1cm. ....	56
Fig. 4.2. The waveforms of the voltage and current in Rx side 1cm. ....	56
Fig. 4.3. The waveforms of the voltage and current in Tx side 2 cm. ....	57
Fig. 4.4. The waveforms of the voltage and current in Rx side 2 cm. ....	57

Fig. 4.5. The waveforms of the voltage and current in Tx side 3 cm. ....	58
Fig. 4.6. The waveforms of the voltage and current in Rx side 3 cm. ....	58
Fig. 4.7. The waveforms of the voltage and current in Tx side 4 cm. ....	59
Fig. 4.8. The waveforms of the voltage and current in Rx side 4 cm. ....	59
Fig. 4.9. The waveforms of the voltage and current in Tx side 5 cm. ....	60
Fig. 4.10. The waveforms of the voltage and current in Rx side 5 cm. ....	60
Fig. 4.11. voltage transmitter simulation and practical according to different distance.	61
Fig. 4.12. voltage Receiver simulation and practical according to different distance....	61
Fig. 4.13. current transmitter simulation and practical according to different distance....	62
Fig. 4.14. current receiver simulation and practical according to different distance.....	63
Fig. 4.15. Case (1) Simulation Result from Table 4.5. ....	66
Fig. 4.16. Case (2) Simulation Result from Table 4.5. ....	67
Fig. 4.17. Practical voltage and current waveforms of the transmitter and receiver coils (No Load (Distance= 7.5cm)). ....	67
Fig. 4.18. Practical voltage and current waveforms of the transmitter and receiver coils (Half Load (Distance= 7.5cm)). ....	68
Fig. 4.19. Practical voltage and current waveforms of the transmitter and receiver coils (Full Load (Distance= 7.5cm)). ....	69
Fig. 4.20. Practical voltage and current waveforms of the transmitter and receiver coils (No Load (Distance= 10cm)). ....	70
Fig. 4.21. Practical voltage and current waveforms of the transmitter and receiver coils (Half Load (Distance= 10cm)). ....	71
Fig. 4.22. Practical voltage and current waveforms of the transmitter and receiver coils (Full Load (Distance= 10cm)). ....	72
Fig. 4.23. Practical voltage and current waveforms of the transmitter and receiver coils (No Load (Distance= 12.5cm)). ....	73
Fig. 4.24. Practical voltage and current waveforms of the transmitter and receiver coils (Half Load (Distance= 12.5cm)). ....	74
Fig. 4.25. Practical voltage and current waveforms of the transmitter and receiver coils (Full Load (Distance= 12.5cm)) ....	75
Fig. 4.26. Stability boundary graphs of controllers' parameters (a) D1 and (b) D2.....	76



# List of Tables

Table 1.1. A comparison between inductive and capacitive WPT.....	7
Table 1.2.A comparison about the contributions between the latest studies and this study.....	26
Table 3.1. System Details components.....	40
Table 3.2. Coils design parameters.....	47
Table 3.3. Parameters the complete transmitter and receiver circuit of the proposed system.....	50
Table 4.1. Experimental results of the small-scale system.....	61
Table 4.2. Simulation vs experimental voltage measurements of the large-scale system.....	62
Table 4.3. Simulation vs experimental current measurements of the large-scale system.....	63
Table 4.4. Simulation vs Experimental Power and Efficiency (Error).....	65
Table 4.5. Experimental and Simulation Flux Linkage, Rotational Speed.....	66
Table 4.6. The Range of Optimal D1.....	77
Table 4.7. The Range of Optimal D2.....	77

# Chapter One: Introduction

## 1.1 INTRODUCTION

Transportation electrification is one of the most effective measures taken to reduce the impacts of climate change as transportation contributes to about 20% of global greenhouse gas emissions [1] and [2]. The importance of decarbonizing the transportation sector was signified by the international community in the commitments made in the latest climate conference COP26 in 2022. Automobile manufacturers and environmental organizations have agreed to cooperate and accelerate the transition to zero emission vehicles by pledging to achieve 100% Electric Vehicles (EV) sales within the next two decades [3]. The widespread use of EV will require new infrastructure and technologies to facilitate efficient and reliable operation of EV fleets. EV charging is one of the vital technologies upon which the commercial and technical success of EV relies on. Therefore, development of fast, efficient, convenient and cost-effective charging methods will be essential to meet the expected demand [4]. Wireless charging using the concept of Wireless Power Transmission (WPT) is an emerging approach developed to meet the power needs of EV besides wired charging. In fact, efficient wireless charging systems are expected to outperform wired charging methods for their advantages of convenience, safety in moist environments, no need for plugs and cables, and inherent galvanic isolation. Nikola Tesla was the first electrical engineer in the world to plant the seed of the WPT idea through his famous yet-overlooked Wardenclyffe Tower experiment that he conducted in New York in the early years of the 20th century [5]. In his experiment he tried to transmit electric power between two distant towers without any wires or cables connecting them. The main application of Tesla's WPT system was for long-distance wireless communication to send

data message across the ocean to England. However, Tesla's WPT idea did not see the light of the day. His invention was not turned into a real product due to financial challenges and global competition. A century after Tesla's attempt, this concept was revived by a research team at MIT that succeeded in transmitting electric power to a 60W load located 2m away from the transmitting source. Although their developed method was able to wirelessly deliver only 40% of the transmitted power, MIT method has shaped the way of modern wireless power transmission technology [6], [7].

## **1.2 OVERVIEW OF WIRELESS POWER TRANSMISSION**

Wireless power transmission is defined as the process of transmitting electrical energy from an energy source to a load without any means of physical connection between them utilizing the electromagnetic phenomena between two passive elements. The absence of wired power connections between source and load makes WPT systems convenient, reliable, galvanically isolated, safe and efficient. These features enable WPT to be used in a wide range of applications including industrial robots, aerospace systems, consumer electronics, medical devices, military applications as well as electric vehicles. WPT systems can be designed with different power levels to cover these applications. For instance, low power WPT system can be found in medical and mobile devices. Medium power systems are used in hand-held electronics, monitors and household appliances. On the other hand, electric vehicle chargers belong to the high power category of WPT system. With such diverse range of applications, WPT global market has been growing steadily as it was valued at \$5,705.1 million in 2020 with a projection of \$35,226 million by 2030 [8].

In designing any WPT system, the coupling coefficient between the coupling elements is a critical consideration because it defines the amount of electromagnetic flux that can be received by the receiver compared to the

transmitted flux from the source. Its typical value ranges from 0 to 1 and depends on the magnetic coupling mechanism used between the coupling components. In WPT systems that utilize a pair of loosely coupled coils, the challenging is to obtain high coupling coefficient because a large amount of the magnetic flux is lost in the air gap. Therefore, the air gap design imposes practical limitations on the transmission distance and alignment angle between the coils to achieve high transmission efficiency. The loosely-coupled nature of the coils has another downside when it comes to modeling WPT systems with multiple receivers that is the crosstalk phenomenon [6], [9].

According to the field and range over which electric energy is transmitted, WPT techniques are found in two main categories: far-field and near-field techniques. In the far-field methods, energy is transmitted through high-frequency electromagnetic waves in the form of radio frequency waves or in the visible spectrum as laser signals, and that is why this technique is also known as the radiative technique. The range of frequency within which radiative methods operates starts from 250 MHz up to 1 THz. With radiative WPT, energy can be transmitted for long distances with high efficiency and directivity. On the other hand, the near-field category includes WPT techniques that operate based on the principle of evanescent electromagnetic coupling between two passive elements where the energy between them is transmitted in forms of magnetic and electric fields. According to the passive elements used, the near-field WPT can be either inductive or capacitive. It is obvious that near-field techniques do not involve any radiation and they are also known as non-radiative methods. Near-field techniques are what is commonly used in EV charging.

### **1.3 CATEGORIES OF WPT SYSTEMS**

As it was mentioned earlier in section 1.2, WPT techniques are classified, based on the nature of the field in which electric energy is

transferred, into two main categories that are far-field and near-field techniques as shown in Fig. 1.1 [10]. As the names suggest, the main difference between these two methods is the distance over which energy can be transmitted. With near-field methods, the transmission distance is less than one wavelength of the frequency with which the WPT technique is operated. On the other hand, far-field methods can be used to transmit energy over long distances that are as long as many wavelengths of the operating frequency. However, both methods work on the same basic principle: the transmitting element energizes its circumference and subsequently drives the receiver element that lies in the surroundings.

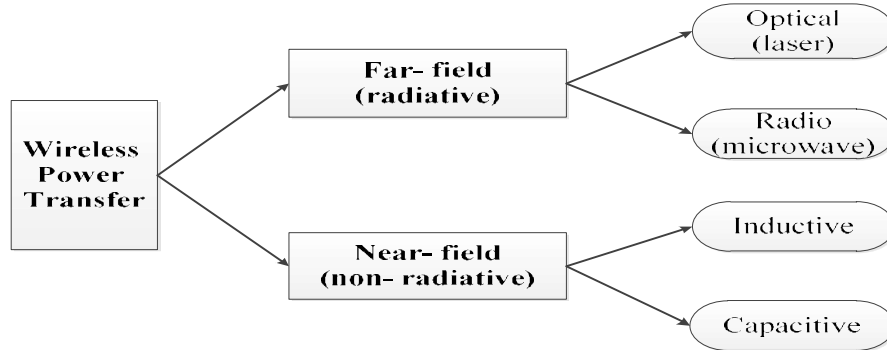


**Fig. 1.1. Classification of WPT Techniques.**

### **1.3.1 Inductive WPT Techniques**

In this technique, two mutually coupled coils are used. One of the coils, defined as the transmitter, is connected to an energy source of high-frequency current. The frequency range in which inductive WPT can be achieved is 50-250 kHz. Based on the electromagnetic induction principle, an electromagnetic force at the same frequency of the source varying magnetic field will be induced at the terminal of the other coil, the receiver, achieving energy transmission between the two coils. This topology can be subdivided into two subcategories based on the method of coupling that are the inductive coupling and resonant coupling. Fig. 1.2 shows the basic structure of an inductive WPT system.

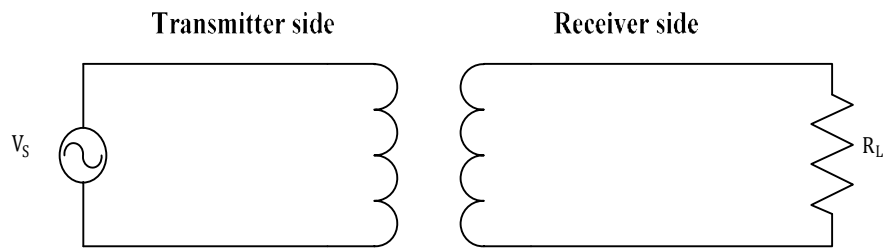


**Fig. 1.2. Inductive WPT coils.**

### **1.3.2 Resonant WPT Technique**

This method depends on the concept of magnetic resonance between two strongly coupled coils. A capacitor is connected in series with the transmitter and receiver coils. The capacitors are tuned to create resonance and reduce the power withdrawn by the transmitter. Thus, energy can be transmitted between a receiver and a transmitter coil that are resonating at a certain frequency. When the frequency of the energizing voltage is equal to the natural frequency of the receiving coil resonance [10]. In such a mechanism, the operating resonance frequency decides the size of the coupling coils and consequently affect the transmission efficiency. Resonant WPT can be operated at high frequencies that can reach the megahertz range. As a result, resonant WPT systems are capable of transmitting energy over distances up to 1 meter which are considered as much as ten times the transmitter's diameter. The concept of operation of this technique makes it suitable for multi-receiver WPT systems because adding more output coils can be as easy as tuning the coil to the resonant frequency of the transmitter. The configuration of a resonant WPT circuit is shown in Fig. 1.3.

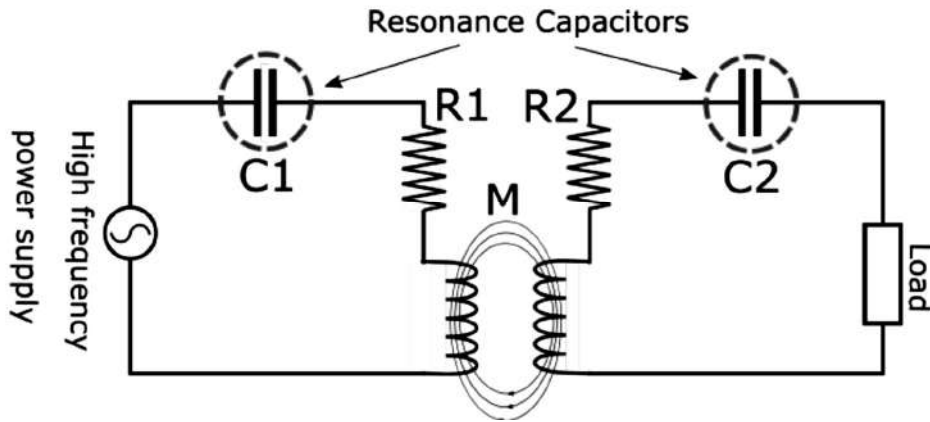


Fig. 1.3. Resonant WPT system. [11]

### 1.3.3 Capacitive WPT Techniques

The capacitive technique is implemented by two capacitors with their corresponding plates on the two different sides of the transmission system, the transmitter and receiver sides as shown in Fig. 1.4. When the transmitter plates are supplied with voltage, potential difference of an opposite polarity will be generated at the receiver plates. These factors impose technical and physical limits on the system and its power capacity. For instance, the maximum value of the electric field intensity between the plates of a capacitor should not exceed 3.4 MV/ m to avoid arc discharge due to air ionization [12]. That is why capacitive WPT system are found in low power applications such as in portable devices and medical devices.

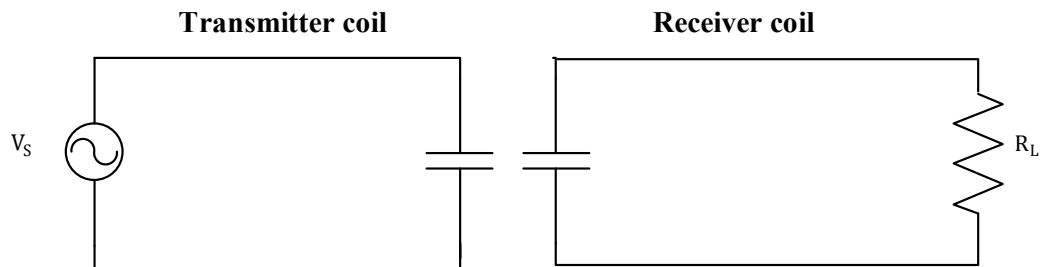


Fig. 1.4. Fundamental capacitive WPT system. [12]

For EV charging purposes, inductive IWPT techniques are commonly used for their capability to transmit much higher power than the capacitive counterpart. Inductive systems are simple to construct and offer high

transmission efficiency over small distances. In other words, they provide a trade-off between power capacity, efficiency and complexity. However, the internal resistance of the coils causes internal heating losses. Inductive IWPT systems are less tolerant to the misalignment between the transmitter and the receiver coils. The other demerit of inductive WPT systems is the generation of electromagnetic interference. Compared to the inductive approach, resonant WPT systems work at a higher frequency range and can achieve higher efficiency. Yet, such features require high inductance and that imposes size and bulkiness challenges. Another requirement in resonant WPT is the compensation circuit that is needed to compensate any inductance leakage and improve the transmission efficiency [13]. A comparison between inductive and capacitive techniques is listed in Table 1.1 [14].

**Table 1.1. A comparison between inductive and capacitive WPT.**

	<b>Inductive power transfer</b>	<b>Capacitive power transfer</b>
Switching frequency	10 kHz ~ 10 MHz	100 kHz ~ 10 MHz
Coupling field	Magnetic	Electric
Heat dissipation	Will generate heat	Will not generate heat
Material	Litz wires, ferrites	Copper/aluminum plates
Cost	High	Low
Safety	Good	Excellent
Size	Small	Large
Misalignment	Poor	Good
Voltage stress	Medium	High
Power level	High	Medium
Stationary or dynamic	Better for stationary	Both

This work focuses on the inductive technique only, and the remaining types including the radiative approaches are out of the scope of this thesis and will not be discussed here.



## 1.4 OPERATION AND ANALYSIS OF INDUCTIVELY-COUPLED WPT SYSTEM

The principle behind the operation of an inductive WPT system is the electromagnetic induction law by Faraday which governs the inductive coupling between two coils [15]. The other equivalent circuit of a fundamental inductive WPT system is shown in Fig. 1.5.

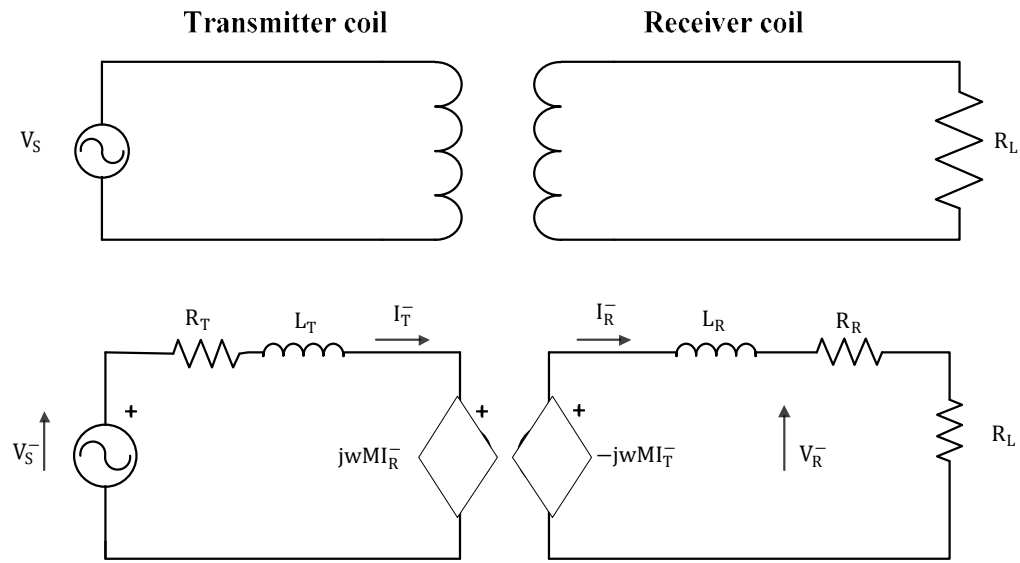


**Fig. 1.5. Equivalent circuit of an inductive WPT system.**

The system is energized with a high frequency alternating voltage source  $V_s$  to transmit power to a load resistance  $R_L$  at the receiving end. In the equivalent circuit,  $R_T$ ,  $L_T$  and  $I_T$  are the internal resistance, the inductance and the current of the transmitter coil respectively. Similarly,  $R_R$ ,  $L_R$  and  $I_R$  are the internal resistance, the inductance and the current of the receiver coil respectively. The two coils are coupled with a mutual inductance  $M$ . The induced voltage in each coil due to the mutual inductance can be written as  $j\omega M I_R$  and  $-j\omega M I_T$ , respectively. Therefore, the voltage equation around the transmitter and receiver loops can be written as follows [15],

$$V_S = Z_T I_T + j\omega M I_R \quad (1.1)$$

$$Z_R I_R = -j\omega M I_T \quad (1.2)$$

Where  $\omega$  is the angular frequency. Defining the loop impedances as  $Z_T = R_T + j\omega L_T$  and  $Z_R = R_R + R_L + j\omega L_R$ , the transmitter and receiver currents can be expressed as follows

$$V_S = Z_T \frac{Z_R I_T}{-j\omega M I_T} + j\omega M I_R \quad (1.4)$$

$$V_S = I_R \left( \frac{Z_T Z_R}{-j\omega M} + j\omega M \right) \quad (1.5)$$

$$I_T = \frac{V_S Z_R}{Z_R Z_T + M^2 \omega^2} \quad (1.6)$$

$$I_R = -\frac{V_S j\omega M}{Z_R Z_T + M^2 \omega^2} \quad (1.7)$$

At this point it is important to specify the system performance parameters that we are interested in. The transmission efficiency is one of these quantities that needs to be formulated, in terms of the input,  $P_{in}$  and output power,  $P_o$ . The input complex power can be obtained as follows

$$S_{in} = V_S I_T^* = V_S \left( \frac{V_S Z_R}{Z_R Z_T + M^2 \omega^2} \right)^* = V_S^2 \frac{Z_R Z_T + M^2 \omega^2}{|Z_R Z_T + M^2 \omega^2|^2} Z_R^* \quad (1.8)$$

The input active power is then given as

$$P_{in} = \text{Real} \left( V_S^2 \frac{Z_R Z_T + M^2 \omega^2}{|Z_R Z_T + M^2 \omega^2|^2} Z_R^* \right) \quad (1.9)$$

The output power on the other hand can be expressed as follows,

$$P_o = |I_R|^2 R_L = \frac{V_S^2 \omega^2 M^2}{|Z_R Z_T + M^2 \omega^2|^2} R_L \quad (1.10)$$

Neglecting the coils internal resistance for simplicity, the efficiency can be written as follows,

$$\eta = \frac{\omega^2 M^2}{R_L + \omega^2 M^2} \quad (1.11)$$

Further formulation can be done in terms of the coils quality factors,  $Q_T = \frac{\omega L_T}{R_T}$  and  $Q_R = \frac{\omega L_R}{R_R}$ , respectively, and the Coupling Coefficient,  $K = \frac{M}{\sqrt{L_T L_R}}$ .

It can be noticed that the transmission efficiency is directly proportional to the coupling coefficient. Since there is no coupling core between the two coils of the WPT system, i.e., the coils are coupled through an air gap, the value of the coupling coefficient will mainly depend on the

size of that air gap and the distance between the coils. The existence of the air gap results in considerable self-inductance and that reduces the mutual inductance and consequently, the coupling coefficient. The typical value of the coupling coefficient in such a configuration is usually around 0.6-0.7. One of the techniques used to improve the coupling coefficient in a coreless pair of coils is to use compensation capacitors connected in series and parallel configurations within the transmitting and receiving circuits. The function of the compensation capacitors is to reduce or completely cancel the reactive component of the transmitter current by resonating at the source frequency with the inductive elements of the circuit. [10]

The transmission efficiency can also be improved by increasing the quality factor of the transmitter and receiver coils. The quality factor of a passive circuit represents the amount of energy that is lost in the circuit when energy oscillates between the passive components. There are different factors that contribute to increase the quality factor of a coil. Increasing the transmission frequency, i.e., the frequency of the source voltage can increase the quality factor of the circuit. However, the operating frequency is restricted to a certain limit for design, safety and noise reasons. Reducing the coil internal resistance also improves the quality of the coil energy storage. The coil resistance depends on the material and dimensions of the coil conductor. [11]

## **1.5 APPLICATIONS OF WPT SYSTEMS**

WPT systems can found in a wide range of applications in modern life including low-power devices such as consumer electronics and high-power systems such as in transportation. Depending on the device size and the amount of energy required to be transferred, each of the different categories discussed in the previous section can be suitable for a certain application. This section lists the emerging applications in which WPT system are used. [12]

### 1.5.1 Biomedical Applications

The use of WPT systems in biomedical applications goes back to the 1960s when an inductive IWPT approach was first used in artificial heart devices. Benefiting from their advantages of contactless operation, which reduces the risk of infection, and comfortable implantation, wireless biomedical devices have since expanded to be used in a variety of biomedical devices including wireless gastric implants, medical endoscopes, deep brain stimulators, gastrointestinal robots, cochlear implants, implanted electrocardiogram recorders and pacemakers [13], [15], [16]. Fig. 1.6 shows an epiretinal prosthesis with a WPT system [17].

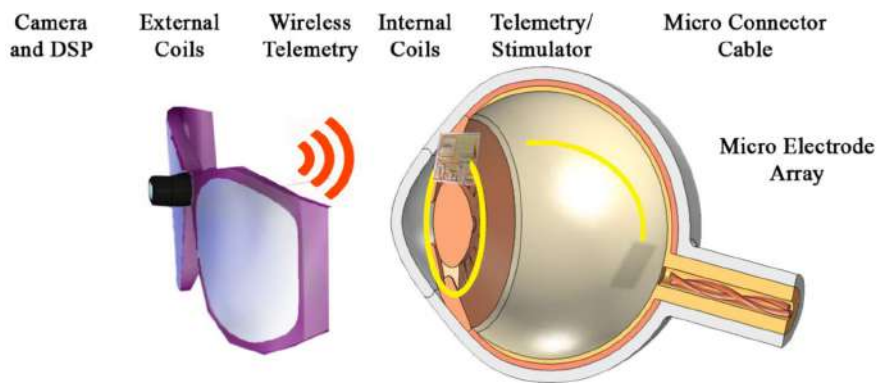


**Fig. 1.6. An epiretinal prosthesis with WPT [17].**

However, the operation of such wireless biomedical devices faces technical challenges represented by electromagnetic effects, attenuation, from the operating medium which is the biological tissues of the human body. The receiver part of the WPT system is implanted inside the human body and that imposes size restriction on the receiver coil. In other words, the receiver circuit should very compact in size to be implanted in the human body. In fact, this challenge is double because the size constrain of the receiver coil also affects the transmission distance which is relatively long given the receiver size and the transmitter location. The other challenge of WPT systems that faced in medical devices is that human body tissues are

considered good conductors of electricity because they mostly consist of an aqueous solution. Therefore, the power transmission process inside the body suffers from conduction losses [18].

### 1.5.2 Military Applications

Manned military applications refer to systems that operate with human involvement such as combat soldiers' wearable batteries used in communication and vision devices. In such wearable chargers, power is transmitted wirelessly to batteries through different configurations of transmitter. [19].

Another approach uses radio frequency in the range of 2-4 GHz to transmit energy from a stationary transmitter to wearable batteries in the vest as shown in Fig. 1.7 [20].

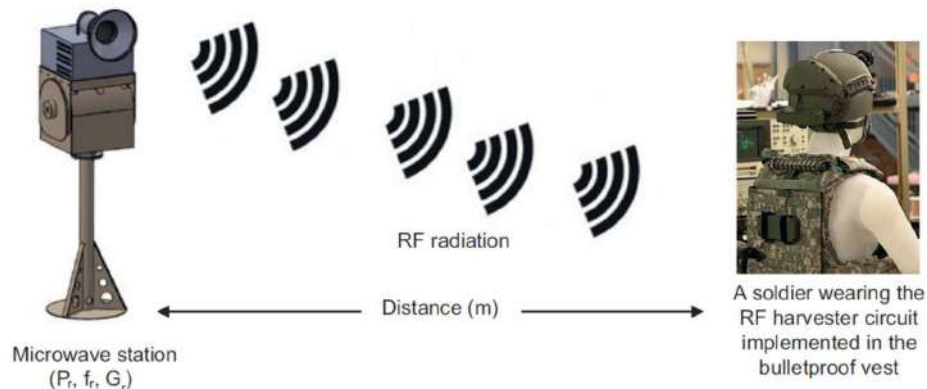


**Fig. 1.7. RF-based WPT system in a military application [20].**

Unmanned military applications include autonomous and semi-autonomous robots that are energized wirelessly from a transmission base. These robotic vehicles can be used in under-water applications [11] or in land robots such as the application presented in shown in Fig. 1.8.

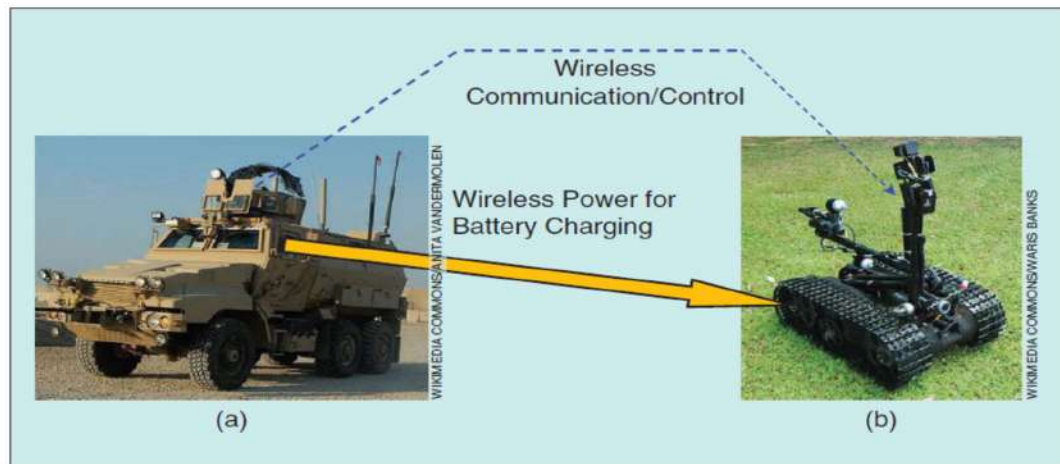


**Fig. 1.8. Wireless charging of a military robotic vehicle [19].**

### 1.5.3 Electric Vehicles

When talking about the use of WPT in the context of EV what comes to mind is the application of wirelessly charging of an electric vehicle. In other words, the dominant application of WPT in EV is in wireless charging, which can be achieved in two different approaches. The first approach is defined as the stationary WPT system in which the vehicle is parked over a wireless charging pad as shown in Fig. 1.9.

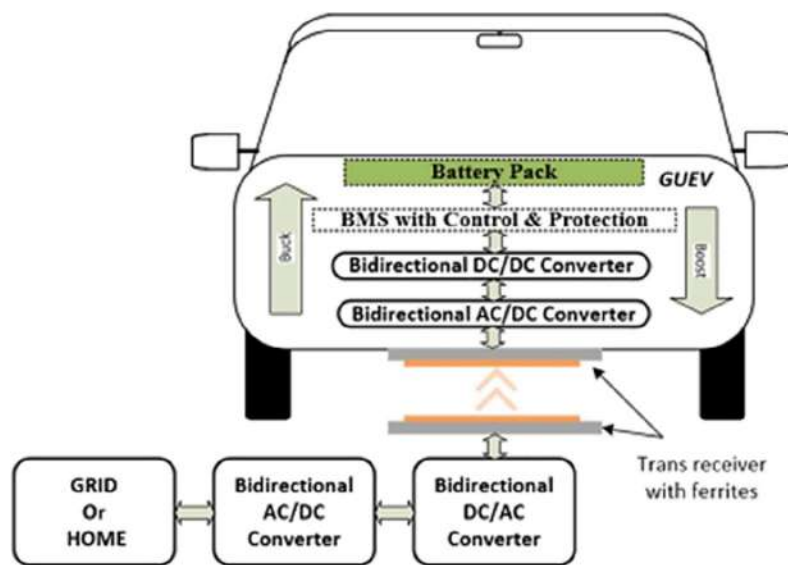


**Fig. 1.7. Scheme of a static charging IWPT system for an electric vehicle [21].**

The convenience of this wireless charging method comes from the dispensability of the conductors. However, it does not fully tap the desired benefits of the WPT because the vehicle still needs to be left for hours at the charging station further to the need for high energy capacity batteries to meet the driving range. The first method faces another inevitable challenge that is the air gap between the receiving and transmitting coils. High air gap between the wireless transmission coils affects the coupling factor between them and deteriorates the transmission efficiency. Besides, the limited availability of EV charging stations is another barrier that might stall the mass adoption of EV [21].

The second approach is the dynamic WPT with the vehicle can be continuously charged while in motion from transmitting coils installed along the road as shown in Fig. 1.10 [22]. Therefore, in-motion charging can contribute to reducing the size and weight of the required batteries and improving the driving range at the same time. Furthermore, with dynamic charging, the receiver coil can be installed around the wheel(s) of the vehicle to ensure that the receiver and transmitter coils are as closest to each other as possible maximizing the coupling coefficient between them as proposed in [23].

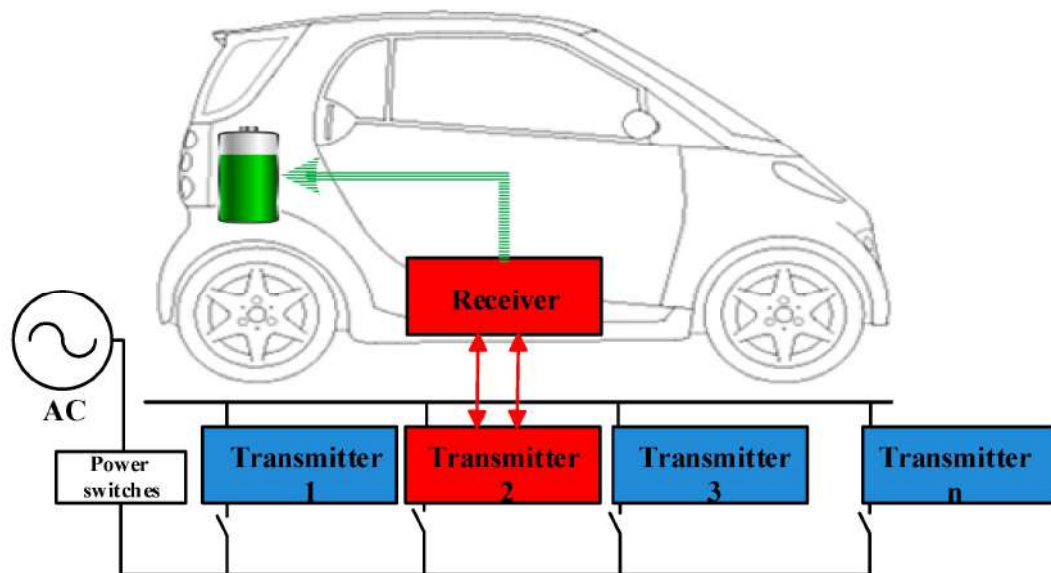


**Fig. 1.8.** The concept of dynamic WPT for EV charging [22].

Dynamic WPT, thus, poses its own drawbacks. First, the power supplied by the road chargers to the vehicle battery is highly pulsating in nature because the value of the power received by the receiver coil changes as it moves from one road transmitter to another. Fig. 1.11 shows the power profile of an electric vehicle receiver when charged from spaced-out road transmitters [12].

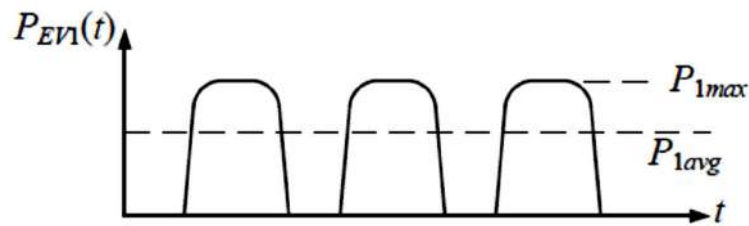


**Fig. 1.9. Power profile from road charging transmitters showing the pulsating nature of dynamic WPT [12].**

This intermittency in charging power requires high-capacity smoothing capacitors to absorb such fluctuations. High capacitance means increase in the size of the capacitors leading to oversize issues in the vehicle-side circuitry. The pulsating profile can also be smoothed out by overlapping the transmitter pads to reduce the spacing between them as proposed in [12]. However, more power fluctuations can also be imposed by the vehicle misalignment with the road charges. The second problem in dynamic WPT chargers is their complexity because optimizing the charging process of moving batteries requires additional sensing and control components [24].

Dynamic WPT can also be bidirectional in which power can also be fed back from the electric vehicle to the mains. Bidirectional power flow enables EV to operate in Vehicle-to-Grid (V2G) mode through which EVs can be utilized in grid ancillary services such as frequency control.



## 1.6 MOTIVATIONS

As it was mentioned earlier, transportation contributes a great deal to global carbon emissions and it is one of the significant industries that needs to be electrified to tackle climate change. This reason along with the emergence of climate action mindset among a large body of automobile customers are behind the growing popularity of Electric Vehicles (EV). For instance, in 2021, about 5 million new electric vehicles were registered in China and Europe combined [25]. In fact, the invention of EV dates back to the 19<sup>th</sup> century when several pioneers in Europe and the US experimented different concepts of a vehicle powered with a battery and electric motor. However, it was not until early 20<sup>th</sup> century that EV became commercially available and achieved market sales. Yet, that rise did not last long and EV were soon overtaken by internal combustion engine vehicles due to manufacturing affordability by mass production and the advent of low-cost oil in early 1900s. And then after that, the growing climate change concerns over the last three-four decades have sparked great interest in EV and revived its market. The adoption of EV technology is however without its hurdles. Driving range and charging time are the major challenges that throw the spanner in the works of smooth transition to electrified transportation. The driving range challenge is related to the battery constraints of energy capacity, energy density, state of health and safety requirements. The advancement in lithium ion battery technologies can alleviate these challenges by developing cost effective batteries with high energy density [26]. The speed of charging an electric vehicle depends on the type of the charger used. Currently, there are three categories of EV charging stations according to the speed of charge: slow chargers, fast chargers. The use of these three types of chargers depends on the electrical compatibility of the electrical vehicle. The first category is represented by cost-effective home chargers that can fully charge a vehicle battery in 24 hours. They are

basically connected to wall plugs and operate at household voltage level. The second type of chargers which can be found in commercial charging stations provides higher power to increase the charging speed by 60% compared to the first type. The third category uses high DC power that can reach up to 350 kW to bring the charging time down to less than two hours [27]. The three categories discussed above refer to hard-wired chargers. i.e., the electric vehicle is connected to the charger through a physical connection. Recently, there have been continued efforts made by researchers and industrial players to improve the speed, efficiency, safety and convenience of EV chargers. One of these advancements is the use of WPT technology in EV charging to achieve safety, convenience, long-range and durability.

## **1.7 RESEARCH PROBLEM**

1-In addition to the charging system, WPT can be used within the electrical circuitry of the electric vehicle such as in the electric drivetrain. Replacing the conventional Internal Combustion Engine (ICE) with an electric motor powered by an onboard battery entails certain modifications in the design of the vehicle drivetrain system.

2-Most EV manufacturers follow the same design principle used in traditional ICE vehicles and mount the traction motor under the hood. In other words, a central electric motor is located in the front end of the vehicle and its power is transferred to the wheels through a driveshaft connecting the motor output to the wheels. Other manufacturers such as Tesla attach their motor on one of the axles, front or rear, in between the wheels through a driveshaft. Such a design reduces the requirements of mechanical power transmission as the motor is located close to the wheels. However, the use of the driveshaft in the two aforementioned designs causes horsepower loss, driving range reduction, and time lag between the motor rotation and the

rotation of the wheels. To avoid this challenge, a new approach is developed by some EV motor manufacturers defined as the in-wheel motor or hub motor [28], [29].

3-The electric motor is attached directly to the wheel to eliminate the need for a driveshaft. As a result, the in-wheel motor technology does not suffer from the power loss associated with the driveshaft components. Besides, with each wheel driven by an individual motor, the wheels can be controlled separately and their acceleration torque response can be improved. The other merit of the in-wheel motors is improving the vehicle handling because left and right wheels can be controlled independently making sharp turns more precise and smooth [30], [31] further to the space that will be saved in the front and rear ends of the vehicle that can be added to the vehicle cargo space. These features in addition to the advancements in electric motor technology has helped direct the attention of not only industry practitioners but also researchers to the in-wheel drive approach [31]–[34].

4-In-wheel motor design faces a practical challenge in connecting the battery pack, which is located on the vehicle body, to the motors on the wheels.

5-The wires and cables that connect the motors to the vehicle chassis experience durability issues because they are susceptible to wear and tear due to continuous steering and exposure to the road rough conditions. This shortcoming can be effectively overcome by utilizing WPT to transmit electric power from the vehicle's body to the wheel motor eliminating all wired connections. This solution was introduced by a research group from the university of Tokyo, Japan.

6-The authors developed and prototyped three generations of Wireless In-Wheel Motor (W-IWM) system based on magnetic resonance coupling. The first generation (W-IWM1) [35] is a practical realization of the concept of using WPT to replace power lines between the in-wheel motors and the vehicle body. The developed system enables bi-directional WPT to support regenerative braking. The W-IWM1 system succeeded in transmitting 3.3

kW in each wheel at an efficiency of 94.3%. In the second generation (W-IWM2) [36], [37], the system was scaled up and upgraded to provide WPT from the wheel side to the body-side coil to improve the regenerative braking via a Lithium-ion Capacitor (LiC) located on the wheel side. Besides, W-IWM2 supports wireless charging from an on-road transmitting coil. The third generation (W-IWM3) is a modification of W-IWM2 which supports in-motion (dynamic) wireless charging instead of static wireless charging [36]. W-IWM3 achieved improvements in power transmission and power density. The authors also discussed the W-IWM system efficiency [38] and investigated a model to evaluate the system losses [39]. In the work surveyed in above, resonant magnetic coupling technique was used for WPT in which two coils are coupled through resonance at the resonance frequency. 7-This technique works at high frequencies that can reach the megahertz level to achieve high coupling coefficient and quality factor and consequently increase the transmission distance. Thus, the usable frequency can be bound by frequency restrictions imposed by Industrial, Scientific and Medical (ISM) international standards for radio bands. The resonance frequency used in W-IWM1, W-IWM2 and W-IWM3 was set to 85 kHz adhering to the Society of Automotive Engineers (SAE) standards [40]. At this frequency, the achieved transmission distance was 10 cm.

8-The technique of WPT using magnetic resonance coupling faces two main challenges. First, it operates in the megahertz range and that poses safety concerns. Second, it requires high inductance to transfer the energy with high efficiency and that necessitates large coils as well as the addition of compensation capacitors resulting increased the system size and weight. Furthermore, other than the contributions of the research group highlighted in above, a scarcity of research on the topic of wireless in-wheel motor has been identified in the literature according to the best of the researcher knowledge.

## 1.8 OBJECTIVES AND CONTRIBUTIONS

The aims of this thesis are.

The first aim presents the design and implementation of a single-input single-output inductive WPT system for EV applications. A small-scale prototype is developed and experimented under different operational conditions. The system performance is discussed in terms of the coefficient of coupling at different transmission distances up to 5 cm.

The Second aim a W-IWM system is designed based on inductive coupling WPT instead of magnetic resonant coupling to explore the effectiveness of the inductive coupling concept in this application for its merits of simplicity, robustness and convenience. The inductive coupling system is based on two planar circular spiral coils resembling the stationary coil (the transmitter to be attached to the vehicle body) and the steering coil (the receiver to be attached to the wheel). A 250 W prototype of the system was built and tested at different transmission distances 7.5, 10 , 12 cm and with different misalignment angles. A simulation model of the system is also developed to confirm the experimental results.

## 1.9 LITERATURE REVIEW

This section presents the related work for this thesis.

[48], U. K. Madawala and D. J. Thrimawithana,2011, this work also suggested a bidirectional IPT system but with focus on EV applications. The system is based on current-source topology and consists of multiple receiving channels. A 1.5 kW prototype of the system was built to transmit power over a 4-cm air gap. The results validated the effectiveness of the system in charging multiple EV.

Attaining high efficiency is one of the critical factors to the success of any WPT system. Thus, a considerable body of research has been carried out on development of high efficiency WPT systems.

[45], H. H. Wu, A. Gilchrist, K. D. Sealy, and D. Bronson, 2012, designed a 5 kW inductive WPT system that achieved a 90 % efficiency over its entire range of loading conditions. To control the charging current of the electric vehicle on-board battery, dual-side control was used in the system to achieve high efficiency at different load and coupling conditions. This system offers higher efficiency at light load 7% and 25% loss reduction over a wider range of loading (175-265) mm.

[57], C. Shuwei, L. Chenglin, and W. Lifang, 2014, discussed a method for vehicle positioning to maintain alignment between the WPT coils. The method uses radio frequency identification to determine the vehicle parking position in real-time and visualize the position data and display it to the driver. The WPT charger will not be initiated until complete alignment is achieved. The method represents a parking-assistant approach, and it was verified with experimental results.

[52], S. Moon, B. C. Kim, S. Y. Cho, C. H. Ahn, and G. W. Moon, 2014, designed an inductive WPT system that utilizes an intermediate coil. The purpose of that additional coil was to enhance the electromagnetic coupling between the transmitter and the receiver by increasing the self-inductance and mutual inductance of the coupling system. Improving the coupling coefficient can increase the transmission efficiency and extend the transmission distance. A prototype of the system was built and optimized to transmit 6.6 kW over 2 cm with 95.57% efficiency.

[46], J. H. Kim *et al.*, 2015, presented a 1 MW inductive WPT system for real-time power supply to an electric vehicle. The system uses a resonant inverter at 60 kHz with a long transmitter that is coupled to 4 receiving coils. The output of each receiving coil is connected to a rectifier that supplies a lumped load. The efficiency of the system was 82.7% at 818 kW and transmission distance of 5 cm. The speed of train is 10Km/H, 128m Transmitter long.

[38], G. Yamamoto, 2015, investigated a model to calculate the transmission efficiency of the I-WPT system presented in [35]–[37]. The findings of the work indicated that the maximum efficiency can be achieved at a certain value of the transmitter voltage and load voltage. The analysis was supported by experimental results.

[35], M. Sato, G. Yamamoto, D. Gunji, T. Imura, and H. Fujimoto, 2016, presented the design and implementation of an experimental setup of a W-IWM system. The work focused on stabilizing the power delivered to the motor under driving and steering conditions. Two control methods were developed to compensate misalignment between the vehicle side coil (The Transmitter) and the in-wheel coil (The Receiver) during wheels steering. The first method is based on a new hysteresis control method to stabilize the voltage of the receiver coil using a hysteresis comparator. The other method is a feedforward controller to control the transmitter coil voltage. The controller estimates the receiver coil output power from the motor speed and uses it in the feedforward control loop. The proposed system and the effectiveness of the control methods used were validated by the experimental results.

[43], M. Suzuki *et al.*, 2017, discussed a low electromagnetic emission series-resonant WPT system for a 44 kW charger used for rapid charging of an electric bus. The system was designed to tolerate sharp misalignments of

up to 10 cm keeping electromagnetic emissions within the limits dictated by the Radio Act. The performance of the developed system was experimentally evaluated at 85 kHz.

[41], V. P. Galigekere et al, 2018, presented a single-stage high-power resonant inductive WPT system for an electric vehicle charging system. The system was designed to transmit 100 kW over a distance of 12.7 cm at a frequency of 22 kHz. The design of the power electronic converters and the coupling coils was optimized and the performance was validated through experimental and simulation results. The wireless charging system achieved 96.9% of efficiency at 50 kW and transmission distance of 12.7 cm.

[44], I. Villar, A. Garcia-Bediaga, U. Iruretagoyena, R. Arregi, and P. Estevez, 2018, a 50 kW inductive WPT system was designed and experimented. The system was based on the conventional inductive category in which the power electronic stage consisted of a frontend three-phase AC-DC rectifier to maintain a constant DC voltage across a DC-link, a DC-DC converter that regulates the transferred current and a high-frequency DC-AC inverter that energizes the transmitter coil. The system functionality was verified through field experimental results. However, the highest transmission efficiency reached was 88 %, which is considered relatively low for today's EV quality standards ( $\pm 1000$  mm) misalignment.

[51], Z. Luo and X. Wei, 2018 analyzed in detail the effectiveness of square and circular planar spiral coils in loosely coupled WPT systems. Analytical models of the two geometries were compared in terms of the self and mutual inductances of the coils by considering the line spacing, coils misalignments and the semi-infinite substrate properties (Fourier Bessel Transfer and Dual Fourier Transfer).

Although inductive WPT systems are widely used for their robustness and simplicity, they can be efficient for short transmission distances because



distance and misalignment affect the efficiency significantly. Therefore, researchers proposed the use of intermediate resonators to increase the transmission distance 600 mm. An intermediate resonator is a coil that receives the transmitted energy from the transmitter and sends it to the receiver coil.

[55], K. A. Kalwar, M. Aamir, and S. Mekhilef, 2018, K. A. Kalwar, M. Aamir, and S. Mekhilef, 2018, designed and optimized an inductive coupling system that tolerates the misalignment between transmitter and receiver coils. The design of the coils enabled the system to achieve acceptable efficiency under different misalignment conditions. Its lowest efficiency was 72% without misaligned when the coils were 40% misaligned. (ICPT) Inductive Coupled Power Transfer 1Kw efficiency 90.5%.

[49], D. H. Tran, V. B. Vu, and W. Choi, 2018, improved the efficiency of a WPT system 66kw prototype, 200mm air gap by adding a pair of intermediate coils with resonant capacitors in order to enhance the effective magnetizing impedance between the source and load-side windings to achieve an efficiency of 97.08% at 3.7 Kw with no ferrites.

Evaluating the efficiency at which power is transferred from the source to the load is another imperative in the WPT design process.

[56], S. Varikkottil and F. D. J. L, 2019, presented a method to tolerate the misalignment by adjusting the operating frequency of the transmitter inverter to achieve optimal mutual inductance and resonance between the coils. The method defines the mutual inductance between the coils in terms of the alignment horizontal and vertical dimensions. Then, the inverter frequency is adjusted accordingly. The proposed method was applied in an experimental 1kW prototype and its effectiveness was verified by experimental results.

[42], J. Pries, V. P. N. Galigekere, O. C. Onar, and G. J. Su, 2019, developed a three-phase inductive WPT system based on bipolar phase windings taking the advantage of rotating magnetic field in achieving the electromagnetic coupling between the transmitter and receiver coils as the three-phase rotating magnetic fields are smoother than the magnetic fields produced by single-phase windings. Besides, three-phase inductive coupling reduces the mass of the ferrite core, filter components requirements, and electromagnetic emissions. A 50 kW experimental prototype was built and tested under aligned and misaligned conditions. The performance was improved in terms of efficiency and power density. However, the efficiency of the proposed design deteriorated in the condition of misalignment due to the interphase mutual inductance. In three-phase configuration, one of the inverter legs that is associated with the weakly-coupled coils pair provides high reactive power reducing the overall transmission efficiency of the system. The coils pair that involves reduced coupling acts more like a single-phase system.

[47], Y.-H. Liao and Y. Lin, 2019, proposed a bidirectional WPT system based on a new 2-switch configuration with dual-side control strategy. Compared to the reviewed topologies, this system is simple to build and control because it consists of two switches only. The system supports bidirectional power flow between the transmitter and receiver ends. Although the system is less complex, it is suitable for only low power applications such as mobile chargers.

[50], D. Ustun, S. Balci, and K. Sabanci, 2020, discussed a novel mathematical approach to evaluate the efficiency of a single phase IWPT system. The derived model was optimized and verified on an experimental system with efficiency 98%.

Design and geometry of the magnetic coupler in WPT system is one of the decisive aspects that influences the quality of mutual inductance between the

receiver and transmitter coils and thus affects the whole system efficiency.

Air gap 200mm prototype build and tested.

[54], S. Aznavi, P. Fajri, and N. Lotfi,2020, misalignment-tolerant coil design techniques, frequency-tuning power electronic topologies, and parking-assistant methods in which the driver is aided by sensors and displays to precisely align the car with the charging pad.

[36] and [37], improved the system of [35] to enable the system to provide bidirectional dynamic WPT between the vehicle and the wheel. This feature allows effective regenerative braking with aid of a Lithium-ion Capacitor (LiC) installed in the wheel-side circuit. This system represents an upgraded version of the system in [35] with improved power density and dynamic performance. The proposed concept was realized and verified experimentally in a real vehicle.

A comparison about the contributions between the latest studies and this study as shown in table.1.2.

Reference	Transmission distance(cm)	Power (kw)	The Weakens of The Paper
[41]	12.7	50	High power transfer
[43]	10	44	High resonant frequency
[48]	4	1.5	Consists of multiple receiving channels

Table 1.2. A comparison about the contributions between the latest studies and this study.

## **1.10 THESIS OUTLINE**

The remaining part of this thesis is structured in four more chapters. Chapter 2 presents a theoretical background about WPT systems and lists the different applications with which WPT can be used.

Chapter 3 discusses the design procedure of the two proposed WPT systems.

Chapter 4 discusses the simulation and experimental results are presented and in.

Chapter 5 concludes the thesis and suggest new paths for further research.

# Chapter Two: Small-Scale WPT System with R-Load

## 2.1 INTRODUCTION

In This chapter the small-scale WPT system was designed. The system contains one-input and one-output, and it is designed for charging an electric vehicle battery. The performance of the small-scale system is analyzed under different operating conditions. The structure and modeling of the different module of the system are also discussed.

## 2.2 SMALL SCALE INDUCTIVE CONFIGURATION

This section demonstrates the configuration of the small-scale inductive WPT and the design of electronic circuits of the transmitter coil, Tx and the receiver coil, Rx especially the inductive coupling circuits. The system is structured in three modules: a power converter, a wireless transmission module, and a compensation network. The power converter functions as an inverter to drive the transmitter coil by converting the DC voltage from the source into an AC voltage at a high frequency corresponding to the transmission frequency. Thus, it determines the amount of power that can be sent to the receiving end. The inverter is implemented with a Class-D inverter topology for its simplicity and high efficiency at high frequencies. The other merit of Class-D is the low voltage across power switches, that is equal to the input DC voltage. Its control can be achieved through PWM and its output power can be controlled in a wide range. The frequency of the PWM control signal is adjusted to the wireless resonant frequency ( $f_{wpt}$ ) for driving the MOSFETs. When the upper MOSFET is turned-on, the current follows from the DC supply to charge the capacitor but only the fundamental component can pass through the circuit. The capacitor is charged up to the magnitude of input DC voltage. In the second

period, the capacitor discharges through the lower MOSFET. This process repeats every cycle, where the upper MOSFET is turned-on from zero to  $(0.5f_{wpt})$  and the lower MOSFET from  $(0.5f_{wpt})$  to  $(1f_{wpt})$ . Compensation is needed on the receive end as well for the same purpose. Therefore, a parallel capacitor is also used at the terminals of the receiving coil to improve the compensation efficiency. The high frequency power received at receiver is fed to a rectifying circuit to convert it to DC power to charge the vehicle battery. Since the main purpose of this work is to shed light on the wireless transmission module, the rectifier circuit was basically implemented using a single diode for charging purposes.

The experimental setup of the small-scale system consists of three parts: (i) the transmitter side; (ii) the inductive coupling resonant circuit and (iii) the receiving side. In the transmitter side, a high-frequency inverter for converting the DC voltage from the source into an AC voltage is designed to generate a sinusoidal waveform. Therefore, the maximum amount of power that can be transfer to the load should be calculated to specify the rated of the power MOSFETs. It is worth to know that the type of the inverter is Class-D due to its features, which are the structure simplicity and the high efficiency at high frequencies. The high-frequency inverter is connected to the inductive coupling circuit, which is composed of two tightly-wound coils aligned electromagnetically. The receiver and transmitter coils are made with planner spiral geometry for low self-inductance and improved efficiency. For the same purpose, a compensation circuit is needed on the Rx side. Therefore, a parallel capacitor is also used at the terminals of the Rx coil to improve the compensation efficiency. The high-frequency power at Rx is fed to a half-wave diode rectifier to generate DC power for charging the battery of the EV. Figs 2.1-2.5 show the schematic and real circuits of the small-scale WPT prototype at Tx and Rx sides.

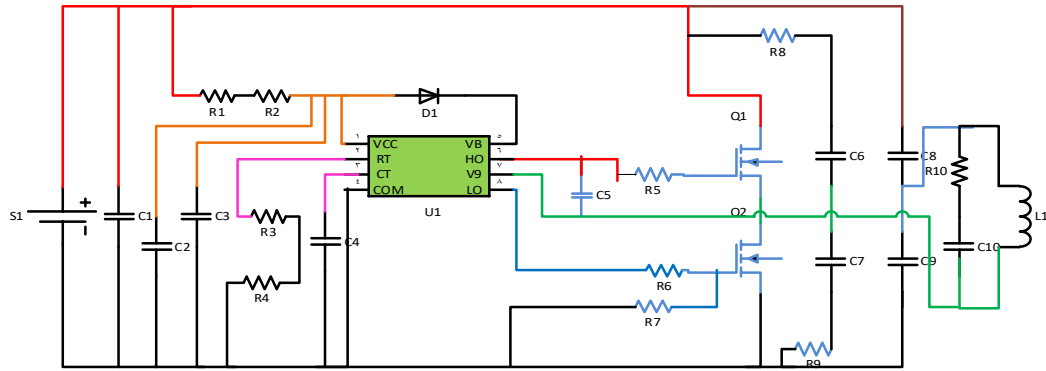


Fig. 2.1. Schematic circuit of the small-scale WPT system, the Tx side.

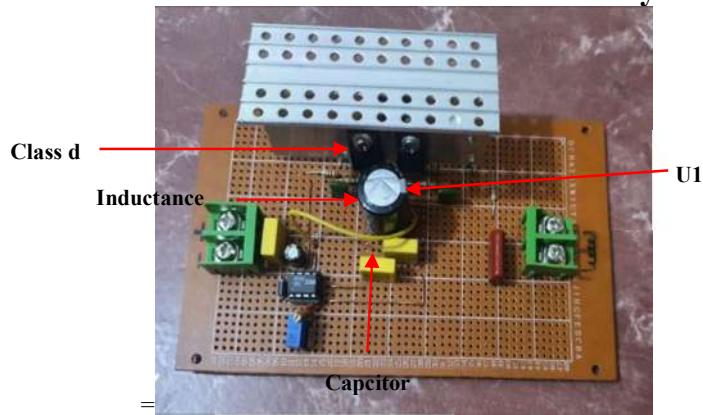


Fig. 2.2. Experimental circuit of the inductive WPT system at the Tx side.

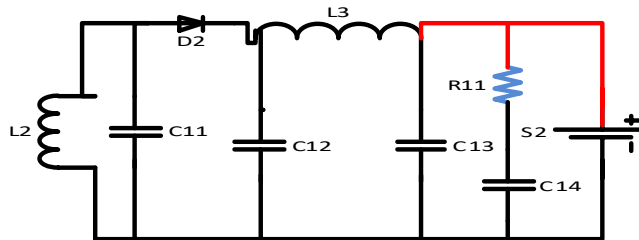
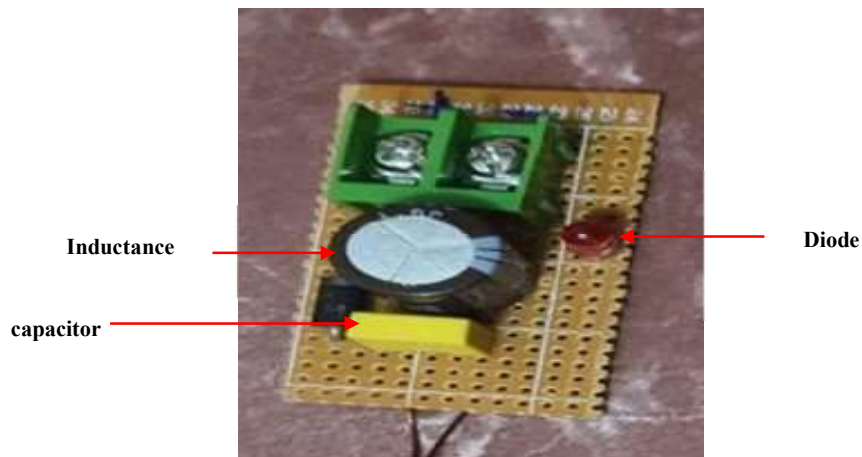
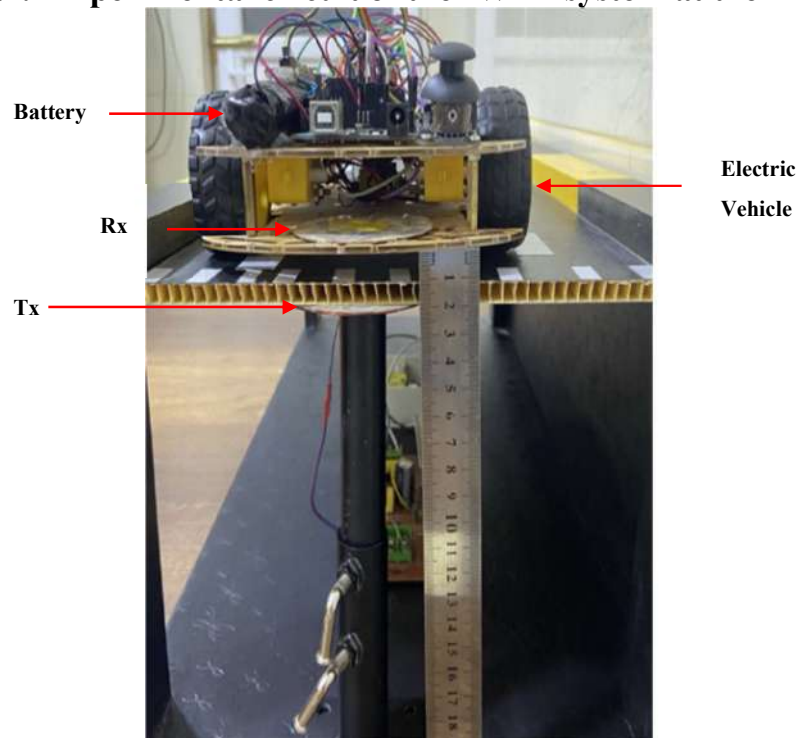


Fig. 2.3. Schematic circuit of the IWPT system at the Rx side.



**Fig. 2.4.** Experimental circuit of the IWPT system at the Rx side.



**Fig. 2.5.** The implemented static charging WPT prototype.

### **2.3 CALCULATIONS OF SELF-INDUCTANCE, MUTUAL INDUCTANCE, COEFFICIENT OF COUPLING, AND RESONANCE-CAPACITANCE PARAMETERS**

One of the key aspects to keep in mind when designing the IWPT coils is to achieve a high coupling coefficient between the receiver and the transmitter. The coupling coefficient can be improved by reducing the self-inductance of the coils; however, it is still required to keep a sufficient



mutual inductance between them. In tightly-wound coils, the self-inductance can be decreased by increasing the distance between the two sides of the coil, i.e., increasing the coil pitch. Reducing the coil pitch will also downgrade the mutual inductance between the two coils but to a smaller extent compared to the extent to which the self-inductance is reduced. The challenge to estimate the optimal pitch is how to achieve the highest coupling coefficient. For circular type, the main empirical equations for designing the coupling coils are given below, which are based on modified Wheelers' formulae [58], where the result of Eq. (2.1) in ( $\mu\text{H}$ ):

$$L = \frac{N^2 a^2}{(30 a - 11 D_{in})} \quad (2.1)$$

$$a = \frac{D_{in} + N*(W+s)}{2} \quad (2.2)$$

The parameters in the above equations are defined as follows:  $D_{in}$  is the inner diameter in inches;  $s$  is the distance between turns in inches;  $w$  is the wire diameter in inches;  $N$  is the number of turns. In this thesis, the self-inductance of the Tx and Rx coils are the same and equal, the mutual inductance is decreased by decreasing the coefficient of coupling as shown in Eq. (2.3).

$$M = k L \quad (2.3)$$

It is worth noting that the wireless resonant frequency,  $f_{wpt}$ , is estimated by varying different parameters affecting the gain of voltage produced within the coils. Parallel resonance or near-to-resonance circuits can be utilized to decrease the power losses. The use of the two types in parallel makes the inductor feed the capacitor, and vice versa, maintaining the same resonant current in the circuit, and converting all the current into useful energy. At  $f_{wpt}$ , the magnitude of inductive reactance and the capacitive reactance are equal as illustrated in Eq. 2.4.

$$f_{wpt} = \frac{1}{2\pi\sqrt{LC}} \quad (2.4)$$

It is based on self-oscillating, which includes a single resistor and a timing capacitor as shown in Fig. 2.4. This circuit exhibits 50% duty cycle and fixed frequency, which is determined by Eq. 2.5 [25]. It is clear that 75-ohm accounts for resistance of the oscillator output pin, RT.

$$f = \frac{1}{1.38 (R_1 + 75\Omega)C_1} \quad (2.5)$$

In this work, the wireless resonance frequency  $f_{\text{wpt}}$  is determined using Eq. (2.4), which is about 95.113 kHz, where  $R_1$  and  $C_1$  are chosen respectively about 12.4 k $\Omega$  and 611 nF. The design parameters of the IWPT prototype are listed as follows:  $D_{\text{out}} = 2.560$  inches;  $D_{\text{in}} = 1.457$  inches;  $W = 0.024$  inches;  $s = 0.029$  inches;  $N = 20$  turns.

The design results are found as follows: the self-inductance,  $L$  is about 28  $\mu\text{H}$  and the wireless resonant capacitance,  $C$  is about 100 nf.

## 2.4 ILLUSTRATION OF THE DIFFERENCE BETWEEN SPIRAL AND RECTANGULAR WIRELESS COIL SHAPES

From the discussion in the previous section and section 1.4, it can be said that the power performance of the inductive coupling link is assessed in terms of its efficiency. The transmission efficiency depends on two main factors that are the quality factor of the coupling coils and the coupling coefficient between them. These parameters are electrical qualities for the coils. However, there are other non-electrical parameters that affect the power transmission process. The geometry and mechanical design of the coupling coils are key factors in the effectiveness of the inductive link because they dictate the pattern and distribution of the induced magnetic field. The efficiency of the wireless transmission will be affected. In other words, the transmission efficiency can be maximized if the coils are geometrically formed and positioned to achieve optimal values of coils quality factors and coupling coefficient for the targeted application and amount of power transmitted. The geometrical design and position of the coils mainly depend on the characteristics of the coil conductor and the way

it is wound because that will affect the quality and distribution of the electromagnetic field and its associated induced electromagnetic force. [58]

WPT coils can be classified based on different aspects such as the type of the coil conductor, the winding pattern, the winding shape and the use of coil core. When it comes to the type of the coil conductor, there are different conductors such as solid (magnet) wire, printed circuit, litz wire, and hollow copper conductor. The importance of conductor type consideration in coil design comes from the skin effect and proximity effect as well as the eddy current phenomenon which affect the pattern and distribution of the electromagnetic field. Depending on the pattern of winding the coil, coils can be either planar spiral or solenoidal with former is the most used in WPT applications. Besides, according to [59], a coreless spiral coil demonstrated a better performance and less internal resistance compared to a rounded winding of coil. These two categories can be further classified according to the shape of the coil that can be circular, rectangular or hexagonal [60], [61].

In EV applications, circular and rectangular planar coils are commonly used [62]. In terms of the polarity of the coil flux density, circular coils can be either non-polarized or unipolar. One of the advantages of circular coils is that they produce uniform flux distribution due to the symmetry in the coil cross section. With uniform flux distribution the coupling coefficient is also uniform resulting in equal power transmission in all directions. Regard the quality factor formula,  $Q = \frac{\omega L}{R}$ , it is obvious that the quality factor can be increase by increasing either the operating frequency or the coil self-inductance, or by decreasing the internal resistance of the coil. Circular design allows for reducing the coil resistance by reducing the coil pitch and in the meantime maintaining high number of turns. The other advantage of circular coils is that they are more tolerant to misalignment. In [63], a technique was discussed to improve misalignment tolerance of circular coils using asymmetrical circular transmitter and

receiver coils and unequal outer diameter of each. On the other hand, rectangular coils are polarized and offer a better magnetic field path compared circular counterpart. As a result, this configuration of planar coils achieves high coupling coefficient compared to other coil shapes. [51] and [59] showed that the power transfer capability can be improved using rectangular or square coils compared to circular coils. Furthermore, rectangular coils are also tolerant to misalignment except in horizontal direction misalignment. Yet, rectangular coils suffer from high leakage flux especially through the lower section of the coil and; therefore, maintaining high transmission efficiency can be challenging. Additionally, for the same coil cross sectional area, rectangular coils require more conductor amount and more space than circular coils [62]. From the comparison above, it can be concluded that circular planar coils can be a feasible option for the studied application and it has been used in this thesis.

## 2.5 MODELLING AND ANALYSIS OF CLASS-D INVERTER

In this work, a class D inverter is used for its high efficiency and simplicity for the sought application. The conventional circuit of a class D inverter with an inductive load is shown in Fig. 2.6. The two switching devices are connected across the DC voltage source. The DC voltage source can be represented by two separate identical sources connected in series across the switching devices. as shown in Fig 2.6a, when a single DC sources is used, two electrolytic as shown Fig 2.6b capacitors are used to achieve two individual voltage sources. The switches are provided with anti-parallel diodes for reverse current of inductive loads. Theoretically, each switch conducts for a half of the switching cycle to achieve alternating voltage at the output. However, practically there must be a dead time between the positive and negative cycles to avoid the shoot through across the switches. After being in steady state operation for some time, the inverter operation can be analyzed as follows. At the beginning of the switching cycle,  $t=0$ , the

upper switch S1 is turned on and the lower switch S2, which was conducting current prior to this switching instance, is turned off. It is worth mentioning here that the class D inverter works at a switching frequency beyond the resonant frequency. After S2 is on the load current continues in the negative direction and flows through the anti-parallel diode D1 before it falls to zero, reverses direction and starts flowing through S1 at  $t=t_1$ . After that, D1 is reversed biased because the current builds up through the loop (S1-load-source V1), and reaches its maximum value at the end of the first half cycle, i.e., at  $t=DT$ , where D is the duty cycle of the switching signal. Next and over the second half of the switching signal, after  $t=DT$ , S1 is switched off and S2 is switched on. Similarly, before S2 starts conducting, the load current continues to flow in the positive direction through the anti-parallel diode D2. However, D2 current will soon diminish and fall to zero because it flows against the direction of the lower voltage source, V2. Then, the current will build up in the negative direction to reach its maximum negative value at the end of the switching cycle resulting in a symmetric current waveform with zero DC value. The different operation periods of the inverter are shown in Fig. 2.7. [61].

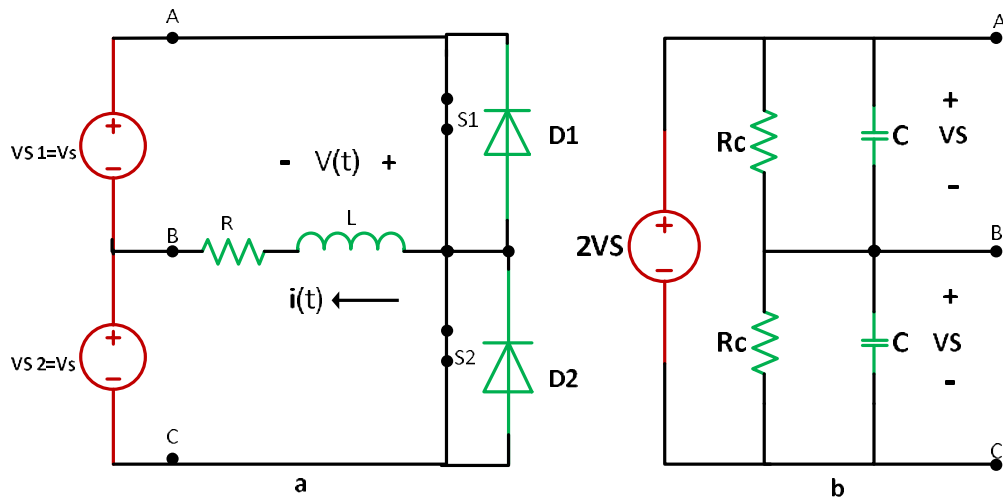


**Fig. 2.6.** Class D inverter circuit diagram with (a) two identical voltage sources and (b) a single voltage source

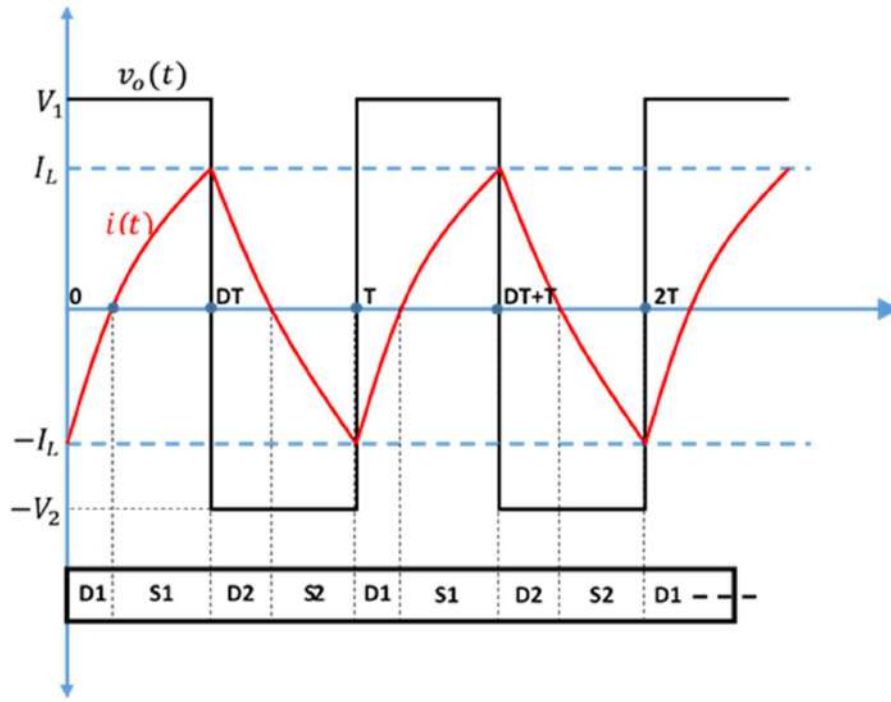


**Fig. 2.7. Voltage and current waveforms of Class D inverter at its different operation stages.**

The current waveform can be mathematically represented by applying KVL around the upper RL loop as follows: [62]

$$V_1 - i(t)R - L \frac{di(t)}{dt} = 0 \quad (2.8)$$

The equation above represents a linear differential equation with a standard solution that can be written as:

$$i(t) = \frac{V_1}{R} + B e^{-\frac{t}{\tau}} \quad (2.9)$$

where  $B$  is a constant and  $\tau = \frac{L}{R}$  is the time constant of the RL circuit.

The constant  $B$  can be evaluated using the initial conditions of the circuit:  $i(0) = I_L$ , where  $I_L$  is the maximum value of the inductor current. Thus, the current equation over the first half of the switching cycle can be given as

$$i(t) = \frac{V_1}{R} \left(1 - e^{-\frac{t}{\tau}}\right) - I_L e^{-\frac{t}{\tau}} \quad (2.10)$$

The maximum value of the inductor current  $I_L$  is reached at the end of the first half cycle. It can be found by substituting the time instant  $t = DT$  in the above equation as follows:

$$I_L = \frac{V_1}{R} \left( \frac{1 - e^{-\frac{DT}{\tau}}}{1 + e^{-\frac{DT}{\tau}}} \right) \quad (2.11)$$

Therefore, the current equation for the time interval from  $t=0$  to  $t=DT$  is given as:

$$i(t) = \frac{V_1}{R} \left( 1 - e^{-\frac{t}{\tau}} \right) - \frac{V_1}{R} \left( \frac{1 - e^{-\frac{DT}{\tau}}}{1 + e^{-\frac{DT}{\tau}}} \right) e^{-\frac{t}{\tau}} \quad (2.12)$$

By the virtue of symmetry, the current equation over the second half of the switching cycle from  $t=DT$  to  $t=T$  can be basically found by negating the above equation as follows [63]:

$$i(t) = -\frac{V_1}{R} \left( 1 - e^{-\frac{t}{\tau}} \right) + \frac{V_1}{R} \left( \frac{1 - e^{-\frac{DT}{\tau}}}{1 + e^{-\frac{DT}{\tau}}} \right) e^{-\frac{t}{\tau}} \quad (2.13)$$

## Chapter Three: Design the Large-Scale WPT Prototype Connecting with an AC Motor

### 3.1 LARGE-SCALE IN-WHEEL WPT SYSTEM

This WPT system is proposed for the purpose of transmitting power wirelessly from the body of the electric vehicle to the wheel(s) motor. The system is also structured in three modules: the power electronic module, the coupling module and the wheel motor module which includes the motor and its conditioning circuit as shown in Fig. 3.1.

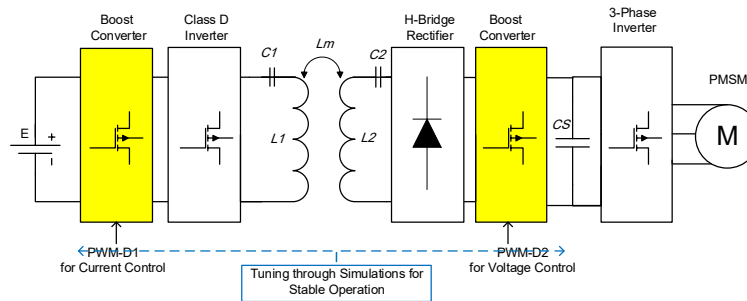


**Fig. 3.1. The structure of the proposed system showing its three modules.**

The power electronic module includes the energy source and the power electronic converter that conditions the power before it is transmitted wirelessly by the coupling module. The coupling module refers to the transmitter and receiver coils along with their compensation components. The motor module represents the motor and its drive circuit. In the following sections, each module will be discussed in details.

### 3.2 DESIGN OF THE PROPOSED WPT SYSTEM

The proposed design in this research is shown in the Fig. 3.2 which includes a DC source, an inverter (DC-AC), a transmitting circuit, receiving



circuit, a power and a rectifier (AC-DC), and a brushless DC motor (BLDCM) load on the wheel.

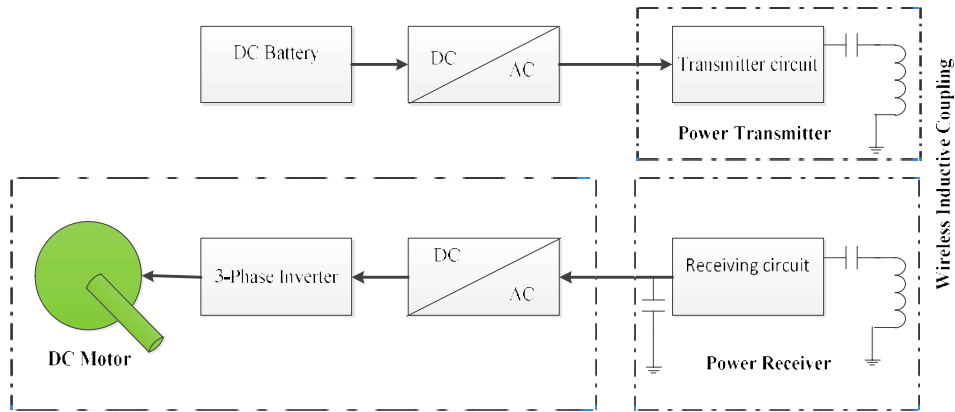


**Fig. 3.2. The proposed wireless drive system for an electric vehicle System component.**

The specifications of the system components are summarized in the Table 3.1.

**Table 3.1. System Details Components.**

component	Technical Specification	
BLDCM	Parameters	Details
	Voltage	48 volts
	Rated Current	3.5 Amp
	Rated Speed	800 RPM
	Rated Torque	1.9 N.m
	Power	250 W
Controller (PWM)	Details	
	Working voltage: DC 9-60V	
	Maximum current: 20A	
	Continuous current: 18A	
	Control frequency: 25KHZ	
Battery	Details	

	E-Bike Battery, 48V 20AH Lithium Li-ion Battery with 4A Charger, for 1000W /1500W E-Bike Kit, Electric
DC-DC	Details
Convert	Boost DC Step Up (9V-80V) 600W Converter

### 3.2.1 The Power Electronic Module

The main function of this module is to provide AC power at a high-frequency voltage to be applied at the terminals of the transmitting coil. High frequency current is necessary to induce an electromagnetic field at the same high frequency and thus achieve high coupling coefficient. Converting the 50 Hz AC voltage from the mains into a high-frequency voltage involves two steps. The first step is to convert the 50 Hz AC voltage into DC voltage at a certain level by a rectifier. This DC voltage is then inverted into AC voltage at the desired frequency by an inverter.

There are different inverter topologies that can be used to drive the transmission coil of a WPT system, and the selection of the suitable topology depends on the application and its operating conditions such as the load power and system frequency. For loads of less than 250 W, conventional inverter topologies such as full-bridge inverters are used for their reliability, high-efficiency and cost effectiveness. These inverters can be realized with switching devices that can achieve switching frequency in the upper hundreds of kilohertz. Increasing the switching frequency improves the power density of the converter as well as the entire WPT system because operating at high frequencies will reduce the footprint of the magnetic components used in the system including the transmission coil. However, driving the power electronic switches at high frequencies will compromise the inverter's efficiency because the switching (turn-on and turn-off) losses increase with frequency. Therefore, working in the megahertz range imposes

design restrictions on the WPT power level [58]. This fact justifies that megahertz frequencies are used in low-power small-size WPT applications such as in portable electronics and medical devices where the load power does not exceed the 1kW level. In such applications, a different set of inverter topologies is typically used that are defined as inverter classes. The first group of inverter classes is called the classical conduction angle amplifiers, aka linear amplifiers. and it includes classes A, B, AB and C. Because of the continuous current conduction, these inverters suffer from low efficiency which can reach its best at 80% with class C inverters making them unsuitable for power applications. The second group of inverter classes used in megahertz applications is defined as the switching (switch mode) inverters which includes class D and class E inverters in which the transistor(s) is continuously turning on and off applying an alternating train of voltage pulses at the inverter output. Thus, class D and class E inverters are characterized by high efficiency which can ideally reach 100% when operated with soft switching schemes [59]. High efficiency feature in addition to circuit simplicity make these two topologies the most preferable choice for low-power high-frequency WPT applications.

Compared to Class D, class E inverter is less complicated because it has one switch instead of two as in class D and that eliminates the need for complemented switching signals with dead-band. Besides, at the same input voltage, class E inverters offer higher power handling capability. However, class E inverter suffers from higher voltage stress on its switch. According to [60], the switch voltage stress in a class E inverter is 3.56 times the source voltage. High voltage stress on the switching device imposes design limitations on the inverter especially in high-input voltage applications. The second disadvantage of the class E inverter is that it resembles a resonant inverter because it contains a series LC resonator in its typical configuration. As a result, it can be designed to operate under certain resonant frequency and load conditions. In other words, a class E inverter cannot be optimized

to operate efficiently under varying load and frequency. EV charging is one of such applications where dynamic load and coils misalignment are expected. Therefore, class E inverters are not an ideal choice for wireless EV charging. Class D inverters on the other hand offer better performance traits that alleviate these shortcomings. The switch voltage stress in a class D inverter is basically the supply voltage and that is one of its advantages that make class D inverters used in high voltage applications. Furthermore, class D inverters can be operated at a fixed switching frequency above the resonant frequency and controlled to cover a wide regulation range of their load[62].

It is worth mentioning here that, besides the two switching inverter, there are different other topologies of switching inverters. According to the nature of their input voltage, switching inverters can be either one-stage or two-stage. In one-stage DC-AC inverters the input DC voltage is directly converted to AC. One-stage inverters are used when there is a stable DC voltage source available such as from a battery or a fuel cell. On the other hand, two-stage AC-AC inverters are more commonly used especially in high-power applications. In two-stage inverters, a front-end AC-DC rectifier is used to supply the inverter input with a stable DC voltage across a DC link capacitor. [63]

### **3.2.2 Inductive link design**

In designing any WPT system, it is significant to analyze and optimize the geometrical dimensions of the coils of the inductive link. Before doing so, let's first understand the physical principle of inductive WPT. According to Faraday's Law, a variable current-carrying conductor generates a variable magnetic field that can be translated into a potential difference between the terminals of the conductor. The strength of the generated magnetic field and the resulting potential difference are intensified if the excited conductor is wound as a coil with multiple turns. The more turns the coil contains the stronger the potential difference becomes. The current intensity also

proportionally contributes to the increase in the value of the potential difference. These parameters are governed by the formula of the coil self-inductance  $L$  which can be described as  $v = iL2\pi f$ , where  $f$  is the frequency at which the supply current changes. The effect of the generated changing electromagnetic field is not limited to the coil itself but also goes beyond that to affect any other coils exposed to the magnetic field. In other words, if a second coil is placed in the proximity of the energized coil, potential difference will also be generated across the second coil in a physical effect that is called mutual inductance which is described by a constant called the mutual inductance (M). Similarly, the induced potential difference across the second coil can be expressed as  $v = iM2\pi f$ . This concept represents the basis of transferring power wirelessly through an inductive link coils separated with an air gap. The existence of the air gap degrades the mutual coupling between the coils and consequently affects the efficiency of power transmission. Thus, there are different coil structures that are designed with one goal in mind that is to improve the mutual coupling and efficiency of the inductive link. The physical structure, geometry and position of the coils play important roles in deciding the individual coil self-inductance, mutual inductance, parasitic equivalent resistance and transmission efficiency. From section 2.4, one of the widely used coil structures in EV applications is the circular spiral configuration for its merits of desirable power transmission performance and tolerance to misalignment [63].

Assuming a circular spiral coil with  $N$  number of turns and  $R$  outer radius, the coupling coefficient between two coils (a transmitter and a receiver) can be given as follows [61].

$$k = \frac{\pi\mu_0(N_1N_2)^{\frac{1}{6}}(2dt - (N_1-1)d)(2dr - (N_2-1)d)}{3.44*10^{-5}h \sqrt{a_1(N_1) \ln \frac{8a_1(N_1)}{c(N_1)} a_2(N_2) \ln \frac{8a_2(N_2)}{c(N_2)}}} \quad (3.1)$$

where  $\mu_0$ : is the vacuum permeability;

$N_1$ : number of turns of Transmitter coil(Turns),

$N_2$ : number of turns of Receiver coil(Turns),

$D_o$ : outer diameter of Transmitter coil(mm),

$D_{in}$ : outer diameter of Receiver coil(mm),

$d$ : Diameter of wire coil(mm);

The other parameters in the equation are defined as follows,

$$a_1(N_1) = R_1 - \frac{(N_1-1)d}{2} \quad (3.2)$$

$$a_2(N_2) = R_2 - \frac{(N_2-1)d}{2} \quad (3.3)$$

$$c(N_1) = N_1 d \quad (3.4)$$

$$c(N_2) = N_2 d \quad (3.5)$$

$a_1(N_1)$ : The average radius of the transmitting coil;

$a_2(N_2)$ : The average radius of the receiver coil;

$c(N_1)$ : The width of the transmitting coil;

$c(N_2)$ : The width of the receiver coil;

$$M = K\sqrt{L_1 L_2} \quad 0 \leq K \leq 1 \quad (3.6)$$

$$W_1 = \frac{1}{\sqrt{L_1 C_1}} \quad (3.7)$$

$$W_2 = \frac{1}{\sqrt{L_2 C_2}} \quad (3.8)$$

$$R_1 = R_s + R_{1P} \quad (3.9)$$

$$R_2 = R_s + R_{2P} \quad (3.10)$$

Reflected impedance  $Z_r$

$$Z_r = \frac{W^2 M^2}{R_l + R_{2P} + j W L_2 + \frac{1}{j W C_2}} \quad (3.11)$$

$$Q_1 = \frac{W L_1}{R_s + R_{1P}} \quad (3.12)$$

$$Q_2 = \frac{W L_2}{R_S + R_{2P}} \quad (3.13)$$

$$Z_r = \frac{W L_1 k^2}{1/Q_2 + j(1 - W_2^2/W_2)} \quad (3.14)$$

Where: -

$M$  is the mutual inductance between the primary and secondary coils

$k$  is the coupling coefficient,

$W_1$  is Resonance frequencies of the primary,

$W_2$  is Resonance frequencies of the secondary,

$Z_r$  is Reflected impedance,

$L_1, L_2$ , are primary and secondary inductance,

$C_1, C_2$  are primary and secondary capacitance.

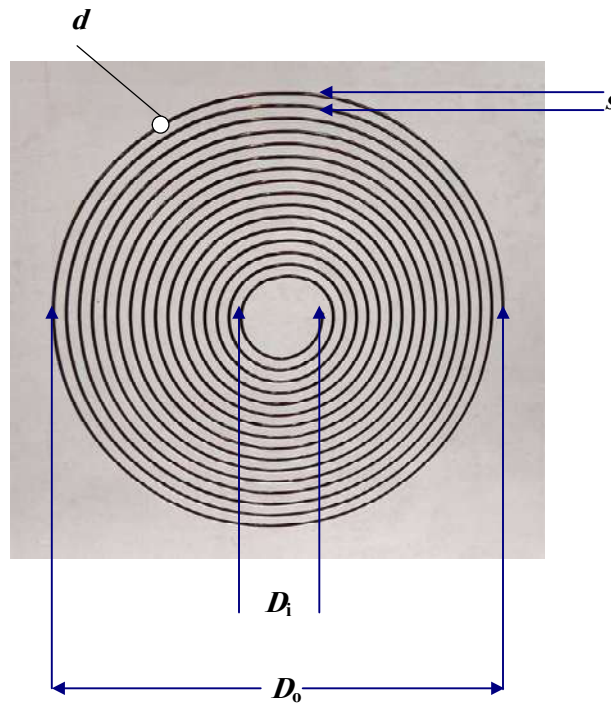


**Fig. 3.3. Real printed wireless coil by CNC machine.**

The coils were designed using the online tools Coil64 [64] and Pronine Electronics Design [65] which are open source online freeware for coil inductance calculation. In Coil64, the coil self-inductance is calculated using *Harold A. Wheeler* formula as follows [62],

$$L(\mu H) = r^2 * \frac{N^2}{8*r+11*w} \tag{3.15}$$

where, L = Inductance μH, r = average winding radius in inches, w = width of winding (in inches), N = number of turns.

From the analysis above, the flat spiral coils were built with outer diameter of 260 mm and inner diameter of 50 mm, and wound with 16 turns spaced by 5 mm gaps. To achieve these diameters, a 9-meter piece of copper wire of a circular cross section with 2 mm diameter was used to form the coils. The wire of each coil was placed in circular grooves engraved in a square MDF plate for physical support and protection. Fig. 3.3 shows the practical spiral coils. The coils design parameters are listed in Table 3.2.

**Table 3.2. Coils design parameters.**

Design Parameters	Ready Design[66]	The Proposed Design
$N_1$ (Turns)	10	16
$N_2$ (Turns)	11	16
$R_1$ (mm)	310	260
$R_2$ (mm)	240	260
$d$ (mm)	1.8	2

**3.2.3 Estimation of the Coupling Coefficient**

Coupling coefficient should be properly estimated from other system parameters such as voltage and current of the transmitting coil or the receiving coil or both [66]. In this section, a method of estimating the coupling coefficient in terms of the transmitter’s voltage, current and phase is presented [66]. First, the equivalent circuit of the coupling module that is



shown in Fig. 3.3 is reconfigured into its T-type form as shown in Fig. 3.4. In this equivalent circuit, coils capacitances were introduced as  $C_T$  and  $C_R$ . The internal impedance of the transmitter voltage source is also incorporated in the circuit as  $Z_S$ . Looking into the circuit through the input terminal, the circuit input impedance  $Z_{in}$  can be expressed as follows: [64]

$$Z_{in} = \frac{V_T}{I_T} (\cos \phi + j \sin \phi) \quad (3.16)$$

Thus, the real and imaginary components of  $Z_{in}$  can be written as follows,

$$Re[Z_{in}] = R_T + \frac{(\omega M)^2 (R_L + R_R)}{(R_L + R_R)^2 + [\omega L_R - (1/\omega C_R)]^2} \quad (3.17)$$

$$Im[Z_{in}] = [\omega L_T - (1/\omega C_T)] - \frac{(\omega M)^2 [\omega L_R - (1/\omega C_R)]}{(R_L + R_R)^2 + [\omega L_R - (1/\omega C_R)]^2} \quad (3.18)$$

Inspecting the imaginary component in (3.18), it can be noticed that it is challenging to measure the imaginary part due to it is highly frequency dependent. Therefore, mutual inductance estimation can be obtained by measuring the real component only as follows,

$$M = \frac{1}{\omega} \sqrt{\frac{[Re[Z_{in}] - R_T][(R_L + R_R)^2 + [\omega L_R - (1/\omega C_R)]^2]}{R_L + R_R}} \quad (3.19)$$

The coupling coefficient can be calculated from the following formula,

$$K = \frac{M}{\sqrt{L_T L_R}} \quad (3.20)$$

The coupling coefficient depends on the distance between the coupling coils. Therefore, it is estimated at different distances to obtain a model that relates  $K$  to the transmission distance,  $d$ .

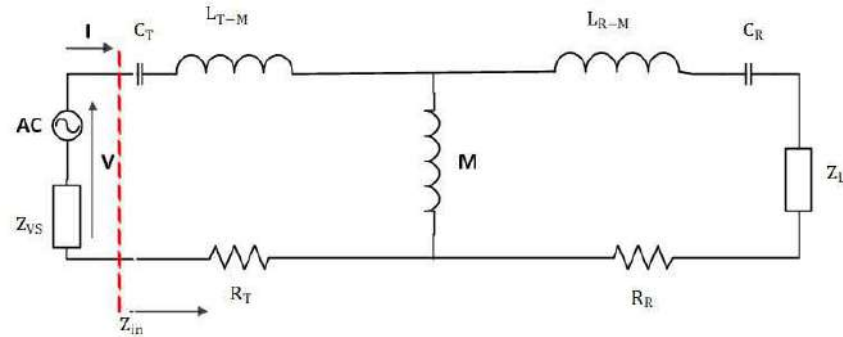


**Fig. 3.4. T-type equivalent circuit of the coupling module.**

### 3.3 DESIGN AND PROCEDURE PROPOSED SYSTEM

The prototype of the wireless power system is designed by selecting the appropriate conductor size that achieves maximum power transfer to the load (motor drive system). The conductor size is chosen according to American Wire Gage (AWG) of 2 mm. The self-inductance is calculated as in Equation 3.15 which contains the input geometry of wireless coils using (The freeware coil inductance calculator coil64) to estimate the approximate number of turns ( $N$ ), outer diameter ( $D_o$ ) and length of wire ( $L_{th}$ ), and then it is determined Wireless resonance frequency is tested from the simulation at full load with long air gap distance without controllers, estimate voltage, current transmitter and voltage, current recover. Then the comparison between the highest and lowest voltage and capacity of the motor, which is compatible with the controller of the motor, which is not less than 48 V and not more than 50 V and not less than 80 W and not more than 295 W. Equation 3.19 is used to estimate the mutual inductance. Test simulations are run with D1 and D2 controllers at varied distances (7.5 cm, 10 cm, and 12.5 cm) with no load, half load, and full load. Through the above values and equations, the simulation system was built according to the parameters of the

complete transmitter and receiver circuit of the Large Scale proposed system shown in Table 3.3, and the flow chart scenario in Fig. 3.5.

**Table 3.3. Parameters the complete transmitter and receiver circuit of the proposed system.**

Parameters	value	unit	Parameters	value	unit
<i>S1</i> =Battery	90-120	V	<i>C6, C7</i>	100	nf
<i>Q1, Q2</i>	IRFP460	----	<i>C9</i>	4.7	nf
<i>U1</i>	IR2153	----	<i>C8, C10, C5</i>	100	nf
<i>R1</i>	3.3	K $\Omega$	<i>L1</i>	36	$\mu$ h
<i>R2</i>	2.2	K $\Omega$	<i>L2</i>	36	$\mu$ h
<i>R3</i>	6.8	K $\Omega$	<i>L3</i>	1	$\mu$ h
<i>R4, R6</i>	15	$\Omega$	<i>C11</i>	168	nf
<i>R5</i>	10	K $\Omega$	<i>D2</i>	HF A15PB60	----
<i>R7, R8</i>	100	$\Omega$	<i>R11</i>	120	K $\Omega$
<i>R9</i>	4.7	$\Omega$	<i>C12</i>	470	$\mu$ f
<i>C1</i>	470	$\mu$ F	<i>C13</i>	10	$\mu$ f
<i>C2</i>	1	nf	<i>C14</i>	1	nf
<i>C3, C4</i>	2.2	nf	<i>S1: DC OUTPUT</i>	(100-400)	Volt

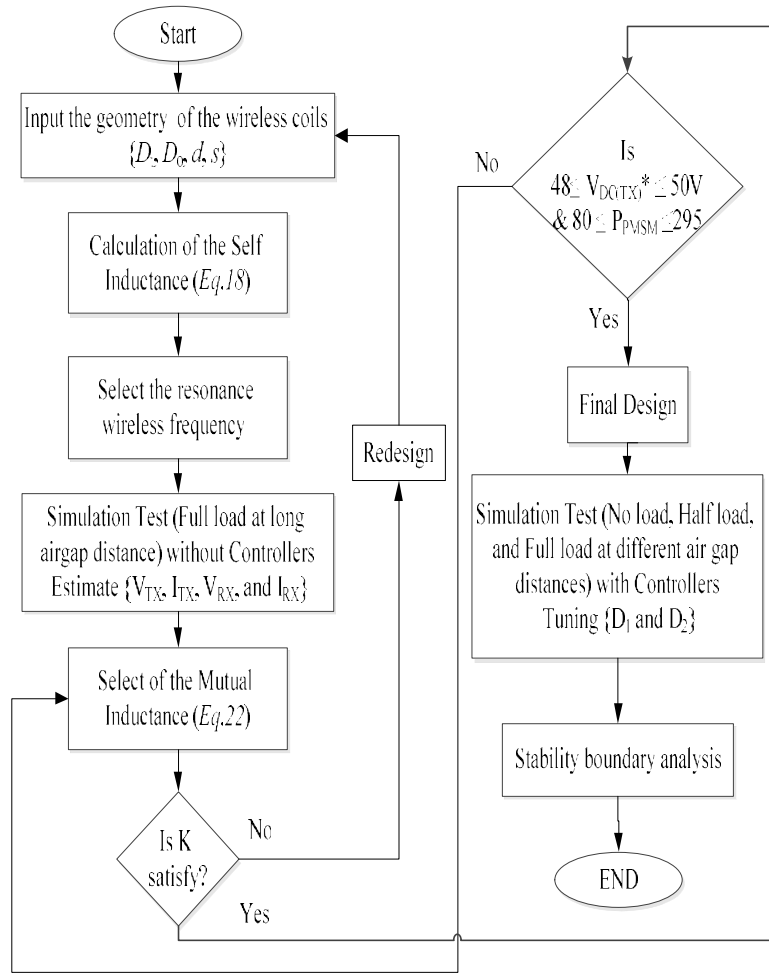


**Fig. 3.5. The Flow Chart the Proposed design procedure and stability validation**

### 3.4 MODELLING AND ANALYSIS OF A BRUSHLESS DC (BLDC) MOTOR

Brushless DC motors (BLDCM) can be found in a wide range of applications where small horsepower and variable speed are required such as in household appliances, industrial processes, automation and aviation systems. The popularity of BLDCM comes from their advantages of reliability, efficiency, compactness, and smooth operation. They also exceed in EV applications for their traction characteristics and high starting torque. For modeling purposes, the BLDCM can be treated as a machine with three stator windings and a permanent magnet rotor modeled in the  $d - q$  frame as follows, [ ]

$$V_d = R \cdot i_d + \frac{d}{dt} L_d \cdot i_d - \omega_r \cdot L_q \cdot i_q \text{ [v]} \quad (3.21)$$

$$V_q = R \cdot i_q + \frac{d}{dt} L_q \cdot i_q + \omega_r \cdot L_d \cdot i_d + \omega_r \cdot \lambda_{pm} \text{ [v]} \quad (3.22)$$

The electromagnetic torque  $T_e$  can be written as:

$$T_e = \frac{p_m}{\omega_m} \text{ [Nm]} \quad (3.23)$$

$$\omega_m = \omega_r \frac{2}{n} \left[ \frac{\text{rad}}{\text{s}} \right] \quad (3.24)$$

$$p_{em} = \frac{3}{2} (\omega_r \cdot \lambda_d \cdot i_q - \omega_r \cdot \lambda_q \cdot i_d) \text{ [W]} \quad (3.25)$$

where,

$V_d$  and  $V_q$  are the voltage equations are represented in the rotating dq reference frame.

$i_d$  and  $i_q$  are the currents are represented in the rotating dq reference frame.

$L_d$  and  $L_q$  the inductances are represented in the rotating dq reference frame.

$\omega_r$  is the electrical angular speed.

$\omega_m$  is the mechanical angular speed.

$T_e$  The electromagnetic torque

$p_m$  mechanical power.

$n$  the number of poles.

A photo of the experimental BLDCM and its drive circuit is shown in Fig. 3.6.



**Fig. 3.6. The practical BLDCM with its drive circuit**

### **3.5 EXPERIMENTAL IMPLEMENTATION OF THE LARGE-SCALE SYSTEM**

The construction of the power electronic circuit is described first. Next, the design parameters and the measurements of the inductive parameters of the spiral coils are presented. After that, the functionality of the complete system is tested under different operating conditions.

As it was mentioned earlier, the power electronic module consists of the DC power supply and the high-frequency inverter. The DC power supply used in the system is a 90-120Volt, 10Amper battery. The Class-D inverter was built using two IRFP460 power MOSFETs from Vishay Siliconix in TO-247 package. These devices were selected for their high switching frequency and simple drive requirements. The drive circuit was designed using a self-oscillating half bridge derive IR2153 from Internal Rectifier to drive the MOSFETs at 65 kHz. The complete circuit diagram of the system with the values of all auxiliary components such as the compensation capacitors and bias resistors are shown in Fig. 3.7.

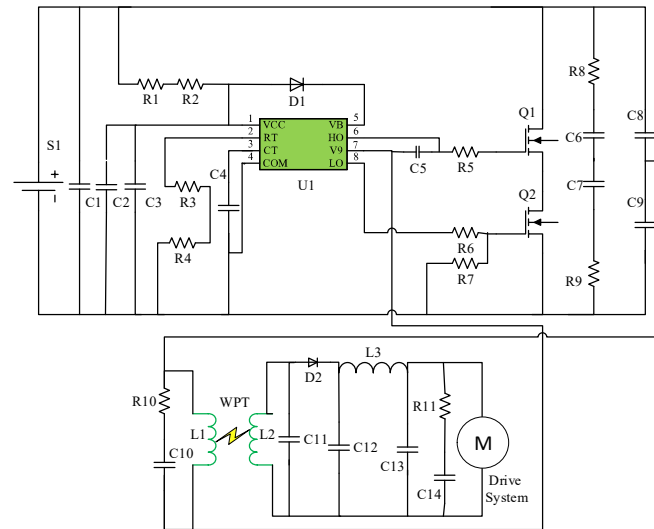


**Fig. 3.7. The complete transmitter and receiver circuit of the proposed system.**

The inductances of the coils of the coupling module were measured using M4070 LCR meter which is an auto-ranging LCR tester that can drive up to 500 KHz. It is suitable for measuring small values inductance and capacitance. This instrument uses LC oscillation technique to measure inductance values up to 100 H. The inductance of the transmitter coil and the receiver coil were measured and found to be 34.5  $\mu\text{H}$  and 34.3  $\mu\text{H}$ , respectively. The inductance measurements confirm the identical design of the two coils. Compared the theoretical value of the inductance, the measured value was slightly higher due to additional inductance from the external wire connections. The mutual inductance between the coils was also calculated in terms of their self-inductances and their series equivalent value using the following formula,

$$M = \frac{L_T + L_R + L_{eq}}{2} \quad (3.27)$$

The complete experimental setup is shown in Fig. 3.8.

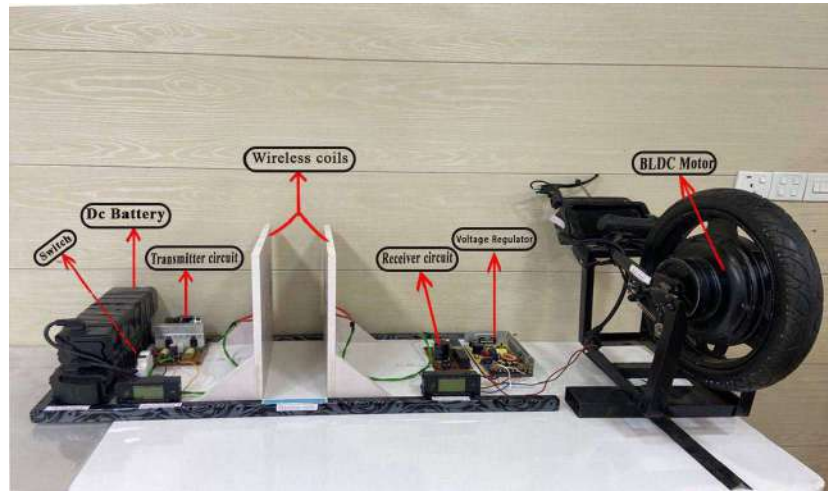


**Fig. 3.8.** The experimental prototype of the Large Scale WPT system.



## Chapter Four: Experimental Results

### 4.1 EXPERIMENTAL RESULTS OF THE SMALL-SCALE SYSTEM

The system was used to charge a 3.7 V, 2 Ah battery of a smart robot car at different transmission distances between the transmitter side (Tx) and the receiver side (Rx). The distance was changed from (1 cm to 5 cm) at a step of 1 cm. At each experimental step, the input and output voltage, current and power as well as the transmission efficiency were measured and calculated. The current values were calculated using the oscilloscope method by connecting the shunt resistance to a value of 20 ohms in parallel, the voltage value in the oscilloscope is shown and divided by the resistance value to measure the current.

The waveforms of voltage and current at Tx and Rx sides at different operating conditions, are shown in Figs. 4.1- 4.10.

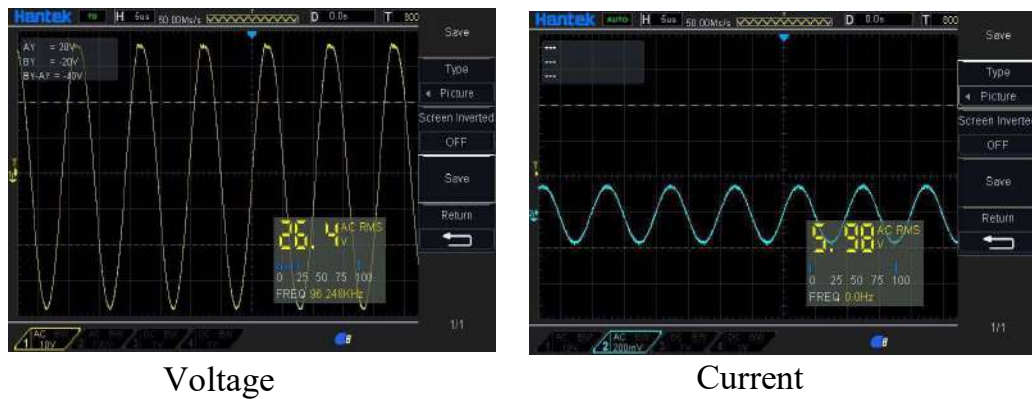


**Fig. 4.1. The waveforms of the voltage and current in Tx side 1cm.**

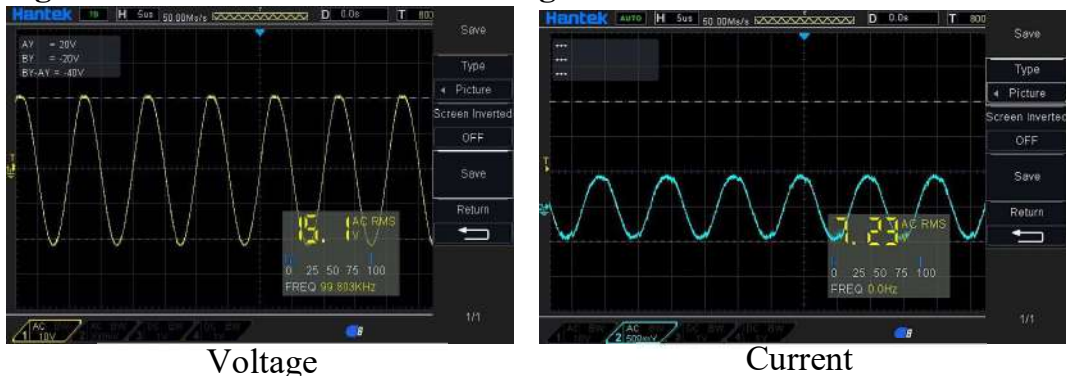


**Fig. 4.2. The waveforms of the voltage and current in Rx side 1cm.**

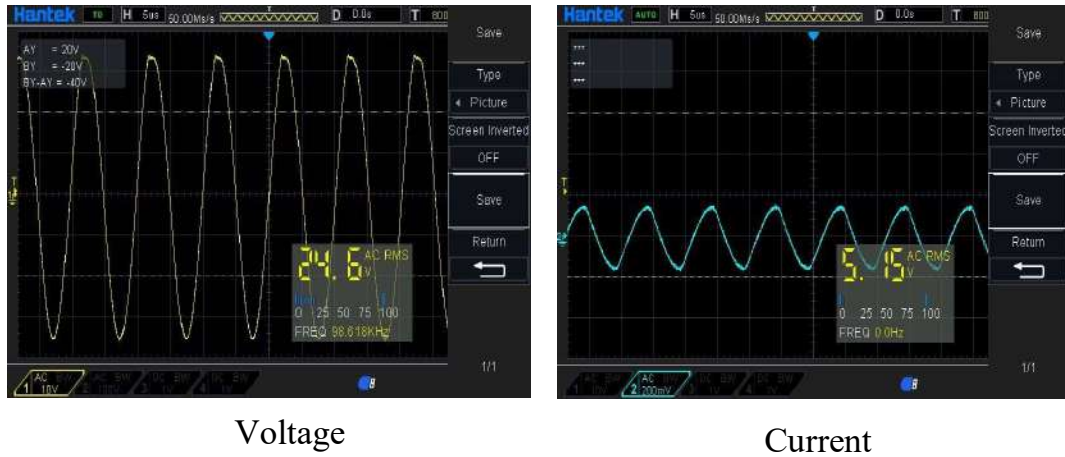


**Fig. 4.3.** The waveforms of the voltage and current in Tx side 2 cm.

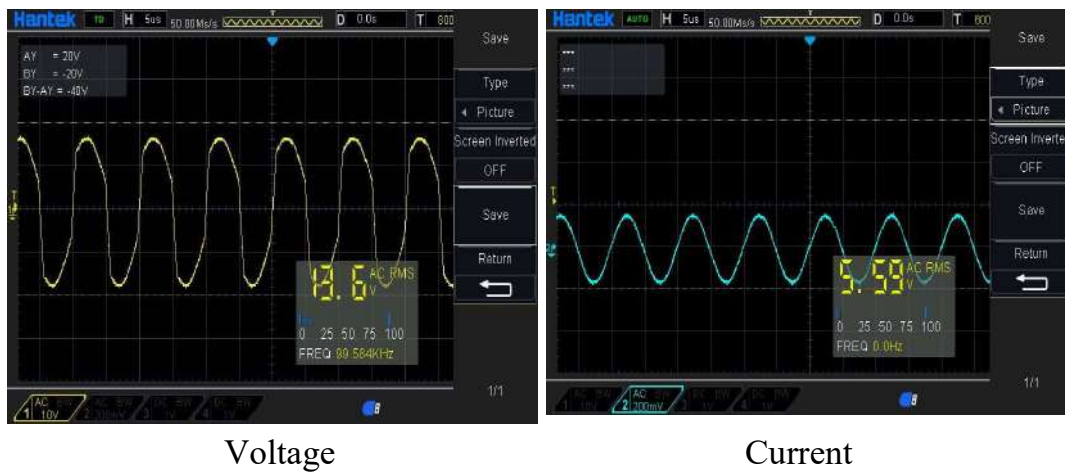
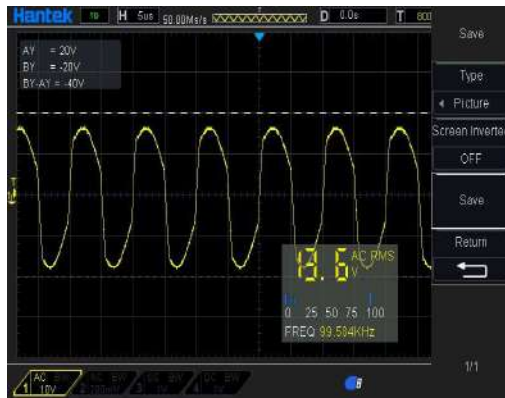
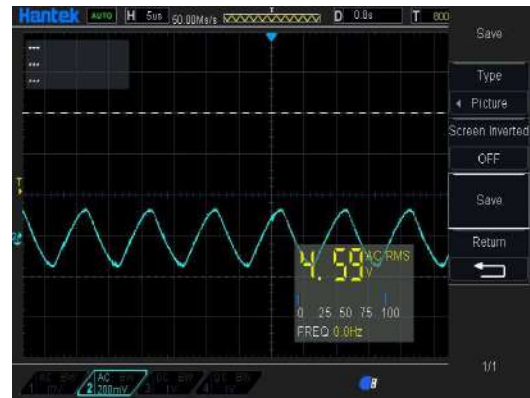


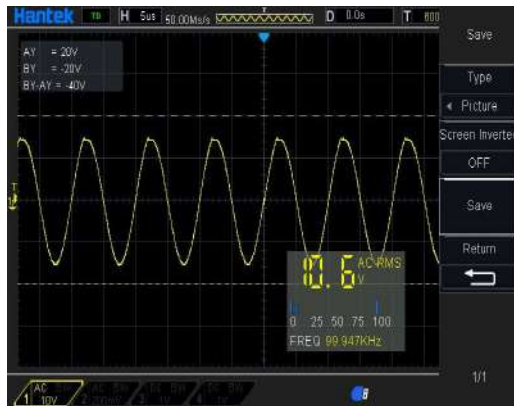
**Fig. 4.4.** The waveforms of the voltage and current in Rx side 2 cm.



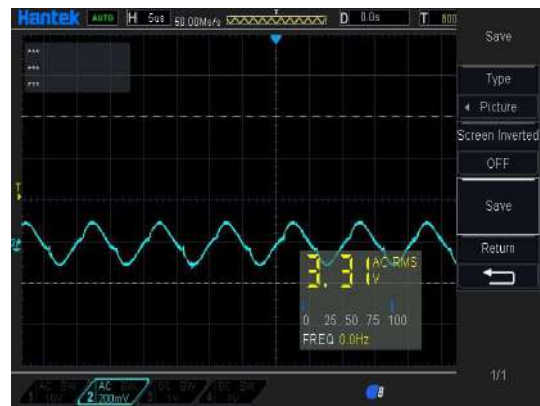
Voltage



Current

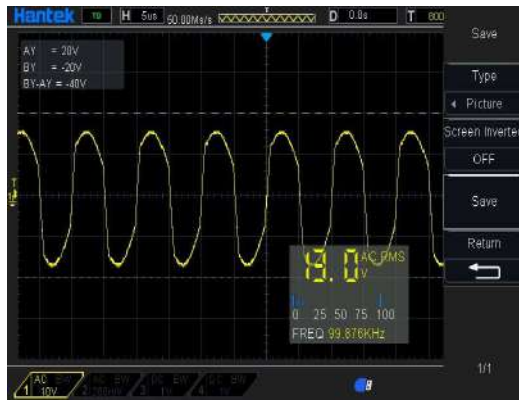
**Fig. 4.5. The waveforms of the voltage and current in Tx side 3 cm.**

Voltage

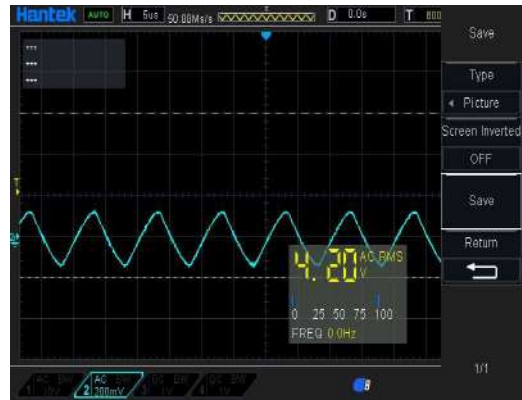


Current

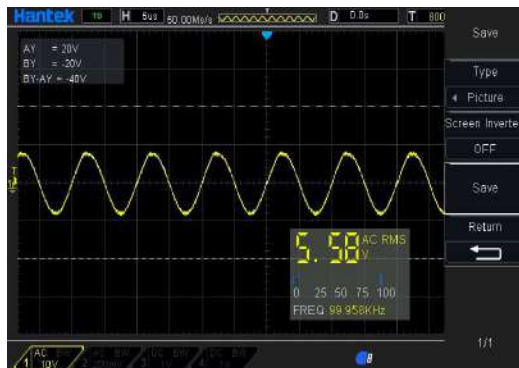
**Fig. 4.6. The waveforms of the voltage and current in Rx side 3 cm.**



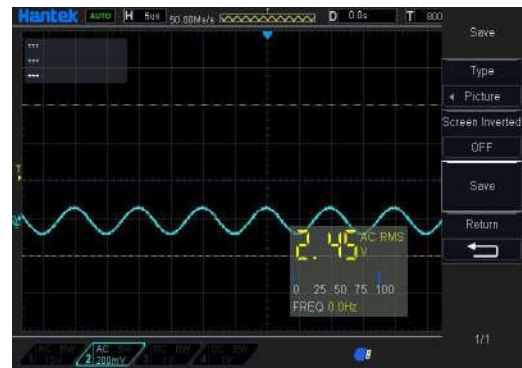
Voltage



Current

**Fig. 4.7. The waveforms of the voltage and current in Tx side 4 cm.**

Voltage



Current

**Fig. 4.8. The waveforms of the voltage and current in Rx side 4 cm**

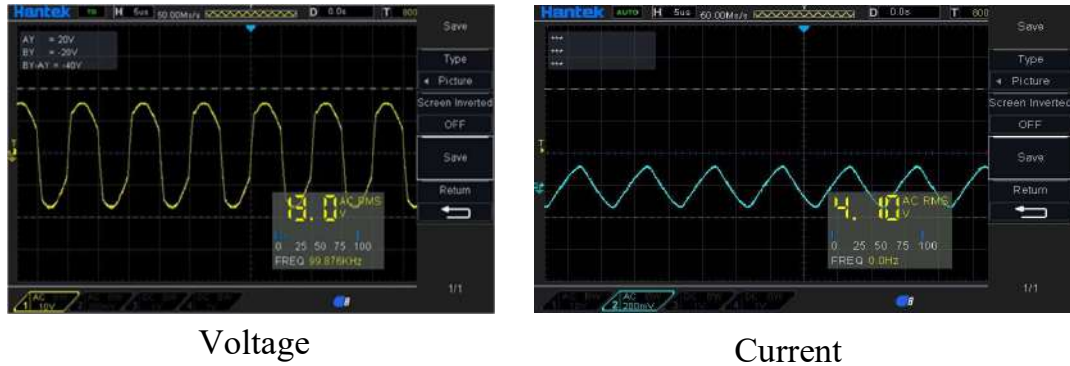


**Fig. 4.9.** The waveforms of the voltage and current in Tx side 5 cm.



**Fig. 4.10.** The waveforms of the voltage and current in Rx side 5 cm.

The experimental measurements of the Tx and Rx voltage and current as well as the transmission efficiency at different distances are listed in Table 4.1. It can be observed that when the distance between the transmitter coil and the receiver coil is increased the RMS voltage decreases. This decrease is attributed to the drop in the air gap flux between the coils. The highest efficiency achieved was at a distance of 1cm and it was about 69%. The efficiency declined with the distance and dropped drastically at 5 cm. The drop in the efficiency is self-explanatory and attributed to the deterioration of the wireless power transmission process at distances longer than 1 cm.

**Table 4.1. Experimental results of the small-scale system.**

D (cm)	Tx		Rx		Power (W)		Eff. (%)
	$V_{Tx}$ RMS (V)	$I_{Tx}$ RMS (A)	$V_{Rx}$ RMS (V)	$I_{Rx}$ RMS (A)	Tx	Rx	
1	26.4	0.598	15.1	0.723	15.8	10.9	69.0
2	24.6	0.515	13.6	0.559	12.6	7.60	60.3
3	13.6	0.459	10.6	0.331	6.20	3.50	56.6
4	13	0.42	5.58	0.245	5.50	1.40	25.5
5	13	0.41	4.18	0.117	5.33	0.49	9.2

## 4.2 EXPERIMENTAL RESULTS OF THE LARGE-SCALE SYSTEM

The large scale system was built and tested to cover a wider range of the transmission distance. It was tested to transmit power to the in-wheel motor at different operating conditions of load and transmission distance between the transmitter and the receiver coils. Three motor load settings were applied that are no load, half-load and full-load, keeping the motor rotational speed control at its rated value of 506.4 rpm. At each load setting, the system was tested at three transmission distances: 7.5, 10 and 12.5 cm. In each experimental step, the system parameters were measured, including the input voltage and current from the battery, the voltage and current of the transmitter and receiver coils as well as the output power delivered to the motor. The transmission efficiency was then calculated at each step.

It is worth mentioning here that the transmission efficiency is calculated in terms of the DC input and output power. A comparison between the experimental and simulation results is listed in tables 4.2 and 4.3. The simulation results showed reasonable agreement with the experimental results, with a percentage error that did not exceed 0.8% in all the studied loading and distance scenarios. It can be noticed that at a certain transmission

distance, the transmission efficiency is relatively equal in the three load conditions. For instance, at 7.5 cm the average value of the transmission efficiency at three loading conditions is 72.7%. However, the efficiency was greatly affected by the transmission distance at a specific load current. At the no load condition, the efficiency dropped from 71.75% to 50.55% when the transmission distance increased from 7.5 cm to 12.5 cm. These trends are depicted in Table 4.4, which shows the efficiency versus load current at different transmission distances.

**Table 4.2. Simulation vs experimental voltage measurements of the large-scale system.**

Operation Mode	Distance (cm)	D1	D2	Sending Voltage (V)		Error (%)	Receiving Voltage (V)		Error (%)
				Sim.	Exp.		Sim.	Exp.	
				No Load	7.5	0.01	0.87	105.7	101
No Load	10	0.1	0.9	116.2	115	1%	252.1	253	0.35%
No Load	12.5	0.172	0.906	126.3	126	0.3%	298.4	298	0.13%
Half Load	7.5	0.015	0.87	106.2	101	4.9%	193.7	195	0.66%
Half Load	10	0.27	0.859	143.3	144	0.5%	245.5	244	0.6%
Half Load	12.5	0.49	0.765	205.1	204	0.5%	244.1	244	0.04%
Full Load	7.5	0.172	0.89	126.3	126	0.3%	205.2	204	0.6%
Full Load	10	0.47	0.8	197.4	198	0.3%	245.3	244	0.5%
Full Load	12.5	0.59	0.71	255.1	253	0.82%	275.4	278	0.93%



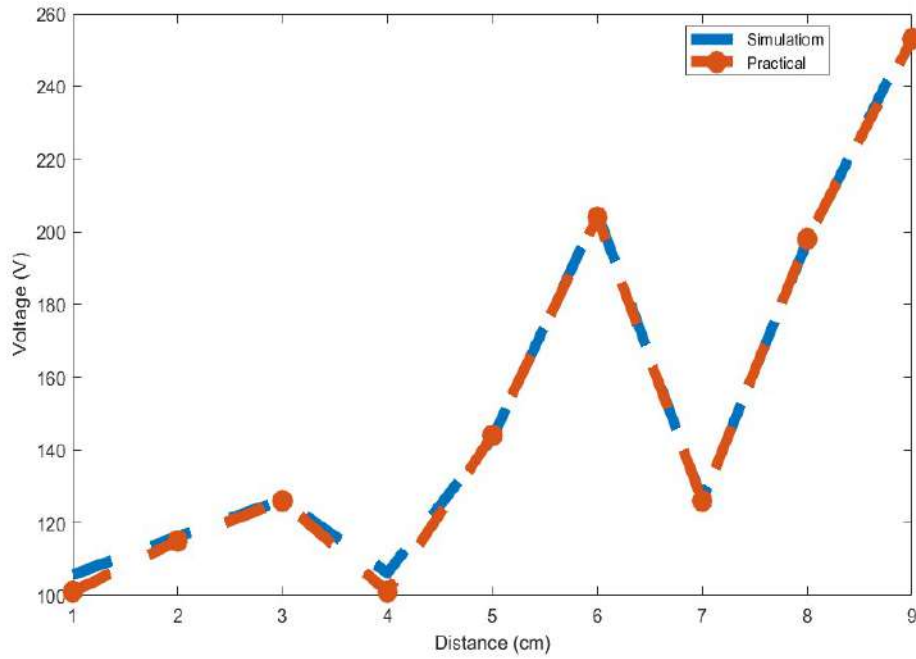


**Fig. 4.11. Voltage of transmitter for simulation and practical results.**

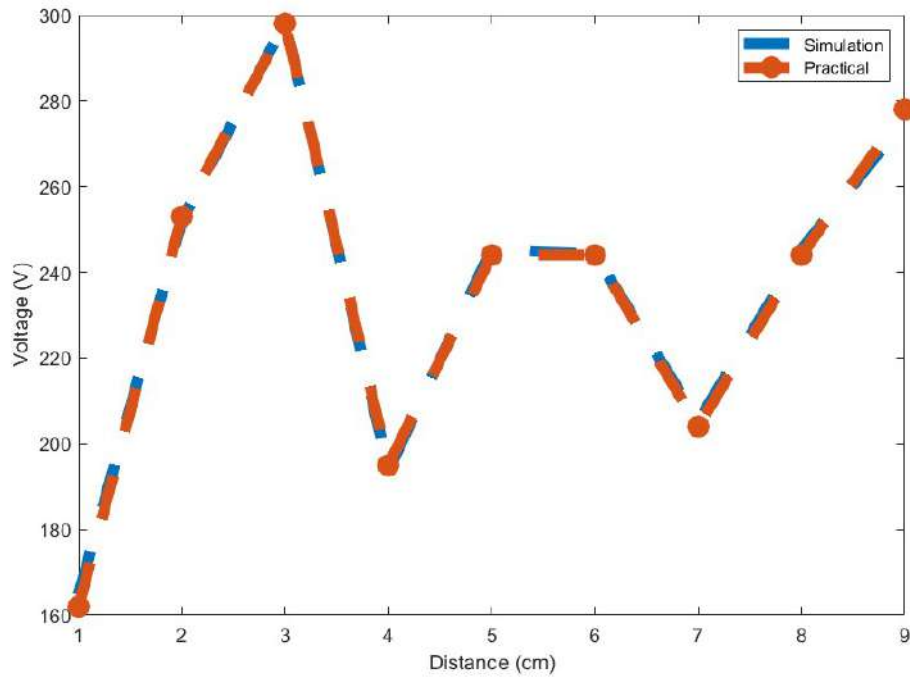


**Fig. 4.12. Voltage of Receiver for simulation and practical results.**



**Table 4.3. Simulation vs experimental current measurements of the large-scale system.**

Operation Mode	Distance (cm)	D3	D5	Sending Current (I)		Error (%)	Receiving Current (I)		Error (%)
				Sim.	Exp.		Sim.	Exp.	
No Load	7.5	0.966	0.858	1.954	1.955	0.05%	0.932	0.935	0.32%
No Load	10	0.945	0.84	2.42	2.45	1.22%	0.77	0.76	1.3%
No Load	12.5	0.925	0.82	2.96	2.93	1.01%	0.5541	0.55	0.73%
Half Load	7.5	0.95	0.86	1.93	1.96	1.53%	0.746	0.76	1.7%
Half Load	10	0.952	0.84	2.98	2.93	1.67%	1.068	1.075	0.65%
Half Load	12.5	0.94	0.89	2.939	3	2.03%	1.416	1.39	6%
Full Load	7.5	0.94	0.925	1.23	1.22	0.81%	0.5573	0.55	1.3%
Full Load	10	0.948	0.903	2.494	2.455	1.56%	1.398	1.39	0.57%
Full Load	12.5	0.925	0.905	3.157	3	4.97%	1.578	1.54	2.4%

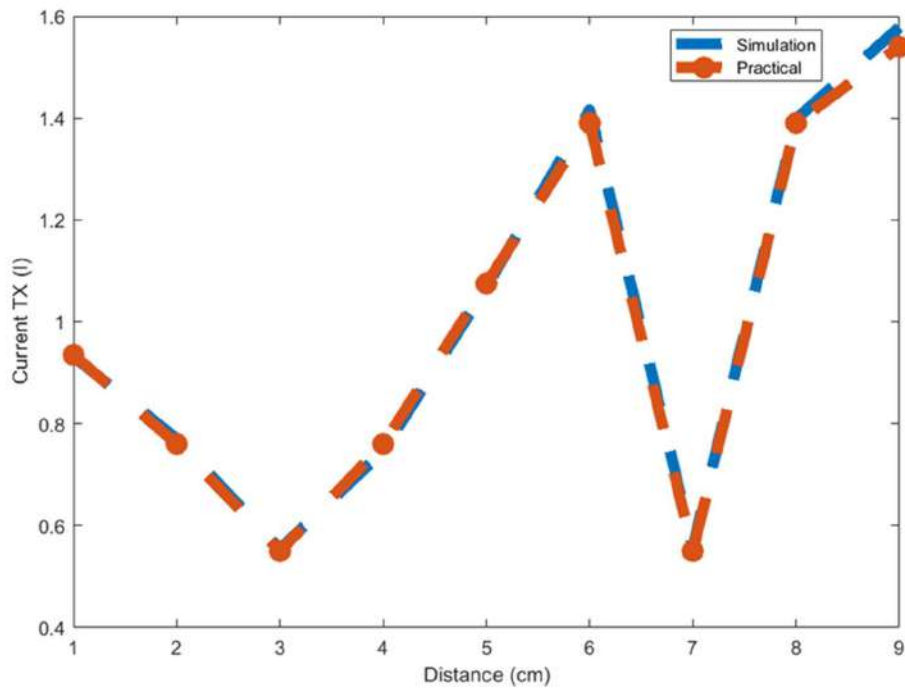


**Fig. 4.13. Current of transmitter for simulation and practical results.**

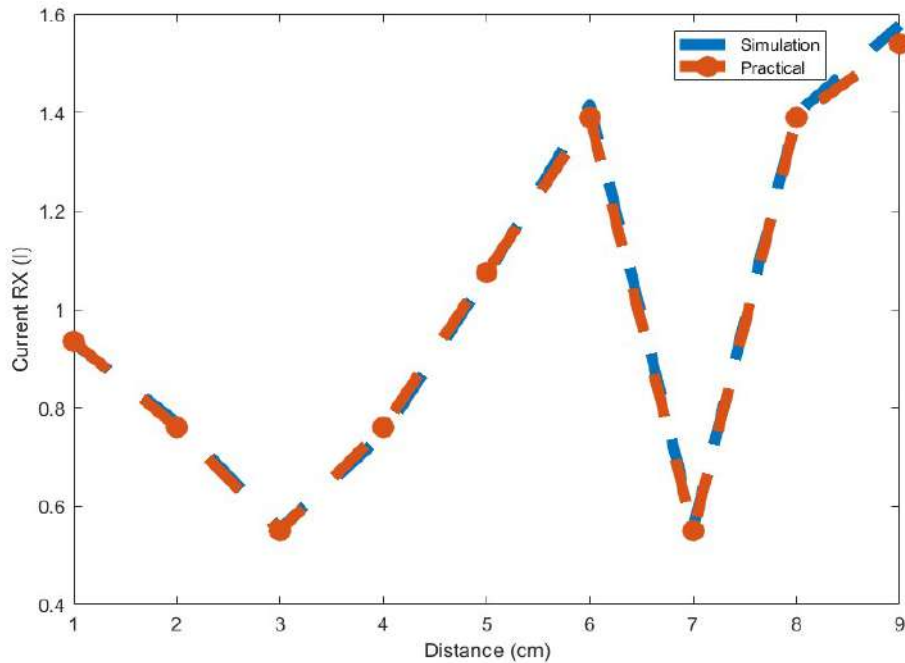


**Fig. 4.14. Current of Receiver for simulation and practical results.**

**Table 4.4. Simulation vs Experimental Power and Efficiency (%Error)**

Operation Mode	Distance (cm)	Sending Power (watt)		Percentage Sending Power Error (%)	Receiving Power (watt)		Percentage Receiving Power Error (%)	Efficiency		Percentage Efficiency Error (%)
		Sim.	Exp.		Sim.	Exp.		Sim.	Exp.	
No Load	7.5	206.5	197.4	4.9%	153.5	151.47	1.28%	74.33%	76.73%	3.12%
No Load	10	281.2	281.75	0.2%	194.11	192.28	0.94%	69%	68.24%	1.1%
No Load	12.5	373.55	369.18	1.17%	165.34	163.9	0.87%	44.2%	44.4%	0.45%
Half Load	7.5	204.96	197.96	3.41%	144.5	148.2	2.5%	70.5%	74.8%	5.7%
Half Load	10	427.03	421.92	1.2%	262.2	262.3	0.03%	61.4%	62.2%	1.28%
Half Load	12.5	602.8	612	1.5%	345.64	339.16	1.87%	57.3%	55.4%	3.31%
Full Load	7.5	155.35	153.72	1.04%	114.35	112.2	1.88%	73.6%	72.98%	0.84%
Full Load	10	492.31	486.1	1.26%	342.9	339.2	4.63%	69.6%	69.7%	0.14%
Full Load	12.5	805.35	759	5.75%	434.58	428.12	1.48%	53.96%	56.4%	4.32%

In Table 4.5, flux linkage and rotational speed were calculated for the load motor in the practical case and the simulation case. Fig. 4.15 and Fig. 4.16 show the simulation model in Matlab/SIMULINK for the two cases in Table 4.5.

**Table 4.5. Experimental and Simulation Flux Linkage, Rotational Speed.**

Experimental					Simulation				
$\omega_r$ (rpm)	$I_{dc}$ (amp)	P Load (w)	T (N.m)	Flux Linkage	$\omega_r$ (rpm)	$I_{dc}(i)$	P Load (w)	T (N.m)	Flux Linkage (We b)
27.7507	0.809	40.6118	1.4634	0.252	27.17	0.8355	40.1	1.46	0.252
55.5015	1.590	79.023	1.4238	0.129	51.27	1.656	79.48	1.423	0.129
83.3569	2.215	108.978	1.3074	0.0875	80.61	2.269	108.9	1.3074	0.0875
111.0029	2.780	135.386	1.2197	0.0653	106.9	2.819	135.3	1.2197	0.0653
138.8584	3.44	165.464	1.1916	0.0525	132	3.45	165.6	1.1916	0.0525
169.4366	5.178	240.25	1.4179	0.0429	157.6	4.991	239.6	1.4179	0.0429

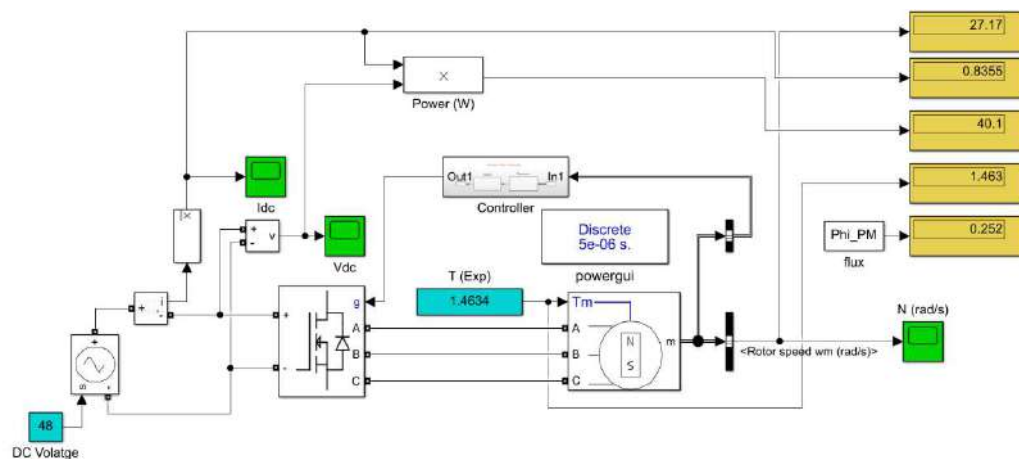


**Fig. 4.11. Case (1) Simulation Result from Table 4.5.**

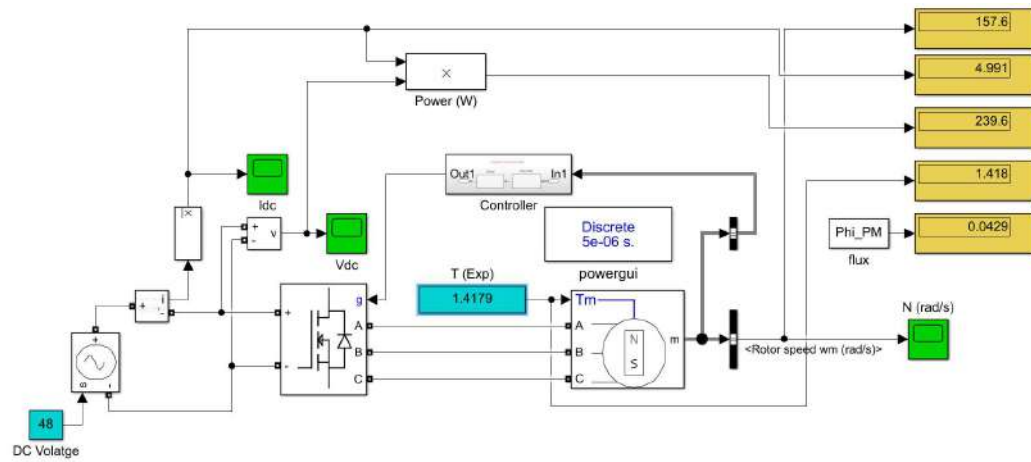
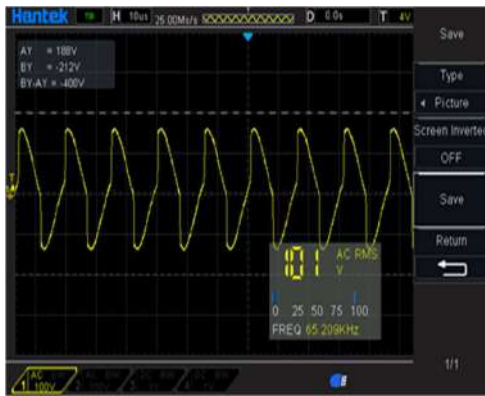
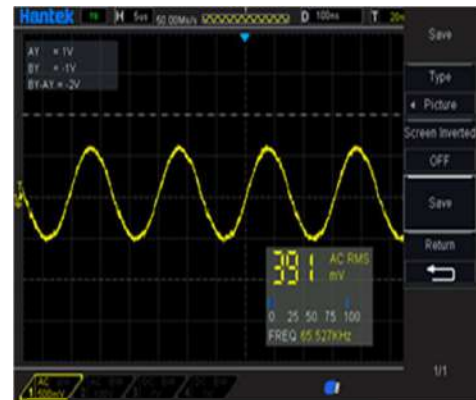


**Fig. 4.12. Case (2) Simulation Result from Table 4.5.**

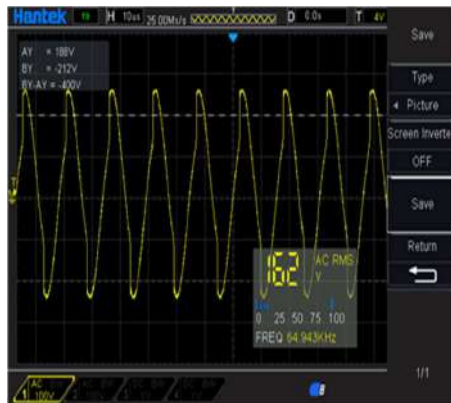
Fig. 4.17 – 4.25 show the practical voltage and current waveforms of the transmitter and receiver coils at different transmission distances and loading conditions.



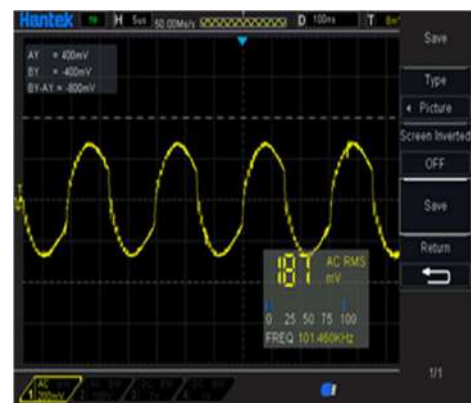
Voltage, Tx



Current, Tx

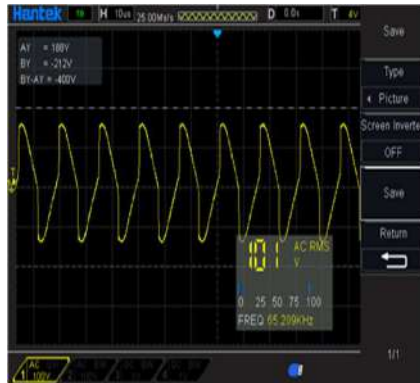


Voltage, Rx

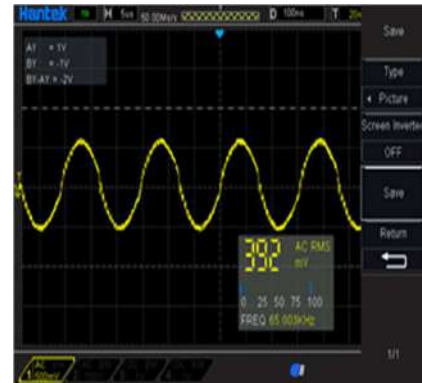


Current, Rx

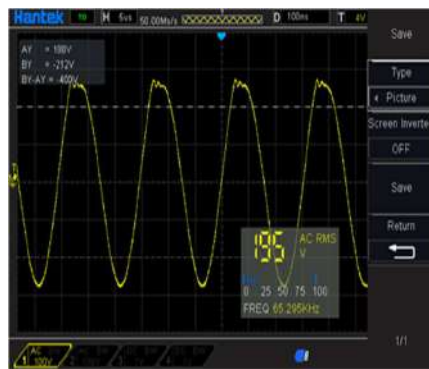
**Fig. 4.13. Practical voltage and current waveforms of the transmitter and receiver coils (No Load (Distance= 7.5cm)).**



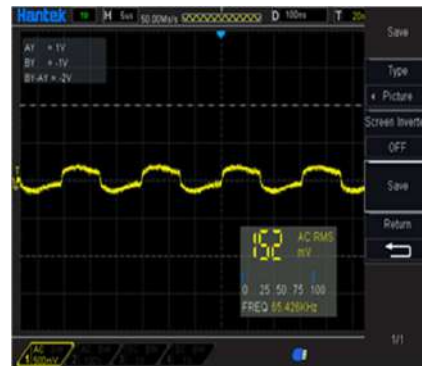
Voltage, Tx



Current, Tx

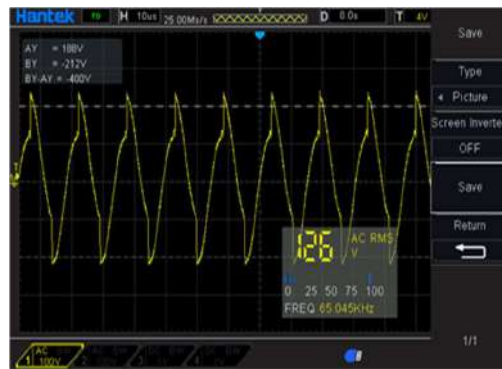


Voltage, Rx

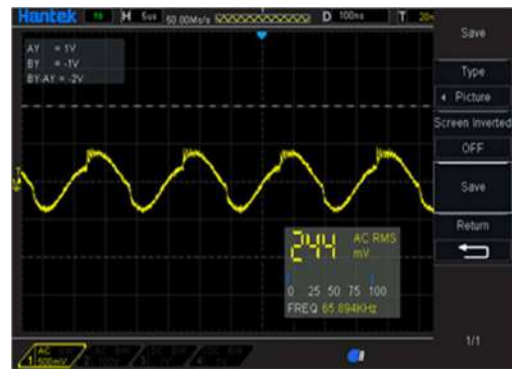


Current, Rx

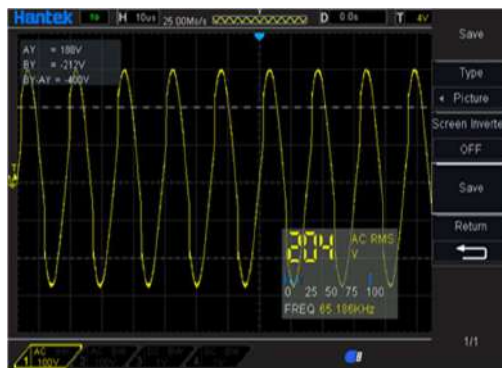
**Fig. 4.14. Practical voltage and current waveforms of the transmitter and receiver coils (Half Load (Distance= 7.5cm)).**



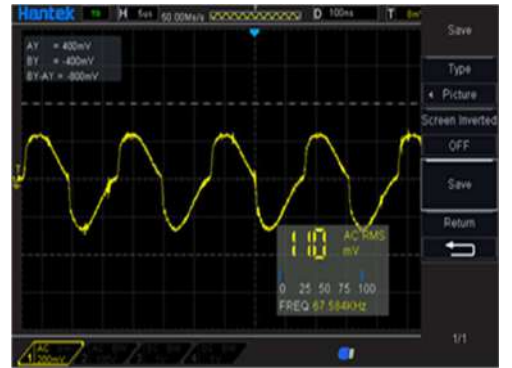
Voltage, Tx



Current, Tx



Voltage, Rx



Current, Rx

**Fig. 4.15. Practical voltage and current waveforms of the transmitter and receiver coils (Full Load (Distance= 7.5cm)).**

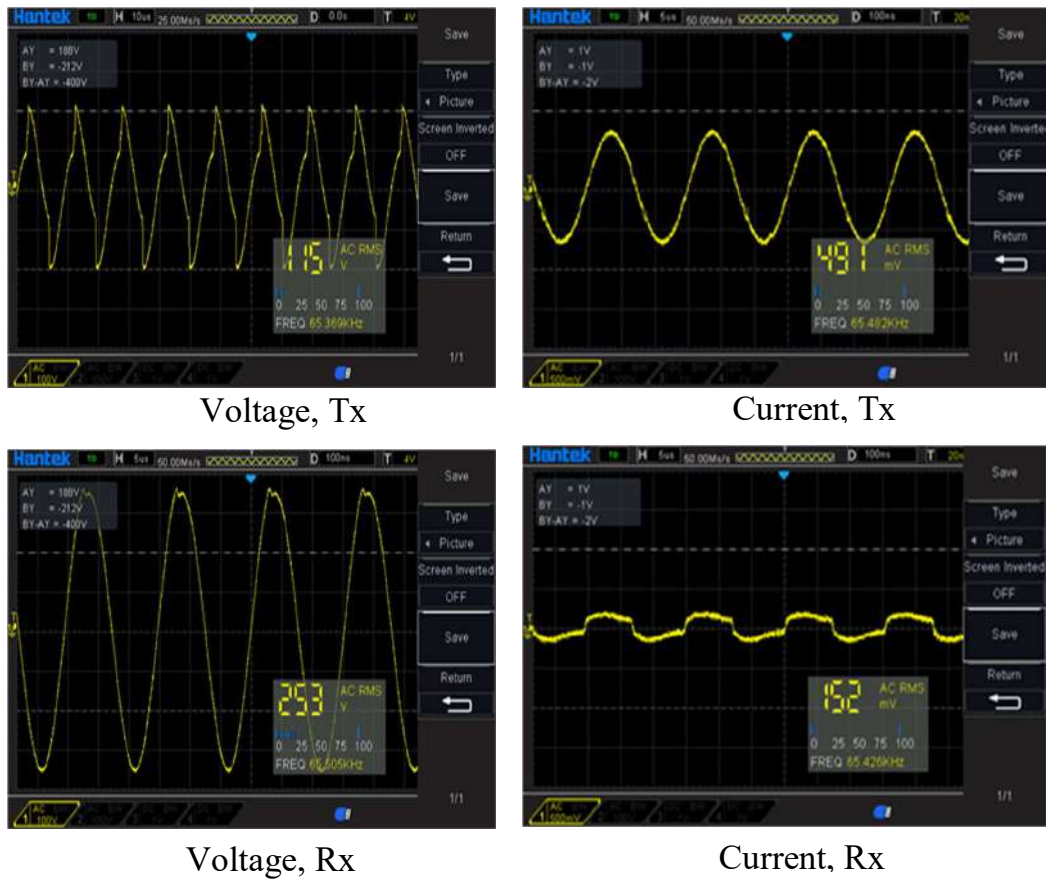
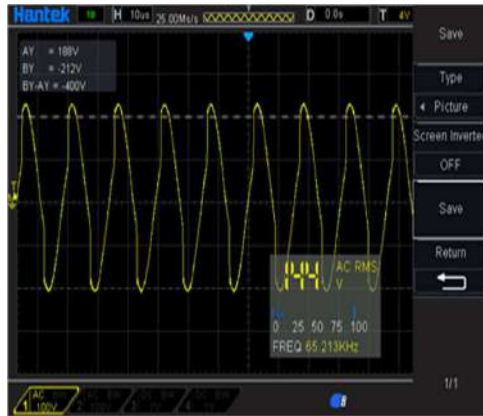
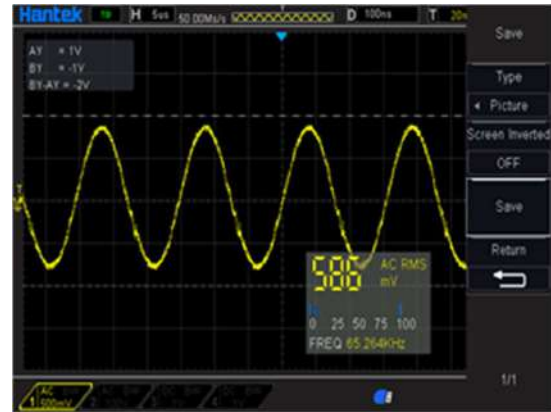


**Fig. 4.20. Practical voltage and current waveforms of the transmitter and receiver coils (No Load (Distance= 10cm)).**

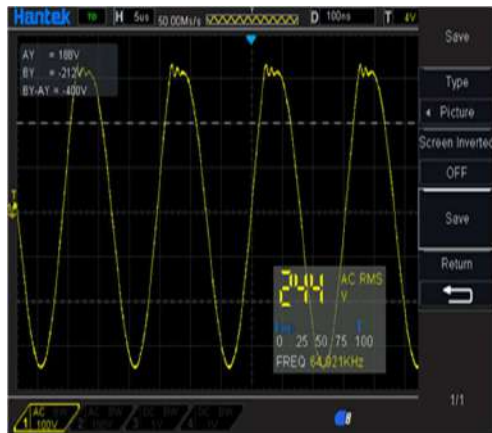




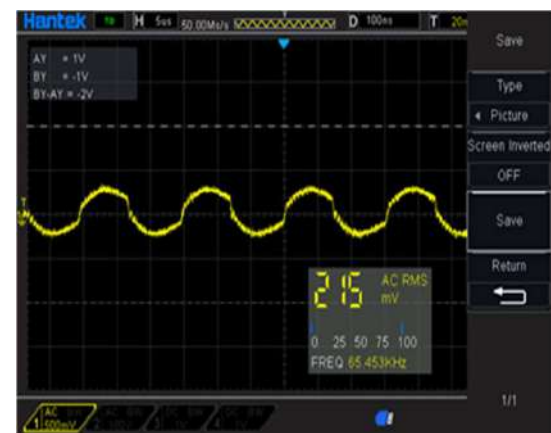
Voltage, Tx



Current, Tx



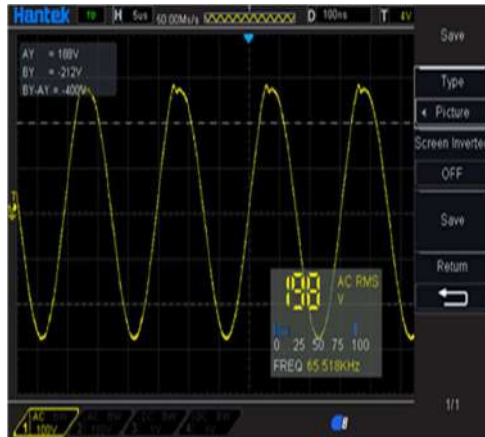
Voltage, Rx



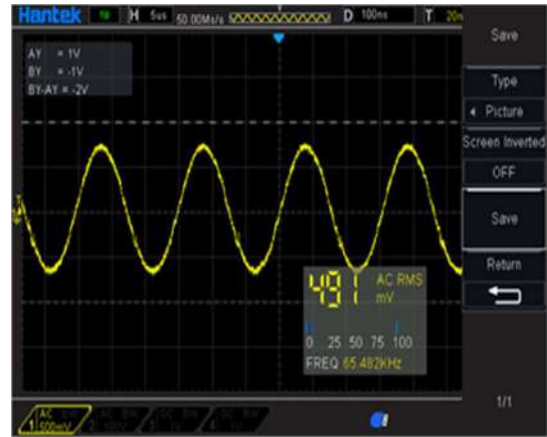
Current, Rx

**Fig. 4.21. Practical voltage and current waveforms of the transmitter and receiver coils (Half Load (Distance= 10cm)).**

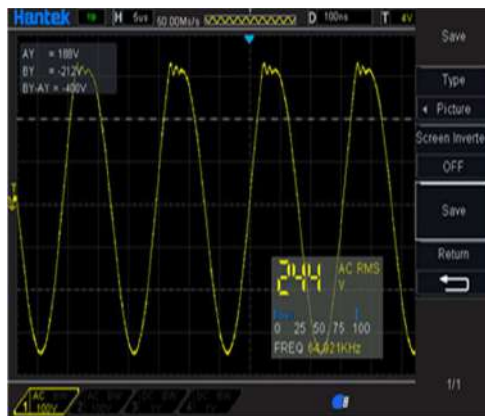




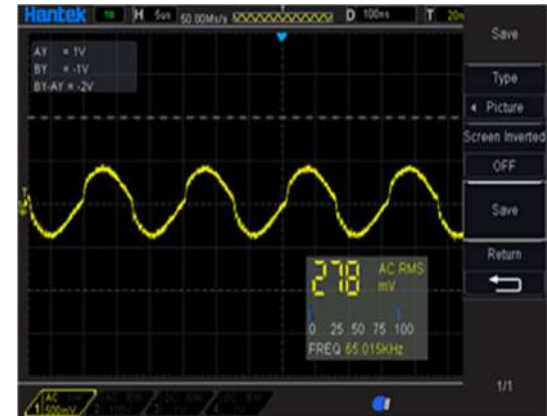
Voltage, Tx



Current, Tx

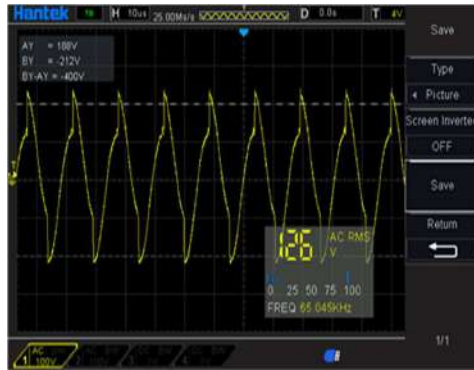


Voltage, Rx

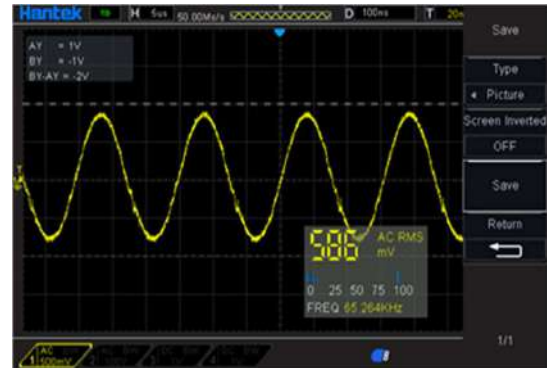


Current, Rx

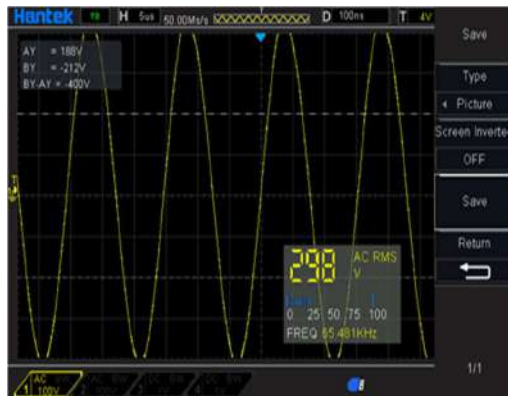
**Fig. 4.22. Practical voltage and current waveforms of the transmitter and receiver coils (Full Load (Distance= 10cm)).**



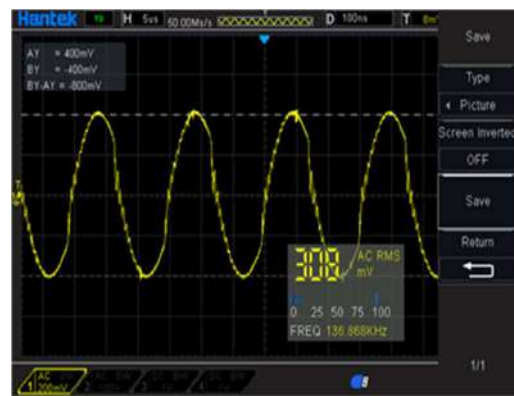
Voltage, Tx



Current, Tx

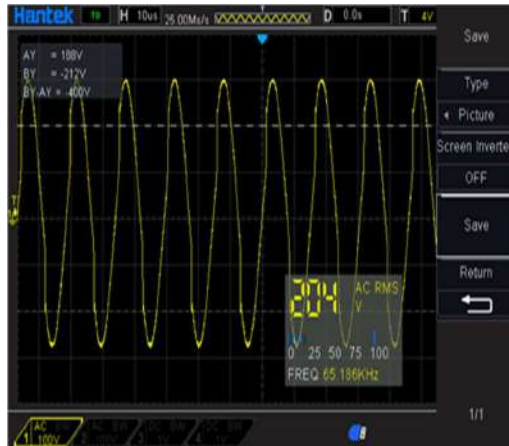


Voltage, Rx

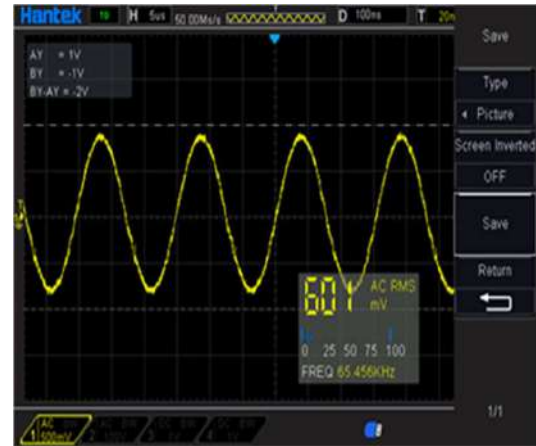


Current, Rx

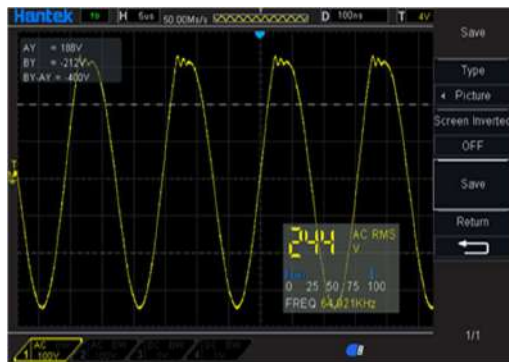
**Fig. 4.23. Practical voltage and current waveforms of the transmitter and receiver coils (No Load (Distance= 12.5cm)).**



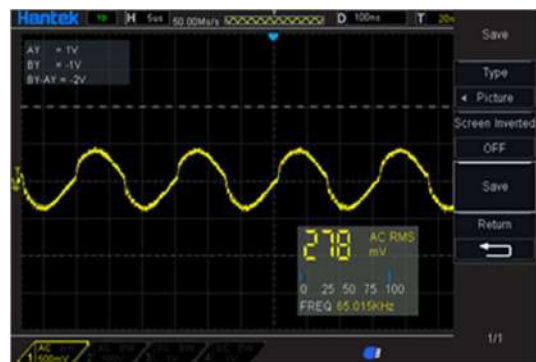
Voltage, Tx



Current, Tx

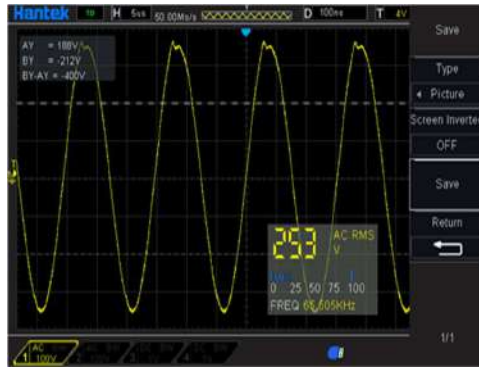


Voltage, Rx

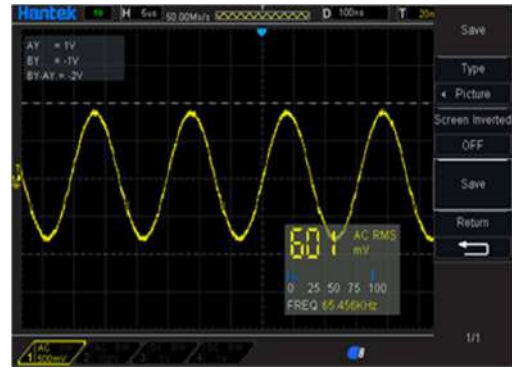


Current, Rx

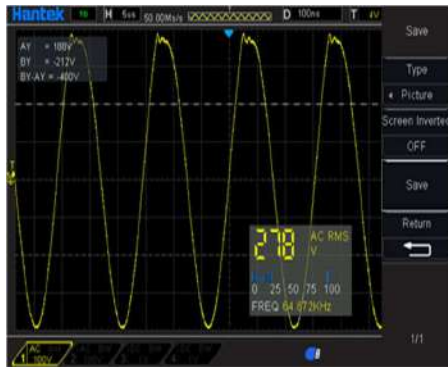
**Fig. 4.16. Practical voltage and current waveforms of the transmitter and receiver coils (Half Load (Distance= 12.5cm))**



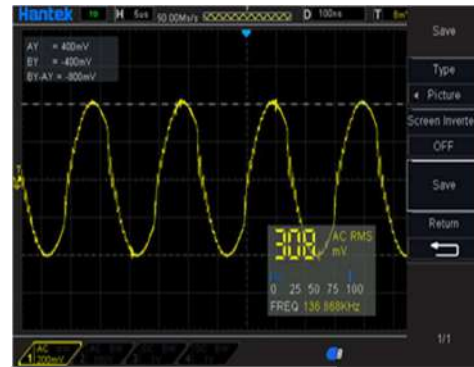
Voltage, Tx



Current, Tx



Voltage, Rx

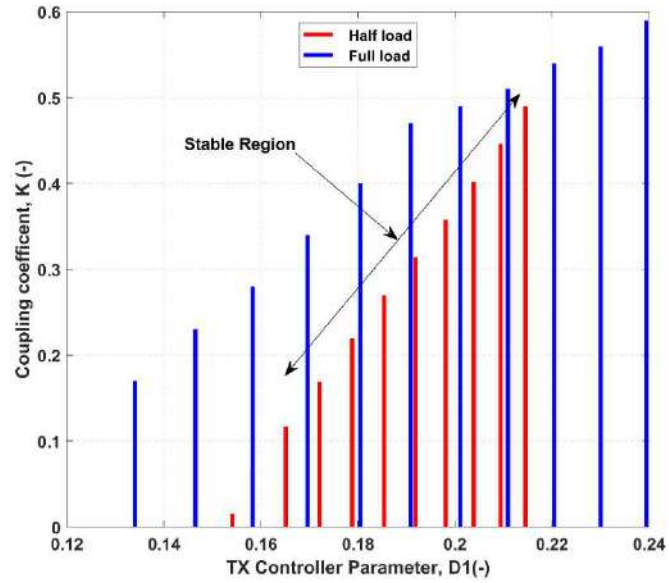


Current, Rx

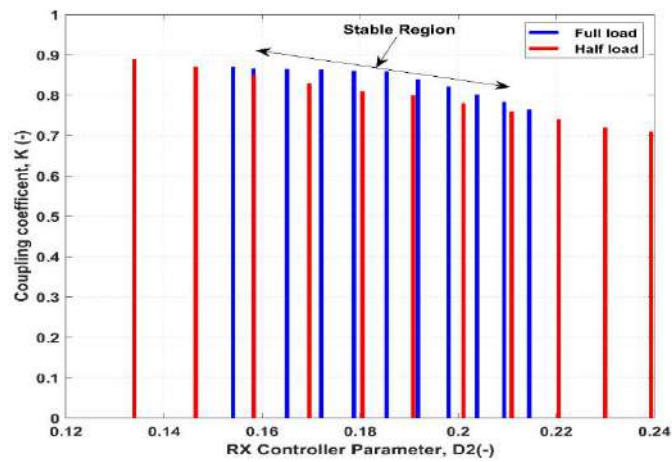
**Fig. 4.17. Practical voltage and current waveforms of the transmitter and receiver coils (Full Load (Distance= 12.5cm))**

#### 4.2.1 Stability for Large Scale Prototype

The parameters' controllers in the Tx & Rx sides and the hardware parameters affect the stability of the WPT system. Hardware parameters are fixed, as for the WPT system, the load impedance  $Z_L(\omega_r, T)$  and mutual inductance  $M(d, k)$  are changed with the system operating conditions. The boundary value of controller parameters ( $D1$  &  $D2$ ), which are related to tuning better  $Z_L$  and  $M$ . In order to analyse the effect of these two parameters on the stability of the system, a three-dimensional stability boundary diagrams of ( $D1$  &  $D2$ ),  $Z_L$  and  $M$  is illustrated, as shown in Fig. 4.26. Tables 4.6 and 4.7 illustrate the optimal duty cycles (e.g.  $D1$  and  $D2$ ) that verify stable region at half and full load operations. It can be estimated the range of motor speeds that achieves stable operation in the range between 68.97 rad/s and 86.20 rad/s.



(a)



(b)

Fig. 4.26. Stability boundary graphs of controllers' parameters (a)  $D1$  and (b)  $D2$ .

**Table 4.6. The Range of Optimal D1.**

<b>D1</b>	<b>K</b>	<b>Region Stability</b>
0.172	0.17	Stable Region
0.179	0.23	Stable Region
0.185	0.26	Stable Region
0.191	0.33	Stable Region
0.198	0.35	Stable Region
0.21	0.44	Maximum value

**Table 4.7. The Range of Optimal D2.**

<b>D2</b>	<b>Load Impedance(<math>\Omega</math>)</b>	<b>Region Stability</b>
0.15	115	Stable Region
0.24	65	Stable Region
0.257	50	Stable Region
0.35	40	Stable Region

## Chapter Five: Conclusion and Future work

### 5.1 CONCLUSION

In this thesis, a wireless power transmission system is built and experimented for wireless charging applications. The system is based on inductive coupling technique where two spiral coils are used for transmission and receiving ends. A Class-D inverter is used as the power converter for high-frequency voltage transformation. A small-scale prototype of the system is tested to charge a 3.7 V, 2 Ah battery of a smart robot car. The experimental results confirmed the functionality of the system in transmitting 15.8 W at a 70% efficiency. The efficiency dropped at distances longer than 1.5 cm because the voltage and current decreased. Although the system presented in this work is a small-scale experimental prototype, it provides useful practical insights on the design and operation of inductive wireless power transmission systems.

Another inductive WPT system has been developed for an in-wheel motor application. The proposed system has been designed and tested at different loading modes and air gap distance between Tx and Rx. In each experimental scenario, the input voltage and current from a battery, the voltage and current of the Tx and Rx coils (as well as the output power delivered to the motor) have been measured. The WPT efficiency has been calculated in terms of the DC input and output power for each scenario. It has been observed from the experimental results that the WPT efficiency strongly depends on the air gap distance because the coupling coefficient deteriorates with distance. The efficiency decreased from 71.75% to 50.55% as the air gap distance increased from 7.5 cm to 12.5 cm at the no-load mode. At a specific air gap distance, the loading factor had a slight effect on the transmission efficiency. Simulation results also verified the functionality of the designed system in supplying power to the in-wheel motor wirelessly.

This research can be extended by scaling up the experimental system and focusing more on the control and stability of the motor.

## **5.2 FUTURE WORK**

The work presented in this thesis is centered around the design and experimental realization of a stationary WPT system for electric vehicle applications focusing on the physical design and characteristics of the system including the coils self-inductance, coupling coefficient, inverter topology and efficiency of transmission. The work can be extended in a further study to investigate the following aspects:

- 1) Investigate the effect of coils misalignment by modifying the system design structure and adding circuit components to compensate any magnetic leakage between the coils under horizontal and vertical misalignments.
- 2) Consider modifying the experimental system to support dynamic wireless charging of the vehicle while in motion. This aspect is worth researching for its importance as a promising approach for EV charging.



## References

- [1] P. Mock and Z. Yang, “ANOTHER CHAPTER IN THE GLOBAL RACE TOWARDS ELECTRIFICATION,” *The International Council on Clean Transportation (ICCT)*, vol. 51, 2022.
- [2] M. Scarfoglio, “Lithium-ion batteries for electric vehicles: A review on aging models for vehicle-to-grid services,” ,vol. 113,2018.
- [3] M. Cardama, C. Dekki, E. Hosek, M. Major, N. Medimorec, K. Peet and A. Steinvorth (SLOCAT Secretariat), “COP26 Outcomes for Sustainable, Low Carbon Transport, ” vol. 17,2021.
- [4] H. Lee and A. Clark, “Recharging the future,” *Harvard Kennedy School*, vol. 54, no. 2, pp. 24–27, 2018.
- [5] S. C. Nambiar and M. Manteghi, “A Simple Wireless Power Transfer Scheme for Implanted Devices Shyam,” in *2014 United States National Committee of URSI National Radio Science Meeting (USNC-URSI NRSM)*, vol.107 ,2014, pp. 650–658. doi: 10.7868/s0023291214050097.
- [6] N. Q. MINH, “Wireless Power Transfer For Medical And Industrial Applications,” The University of Texas at Arlington, vol. 23, 2016.
- [7] A. El-Shahat, E. Ayisire, Y. Wu, M. Rahman, and D. Nelms, “Electric vehicles wireless power transfer state-of-the-art,” *Energy Procedia*, vol. 162, pp. 24–37, 2019, doi: 10.1016/j.egypro.2019.04.004.
- [8] S. Wankhede, S. Sachan, and V. Kumar, “Wireless Power Transmission Market,” *Allied Market Research*, vol. 74, 2021.
- [9] D. Ahn and S. Hong, “Effect of coupling between multiple transmitters or multiple receivers on wireless power transfer,” *IEEE Trans. Ind. Electron.*, vol. 60, no. 7, pp. 2602–2613, 2013, doi: 10.1109/TIE.2012.2196902.
- [10] X. Lu, P. Wang, D. Niyato, D. I. Kim, and Z. Han, “Wireless Charging

- Technologies: Fundamentals, Standards, and Network Applications,” *IEEE Commun. Surv. Tutorials*, vol. 18, no. 2, pp. 1413–1452, 2016, doi: 10.1109/COMST.2015.2499783.
- [11] A. Mahesh, B. Chokkalingam, and L. Mihet-Popa, “Inductive Wireless Power Transfer Charging for Electric Vehicles—A Review,” *IEEE Access*, vol. 45, 2021, pp. 137667–137713.
- [12] V. B. Vu, M. Dahidah, V. Pickert, and V. T. Phan, “A High-Power Multiphase Wireless Dynamic Charging System with Low Output Power Pulsation for Electric Vehicles,” *IEEE J. Emerg. Sel. Top. Power Electron.* vol. 8, pp. 3592–3608. 2020.
- [13] D. B. Ahire, V. J. Gond, and J. J. Chopade, “Compensation topologies for wireless power transmission system in medical implant applications: A review,” *Biosens. Bioelectron. X*, vol. 11, no. April, p. 100180, 2022.
- [14] S. Shen, Member, IEEE, J. Kim, Member, IEEE, C. Song, Member, IEEE, and B. Clerckx, Senior Member, IEEE, “Wireless Power Transfer with Distributed Antennas: System Design, Prototype, and Experiments,” vol. 27, 2020.
- [15] M. Rashid, *Power Electronics Handbook*, 4th ed. Elsevier, 2018.
- [16] B. Ghosh, S. Chakraborty, S. Bhunia and S. Pall, “Wireless power transmission system,” *IJIP*, Vol. 2, Issue 1, 2020.
- [17] I. A. Mashhadi, M. Pahlevani, S. Hor, H. Pahlevani, and E. Adib, “A new wireless power-transfer circuit for retinal prosthesis,” *IEEE Trans. Power Electron.*, vol. 34, no. 7, pp. 6425–6439, 2019, doi: 10.1109/TPEL.2018.2872844.
- [18] H.-D. Lang, “Optimization of Wireless Power Transfer Systems with Multiple Transmitters and Receivers,” p. 262, 2018, [Online]. Available: <https://tspace.library.utoronto.ca/handle/1807/89697>
- [19] M. A. Masrur and M. Cox, “A Unique Military Application of Wireless Power Transfer: Wireless Charging through a Vehicle Seat with

- Simplified Design Considerations,” *IEEE Ind. Electron. Mag.*, vol. 13, no. 4, pp. 19–30, 2019, doi: 10.1109/MIE.2019.2937469.
- [20] M. Z. Chaari, R. Al-Rahimi, and O. Aghzout, “High power wireless power transfer for the future of the battlefield challenges,” *Secur. Def. Q.*, vol. 40, no. September 2022, pp. 9–26, 2022, doi: 10.35467/sdq/152548.
- [21] Taylor M. Fisher, K. Blair Farley, Y. Gao, H. Bai, and Z. T. H. Tse, “Electric vehicle wireless charging technology: A state-of-the-art review of magnetic coupling systems,” *Wirel. Power Transf.*, vol. 1, no. 2, pp. 87–96, 2014, doi: 10.1017/wpt.2014.8.
- [22] A. Rakhymbay, A. Khamitov, M. Bagheri, B. Alimkhanuly, M. Lu, and T. Phung, “Precise analysis on mutual inductance variation in dynamic wireless charging of electric vehicle,” *Energies*, vol. 11, no. 3, 2018, doi: 10.3390/en11030624.
- [23] Y. J. Hwang and J. Y. Jang, “Design and analysis of a novel magnetic coupler of an in-wheel wireless power transfer system for electric vehicles,” *Energies*, vol. 13, no. 2, p. 1V, 2020, doi: 10.3390/en13020332.
- [24] V. B. Vu, M. Dahidah, V. Pickert, and V. T. Phan, “A High-Power Multiphase Wireless Dynamic Charging System with Low Output Power Pulsation for Electric Vehicles,” *IEEE J. Emerg. Sel. Top. Power Electron.*, vol. 8, no. 4, pp. 3592–3608, 2020, doi: 10.1109/JESTPE.2019.2932302.
- [25] P. Mock and Z. Yang, “2021: Another Chapter in The Global Race Towards Electrification,” *The International Council on Clean Transportation (ICCT)*, 2022.
- [26] M. Scarfogliero, “Lithium-ion batteries for electric vehicles: A review on aging models for vehicle-to-grid services,” vol. 61, 2018.
- [27] Y. J. Hwang and J. Y. Jang, “Design and analysis of a novel magnetic coupler of an in-wheel wireless power transfer system for electric

- vehicles," *Energies*. vol. 13, (2020).
- [28] M. Biček, R. Kunc, and S. Zupan, "Mechanical Impact on In-Wheel Motor's Performance," *J. Mech.*, 33.607–618, vol. 29 ,(2017).
- [29] R. N. Tuncay, O. Ustun, M. Yilmaz, C. Gokce, and U. Karakaya, "Design and implementation of an electric drive system for in-wheel motor electric vehicle applications," 2011 IEEE Veh. Power Propuls. Conf. VPPC . vol. 15, (2011).
- [30] Y. O. Toshiyuki Fujita, Sakahisa Nagai, Hiroshi Fujimoto, "Development of dynamic wireless power transfer coils for 3rd generation wireless in-wheel motor," *IEEJ Trans. Ind. Appl.* 141. vol.8. (2021).
- [31] S. I. Sakai, H. Sado, and Y. Hori, "Motion control in an electric vehicle with four independently driven in-wheel motors," *IEEE/ASME Trans. Mechatronics*, vol. 4, no. 1, pp. 9–16, 1999, doi: 10.1109/3516.752079.
- [32] R. N. Tuncay, O. Ustun, M. Yilmaz, C. Gokce, and U. Karakaya, "Design and implementation of an electric drive system for in-wheel motor electric vehicle applications," 2011 IEEE Veh. Power Propuls. Conf. VPPC 2011, 2011, doi: 10.1109/VPPC.2011.6043070.
- [33] M. Terashima, T. Ashikaga, T. Mizuno, K. Natori, N. Fujiwara, and M. Yada, "Novel motors and controllers for high-performance electric vehicle with four in-wheel motors," *IEEE Trans. Ind. Electron.*, vol. 44, no. 1, pp. 28–38, 1997, doi: 10.1109/41.557496.
- [34] K. M. Rahman, N. R. Patel, T. G. Ward, J. M. Nagashima, F. Caricchi, and F. Crescimbin, "Application of direct-drive wheel motor for fuel cell electric and hybrid electric vehicle propulsion system," *IEEE Trans. Ind. Appl.*, vol. 42, no. 5, pp. 1185–1192, 2006, doi: 10.1109/TIA.2006.880886.
- [35] M. Sato, G. Yamamoto, D. Gunji, T. Imura, and H. Fujimoto, "Development of Wireless In-Wheel Motor Using Magnetic Resonance Coupling," *IEEE Trans. Power Electron.*, vol. 31, no. 7, pp.

- 5270–5278, 2016, doi: 10.1109/TPEL.2015.2481182.
- [36] H. Fujimoto, O. Shimizu, S. Nagai, T. Fujita, D. Gunji, and Y. Ohmori, “Development of wireless in-wheel motors for dynamic charging: From 2nd to 3rd generation,” pp. 56–61, vol.11, 2020, doi: 10.1109/WoW47795.2020.9291287.
- [37] T. Takeuchi, T. Imura, H. Fujimoto, and Y. Hori, “Power management of wireless in-wheel motor with dynamic-wireless power transfer,” *EVS 2017 - 30th Int. Electr. Veh. Symp. Exhib.*, vol. 2, 2017.
- [38] G. Yamamoto, “Investigation on Maximizing Power Transfer Efficiency of Wireless In-wheel Motor by Primary and Load-Side Voltage Control” ,vol. 59,2015.
- [39] M. Sato, G. Guidi, T. Imura, and H. Fujimoto, “Model for loss calculation of wireless in-wheel motor concept based on magnetic resonant coupling,” *2016 IEEE 17th Work. Control Model. Power Electron. Compel*, 2016, doi: 10.1109/COMPEL.2016.7556776.
- [40] T. Beh, T. Imura, M. Kato, and Y. Hori, “Wireless Power Transfer System via Magnetic Resonant Coupling at Restricted Frequency Range,” *Ind. Appl. Soc. ...*, vol. 4, no. 1, pp. 744–753, 2010.
- [41] V. P. Galigekere *et al.*, “Design and Implementation of an Optimized 100 kW Stationary Wireless Charging System for EV Battery Recharging,” *2018 IEEE Energy Convers. Congr. Expo. ECCE 2018*, pp. 3587–3592, 2018, doi: 10.1109/ECCE.2018.8557590.
- [42] J. Pries, V. P. N. Galigekere, O. C. Onar, and G. J. Su, “A 50-kW Three-Phase Wireless Power Transfer System Using Bipolar Windings and Series Resonant Networks for Rotating Magnetic Fields,” *IEEE Trans. Power Electron.*, vol. 35, no. 5, pp. 4500–4517, 2020, doi: 10.1109/TPEL.2019.2942065.
- [43] M. Suzuki *et al.*, “Design method for low radiated emission of 85 kHz band 44 kW rapid charger for electric bus,” *Conf. Proc. - IEEE Appl. Power Electron. Conf. Expo. - APEC*, pp. 3695–3701, 2017, doi:

- 10.1109/APEC.2017.7931229.
- [44] I. Villar, A. Garcia-Bediaga, U. Iruretagoyena, R. Arregi, and P. Estevez, "Design and experimental validation of a 50kW IPT for Railway Traction Applications," *2018 IEEE Energy Convers. Congr.*, pp. 1177–1183, 2018, doi: 10.1109/ECCE.2018.8558441.
- [45] H. H. Wu, A. Gilchrist, K. D. Sealy, and D. Bronson, "A High Efficiency 5 kW Inductive Charger for EVs Using Dual Side Control," *IEEE Trans. Ind. Informatics*, vol. 8, no. 3, pp. 585–595, 2012.
- [46] J. H. Kim *et al.*, "Development of 1-MW Inductive Power Transfer System for a High-Speed Train," *IEEE Trans. Ind. Electron.*, vol. 62, no. 10, pp. 6242–6250, 2015, doi: 10.1109/TIE.2015.2417122.
- [47] Y.-H. Liao and Y. Lin, "A Novel Bidirectional Wireless Power Transfer System for Mobile Power Application," *Appl. Sci.*, vol. 9, no. 18, pp. 1–12, 2019.
- [48] U. K. Madawala and D. J. Thrimawithana, "A Bidirectional Inductive Power Interface for Electric Vehicles in V2G Systems," *IEEE Trans. Ind. Electron.*, vol. 58, no. 10, pp. 4789–4796, 2011.
- [49] D. H. Tran, V. B. Vu, and W. Choi, "Design of a High-Efficiency Wireless Power Transfer System With Intermediate Coils for the On-Board Chargers of Electric Vehicles," *IEEE Trans. Power Electron.*, vol. 33, no. 1, pp. 175–187, 2018.
- [50] D. Ustun, S. Balci, and K. Sabanci, "A parametric simulation of the wireless power transfer with inductive coupling for electric vehicles, and modelling with artificial bee colony algorithm," *Measurement*, vol. 150, pp. 1–8, 2020.
- [51] Z. Luo and X. Wei, "Analysis of Square and Circular Planar Spiral Coils in Wireless Power Transfer System for Electric Vehicles," *IEEE Trans. Ind. Electron.*, vol. 65, no. 1, pp. 331–341, 2018, doi: 10.1109/TIE.2017.2723867.
- [52] S. Moon, B. C. Kim, S. Y. Cho, C. H. Ahn, and G. W. Moon, "Analysis

- and design of a wireless power transfer system with an intermediate coil for high efficiency,” *IEEE Trans. Ind. Electron.*, vol. 61, no. 11, pp. 5861–5870, 2014, doi: 10.1109/TIE.2014.2301762.
- [53] Y. Gao, A. Ginart, K. B. Farley, and Z. T. H. Tse, “Misalignment effect on efficiency of wireless power transfer for electric vehicles,” in *2016 IEEE Applied Power Electronics Conference and Exposition (APEC)*, 2016, pp. 3526–3528.
- [54] S. Aznavi, P. Fajri, and N. Lotfi, “Misalignment correction in wireless power transfer of electric vehicles by angular compensation,” *2020 IEEE Transp. Electrification Conf. Expo, ITEC 2020*, pp. 974–978, 2020, doi: 10.1109/ITEC48692.2020.9161481.
- [55] K. A. Kalwar, M. Aamir, and S. Mekhilef, “A design method for developing a high misalignment tolerant wireless charging system for electric vehicles”, vol. 118, pp. 237–245, 2018.
- [56] S. Varikkottil and F. D. J. L., “Estimation of Optimal Operating Frequency for Wireless EV Charging System under Misalignment,” *Electronics*, vol. 8, no. 3, pp. 1–15, 2019.
- [57] C. Shuwei, L. Chenglin, and W. Lifang, “Research on positioning technique of wireless power transfer system for electric vehicles,” in *2014 IEEE Conference and Expo Transportation Electrification Asia-Pacific (ITEC Asia-Pacific)*, 2014, pp. 1–4.
- [58] A. Mahesh, B. Chokkalingam, and L. Mihet-Popa, “Inductive Wireless Power Transfer Charging for Electric Vehicles—A Review,” *IEEE Access*, vol. 9, pp. 137667–137713, 2021.
- [59] M. F. Romlie, K. Lau, M. Z. Zainol, M. F. Abdullah, and R. Kannan, “Performance of Inductive Coupled Power Transfer Versus the Coil Shape - Investigation using Finite Element Analysis,” *MATEC Web Conf.*, vol. 225, 2018, doi: 10.1051/mateconf/201822501017.
- [60] P. Pérez-Nicoli, F. Silveira, and M. Ghovanloo, “*Inductive Links for Wireless Power Transfer*” vol. 24. 2021. doi: 10.1007/978-3-030-

- 65477-1.
- [61] Jin Xua,\* , Yuhui Xub , Qian Zhanga“Calculation and analysis of optimal design for wireless power transfer,” Contents lists available at ScienceDirect Computers and Electrical Engineering. vol. 39, 2019.
- [62] S. Chatterjee, A. Iyer, C. Bharatiraja, I. Vaghasia, and V. Rajesh, “Design Optimisation for an Efficient Wireless Power Transfer System for Electric Vehicles,” *Energy Procedia*, vol. 117, pp. 1015–1023, 2017, doi: 10.1016/j.egypro.2017.05.223.
- [63] R. Vaka and R. K. Keshri, “Design Considerations for Enhanced Coupling Coefficient and Misalignment tolerance Using Asymmetrical Circular Coils for WPT System,” *Arab. J. Sci. Eng.*, vol. 44, no. 3, pp. 1949–1959, 2019, doi: 10.1007/s13369-018-3219-x.
- [64] “Coil64.” <https://coil32.net/online-calculators/flat-spiral-pancake-tesla-coil.html>
- [65] “Pronine.” <http://www.pronine.ca/spiralcoil.htm>
- [66] V. Jiwariyavej, T. Imura, and Y. Hori, “Coupling coefficients estimation of wireless power transfer system via magnetic resonance coupling using information from either side of the system,” *IEEE J. Emerg. Sel. Top. Power Electron.*, vol. 3, no. 1, pp. 191–200, 2015, doi: 10.1109/JESTPE.2014.2332056.



## Appendix A: Photos of the Experimental Setup

### A.1 SMALL SCALL PROTOTYPE



*Fig. A.1.* Small Scale Prototype

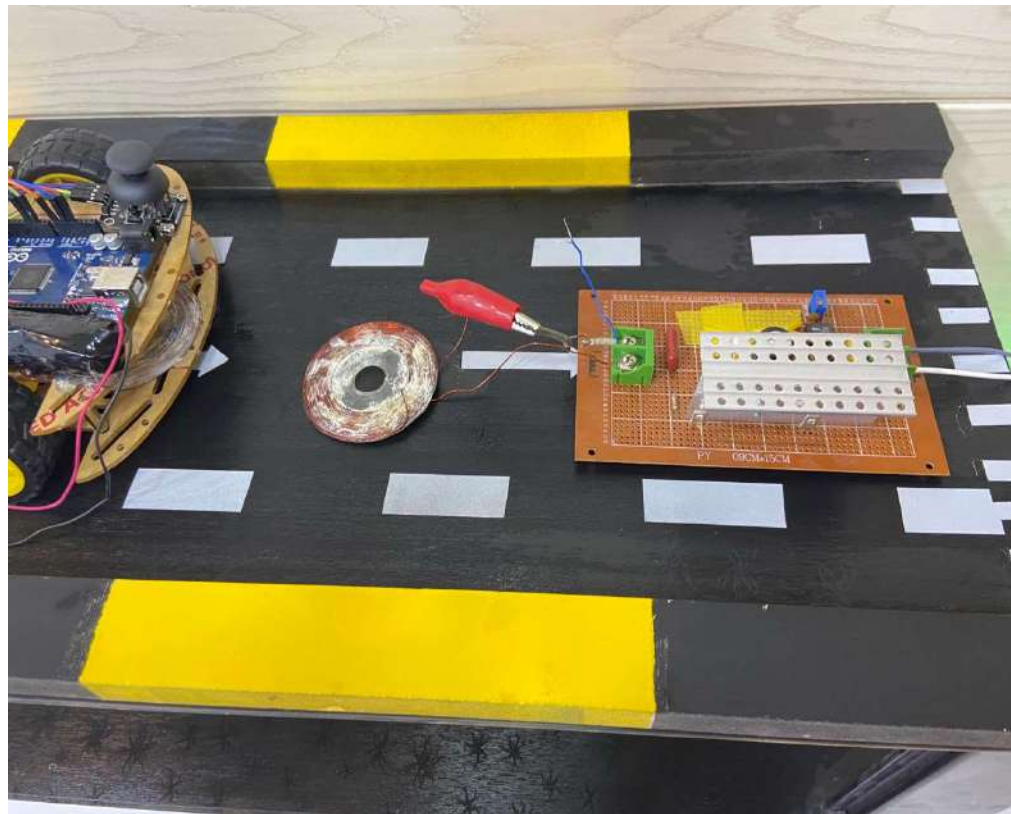


**Fig A.2.** Small Scale Prototype



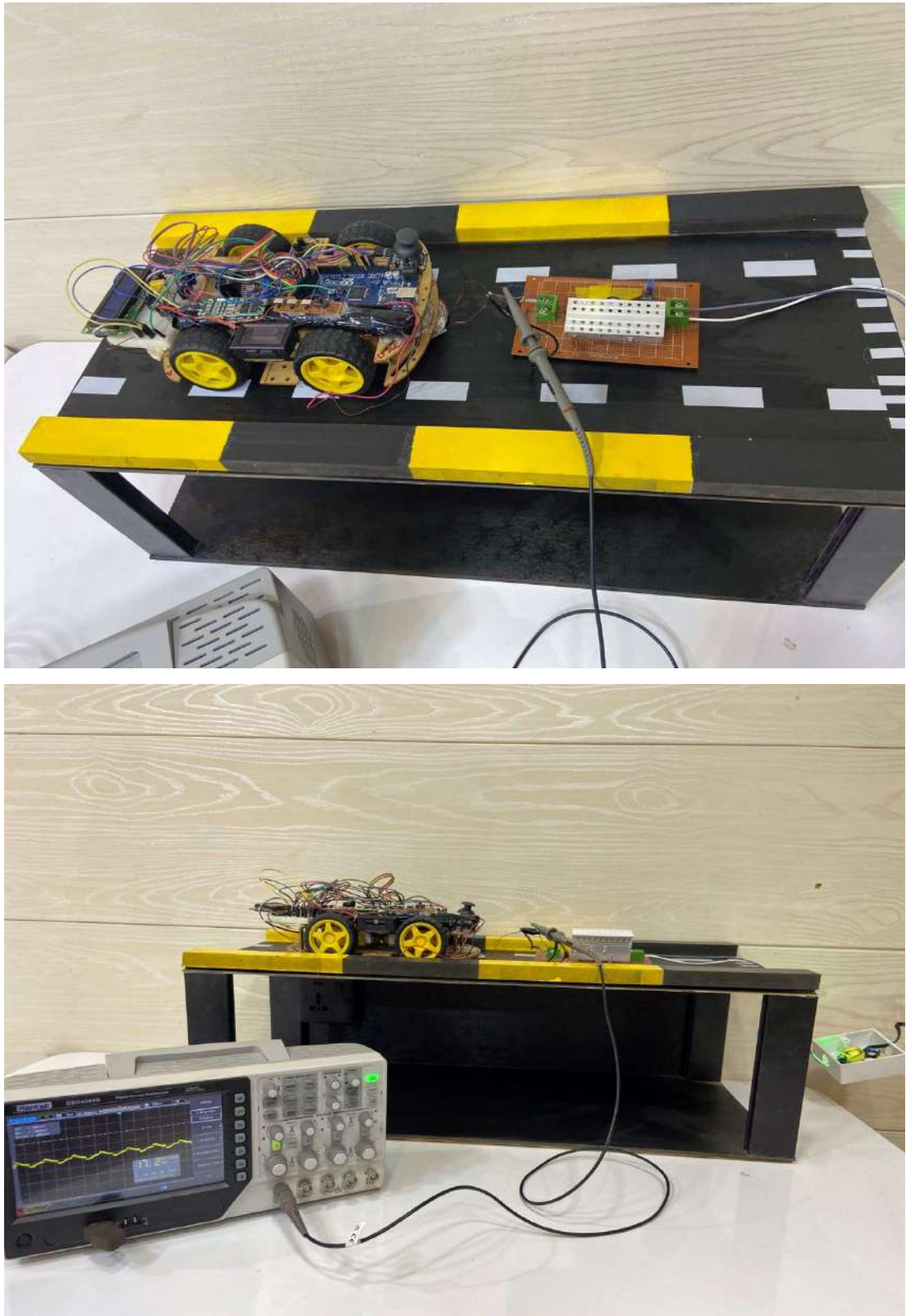


**Fig A.3. Small Scale Prototype**

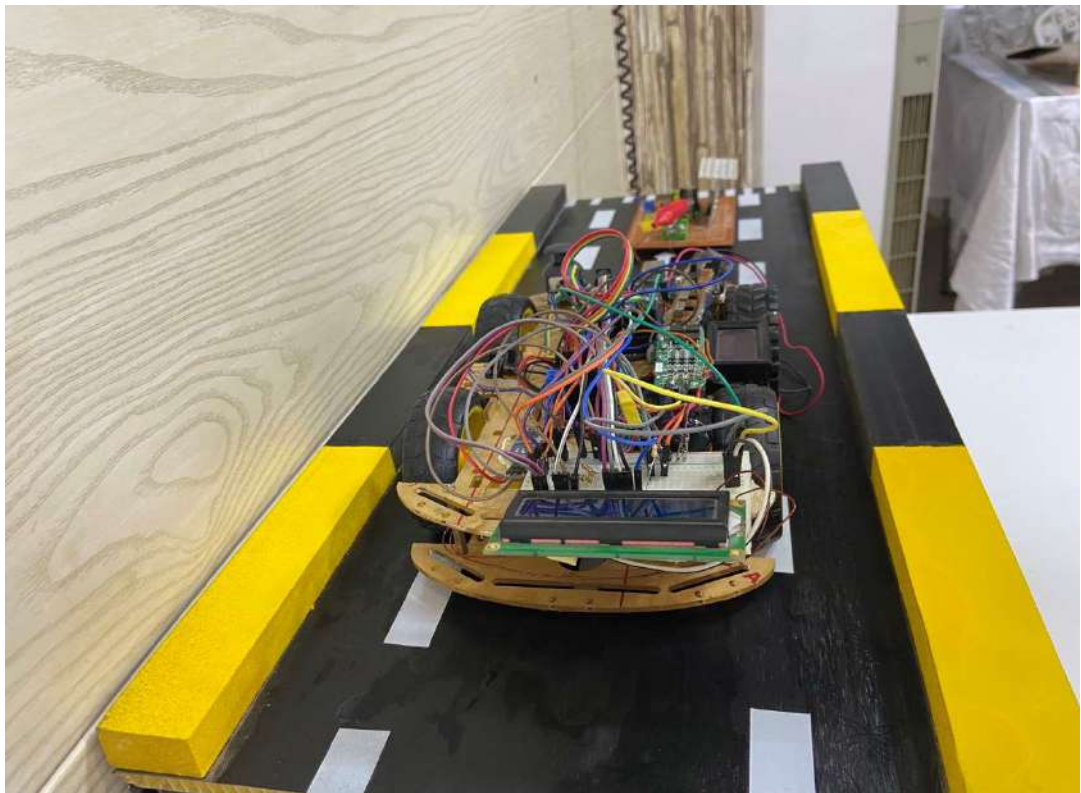
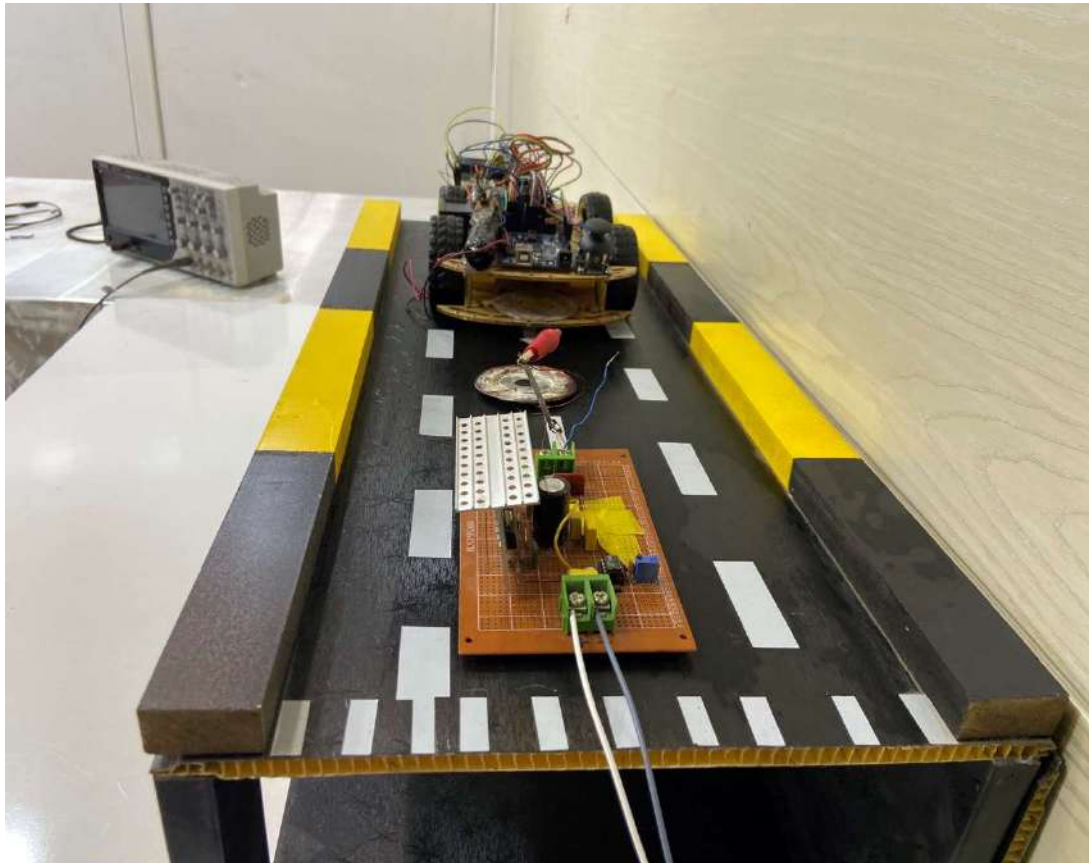


**Fig A.4. Small Scale Prototype**

## A.2 SMALL SCALL PROTOTYPE

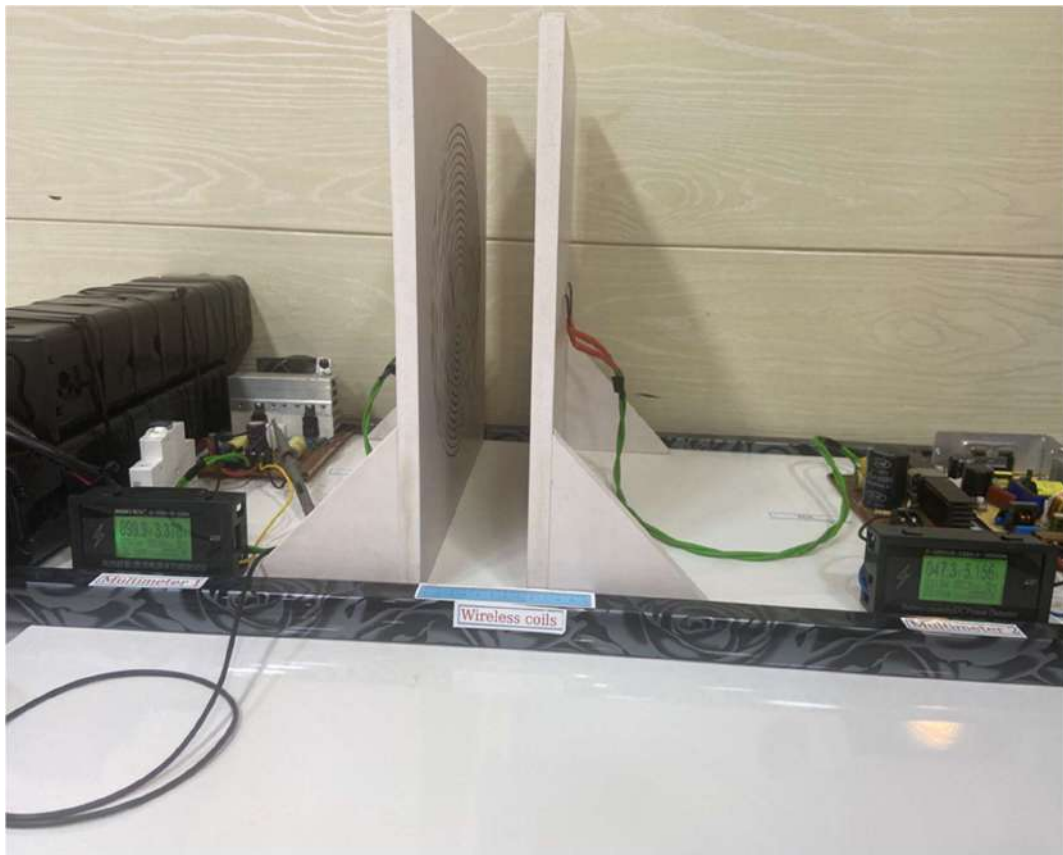


*Fig A.2.1* Wireless Coils Large Scale Prototype



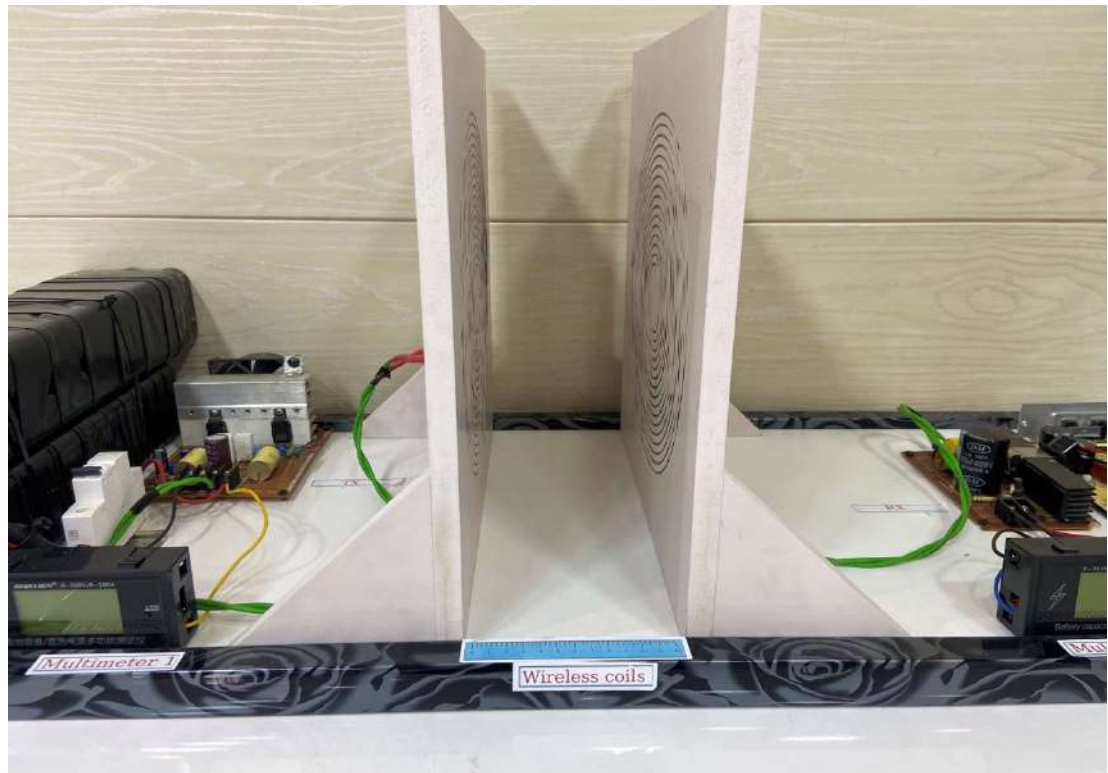


**Fig A.2.2**Battery and TX Circuit Large Scale Prototype



**Fig A.2.3** Measuring BLDCM Resistance





**Fig A.2.4** Measuring BLDCM Inductance





**Fig A.2.5** Measuring BLDCM RPM



**Fig A.2.6 LARGE SCALE PROTPTYPE**







**Fig A.2.8. BLDCM**

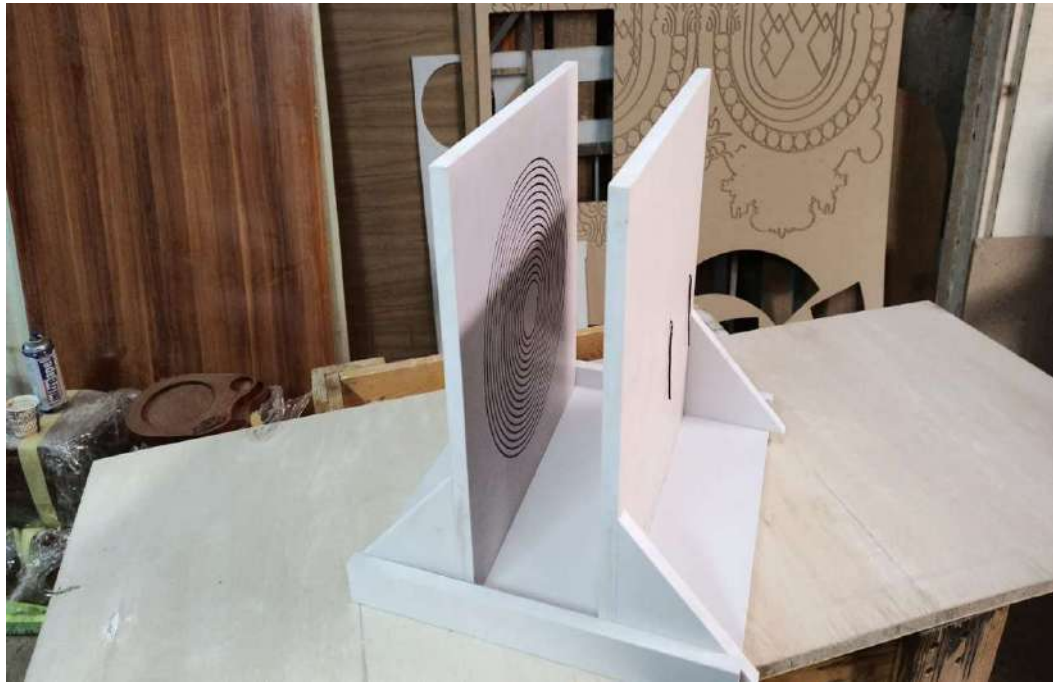


**Fig A.2.9.CNC COIL FLAT**





**FigA2.10. BLDCM**

**Published Papers**

<b>Number</b>	<b>Paper Name</b>	<b>Paper Status</b>
1	A Small-scale Inductive Wireless Power Transmission Prototype for Charging Electric Vehicles	Published
2	Performance Validation of a Wireless Power Transfer Drive Prototype for Electric Vehicles	Under Review

## الخلاصة

تم اعتماد نقل الطاقة اللاسلكية الاستقرائي (WPT) على نطاق واسع في تقنيات الشحن اللاسلكي في تطبيقات المركبات الكهربائية لقدرته على نقل مستويات عالية من الطاقة بكفاءة عبر مسافات طويلة يمكن أن تصل إلى 5 سم. يتجاوز استخدام WPT الاستقرائي تطبيق الشحن ويمكن استخدامه في مجموعة نقل الحركة في السيارة الكهربائية. المحرك داخل العجلة هو تصميم مبتكر لمجموعة نقل الحركة حظي مؤخرًا باهتمام المجتمع البحثي. في هذا التكوين، يتم تثبيت المحركات الكهربائية في عجلات السيارة ويتم تشغيلها لاسلكيًا مما يلغي الحاجة إلى كابلات الطاقة وعلبة التروس أو عمود الإدارة، مما يقلل من فقد الطاقة الميكانيكية، ويوفر حرية التحكم ويوفر مساحة أكبر في تصميم هيكل السيارة. في هذه الأطروحة، تم تصميم نموذج أولي لنقل الطاقة اللاسلكية الاستقرائي بمدخل واحد ومخرج واحد لشحن المركبات الكهربائية ويتم تحديد الكفاءة تحت مسافات الشحن المختلفة عمليًا. يتم تقديم الجهد الحقيقي وأشكال الموجة الحالية للجهود والتيارات (في الجانبين المرسل والمستقبل) للتحقق من قوة النموذج الأولي المقترح لشحن البطارية تحت مسافات فجوة هوائية مختلفة. بعد ذلك، تم تصميم وتنفيذ نظام نقل الطاقة اللاسلكي بنظام نموذج أولي للمحرك الكهربائي بقدرة 250 واط. يعتمد النظام على تقنية نقل الطاقة اللاسلكية الاستقرائي حيث يتم تصميم ملفين ومقارنتهما بشكل متبادل عند 65 كيلو هرتز. يتم تشغيل ملف جهاز الإرسال بواسطة عاكس من الفئة D يتم توفيره بواسطة بطارية 120 فولت و 10 أمبير. يقوم ملف المستقبل بتزويد دائرة المحرك في ظروف تحميل مختلفة. يتم إجراء تحليل الأستقرارية لنموذج WPT المقترح بناءً على نقاط التقاطع على الرسوم البيانية لاقتران المعاملات مقابل معاملات وحدات التحكم (أي دورات عمل المحولات في جانبي الإرسال والاستقبال). تظهر النتائج أن نموذج WPT مستقر في النطاق المحدود لدورات العمل التي تحقق أفضل اقتران للمعاملات.





جمهورية العراق  
وزارة التعليم العالي و البحث العلمي  
جامعة كربلاء  
كلية الهندسة  
قسم الهندسة الكهربائية والالكترونية

## تصميم وتنفيذ نماذج نقل الطاقة اللاسلكية للتحقق من صحة البحث

رسالة مقدمة الى مجلس كلية الهندسة / جامعة كربلاء وهي جزء من متطلبات نيل درجة  
الماجستير في علوم الهندسة الكهربائية

من قبل:

حيدر حميد حسين

بإشراف :

أ.د. علي جعفر مهدي